UNIVERSITY OF CALIFORNIA
RIVERSIDE

Flow Field Flow Fractionation Method Development for Applied Bioanalysis

A Dissertation submitted in partial satisfaction
of the requirements for the degree of

Doctor of Philosophy

in

Chemistry

by

Samantha Lynn Schachermeyer

June 2013

Dissertation Committee:
Dr. Wenwan Zhong, Chairperson
Dr. Cynthia Larive
Dr. Yinsheng Wang

The Dissertation of Samantha Lynn Schachermeyer is approved:

_____

_____

_____

Committee Chairperson

University of California, Riverside

ACKNOWLEDGEMENTS

I would like to thank my research advisor, Dr. Wenwan Zhong, for her support and guidance. She played a crucial part in my transformation from cookbook chemist into an independent scientist. Also, the input and help over the years from my coworkers were vital to my graduate career.

This dissertation is dedicated to my parents, Brian and Mary Schachermeyer, who have always supported my choices in life and taught me to value hard work and remaining true to myself.

ABSTRACT OF THE DISSERTATION

Flow Field Flow Fractionation Method Development for Applied Bioanalysis

by

Samantha Lynn Schachermeyer

Doctor of Philosophy, Graduate Program in Chemistry
University of California, Riverside, June 2013
Dr. Wenwan Zhong, Chairperson

Flow field flow fractionation (F4) and asymmetric F4 (AF4) are open channel separation instruments relying on an axial-flow and a perpendicular cross-flow to separate analytes based on hydrodynamic radius. The cross-flow provides enough force to simultaneously separate non-binding analytes based on size and remove non-specific binding giving F4 potential as a method for bioanalysis. With the desire to apply F4 in bioanalysis, a need to understand how a complex sample, containing a variety of biomolecules and nanomaterials, would behave in the system was created. The effects of changes in carrier solution (CS) and binding buffer (BB) composition such as ionic strength, cation type, and pH, on particle and protein recoveries, and on the binding between protein and a ssDNA were investigated.

Proteins required higher ionic strength to prevent adsorption in the channel, while nanoparticles had the opposite trend with increased ionic strength causing lower recoveries. No effect was seen from varying the BB, but the CS had

played a significant role. During AF4's unique focusing step, the BB is replaced with the CS rapidly, indicating that on-line incubation is a possibility for F4 bioanalysis reducing the amount of sample handling time. The presence of $MgCl_2$ in the CS, which plays an important role in DNA folding, was necessary for binding to occur. An experimental detection limit of 33 nM was achieved for immunoglobulin E, limited by the labeling of one fluorophore per protein.

The study on protein-ssDNA analysis was expanded to calculate the dissociation constant (K_d) of the model system which was in very good agreement with K_d values obtained by other methods. A variety of ssDNA were investigated to determine the effect different lengths and secondary structures had on the recovery and retention times in F4. With the ability to possibly bind both intramoleculary and intermoleculary, ssDNA showed unique elution profiles from more globular analytes. Folding equilibra were calculated for ssDNA with known secondary structure by comparing the elution times of linear DNA that was unlikely to form intramolecular bonds. This work has shown the versatility F4/AF4 could have for future applications of ssDNA as labeling agents.

TABLE OF CONTENTS

TABLE OF FIGURES

FIGURE PAGE

TABLE OF TABLES

Chapter One

Introduction

The study of biomolecular interactions is an area of great importance for biosensing. To simplify the system and reduce background, separation methods are used to remove biological complexes from free molecules. Some of the most common separation tools used are high performance liquid chromatography (HPLC) and size exclusion chromatography (SEC). HPLC separates molecules based on their hydrophobicity, while SEC separates based on size. Both methods are well understood and developed with a wide range of applications. However, they are packed channel systems which can be harsh on biomolecular interations and even the physiological structure of the biomolecules.[1-3] For this reason, open channel separation tools are an attractive alternative to more traditional chromatography methods as these methods are devoid of the disruptive packing material. A popular open channel separation tool for bioanalysis is capillary electrophoresis (CE). CE separates analytes based on their size to charge ratio. A couple of advantages of CE are a nanoliter injection size, limiting the amount of sample needed for analysis, and fast analysis time. The main disadvantage to CE is the need to keep the ionic strength of the running buffer low to reduce Joule heating.[4] In this dissertation, the open channel separation method, flow field flow fractionation (F4), was investigated for use in bioanalysis and as a cleanup tool for biological samples.

Field Flow Fractionation

Field flow fractionation (F3) was first developed by Calvin Giddings in 1986.[5] Similar to chromatography, F3 is a flow based separation technique. It is an open channel separation tool with a two dimensional separation force. F3 works by having an axial flow that carries the analytes through the channel, while a perpendicular force acts on the analytes to separate them (Figure 1.01). Many sub-types of F3 have been developed, each having their own unique separating force. These include centrifugal, thermal, gravity, sedimentation, and flow.[5] The two most popular F3 subtypes are sedimentation (SdFFF) and flow (F4). SdFFF uses a perpendicular centrifugal force that separates analytes based on mass and is popular for colloidal studies. It has also been applied to study cells and nanoparticles.[6-9]

Flow Field Flow Fractionation

F4 utilizes a secondary carrier solution flow, or cross-flow, perpendicular to the axial-flow to separate analytes based on hydrodynamic size (Figure 1.02a).[10] The instrument channel is made of two frits through which the cross-flow enters (top frit) and then leaves (bottom frit) the channel (Figure 1.02b). The channel dimensions are created via a spacer. The spacer thickness determines the channel depth and can range from 50 to 500 μm. Loading capacity is also determined by the spacer thickness. The larger the spacer, the greater the loading capacity; however, this is at the detriment of separation resolution.

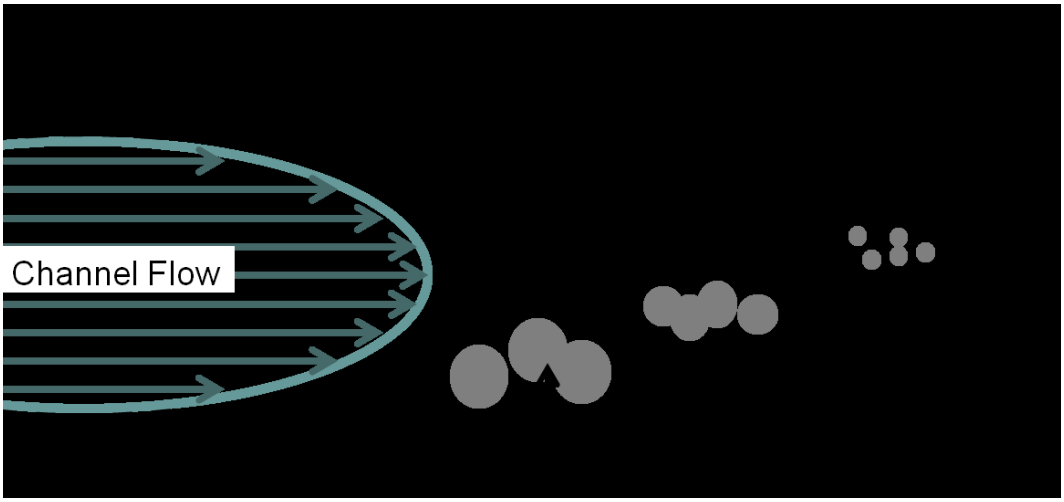

Figure 1.01. Schematic of field flow fractionation illustrating the balance of the separation force with the diffusional force.

a)

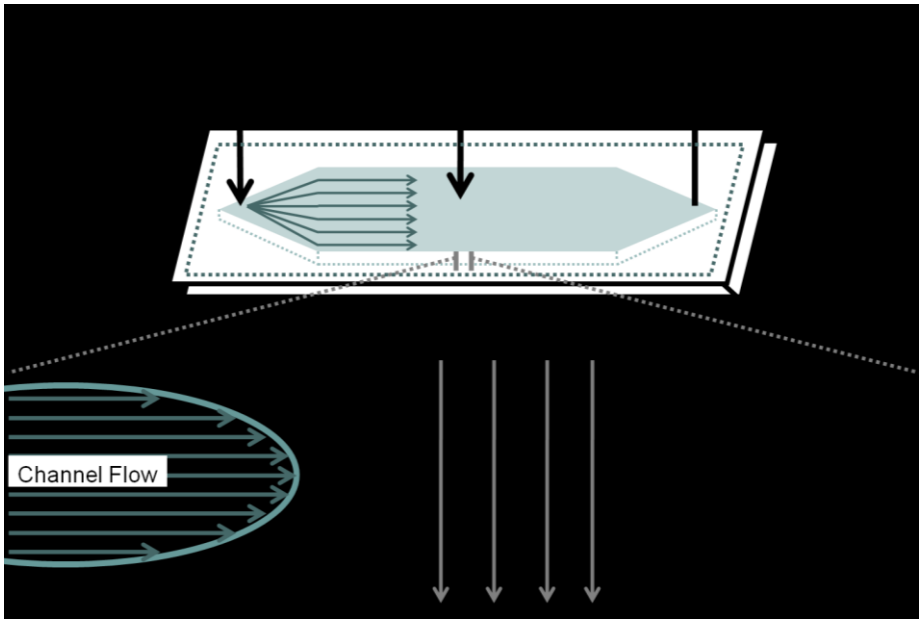

b)

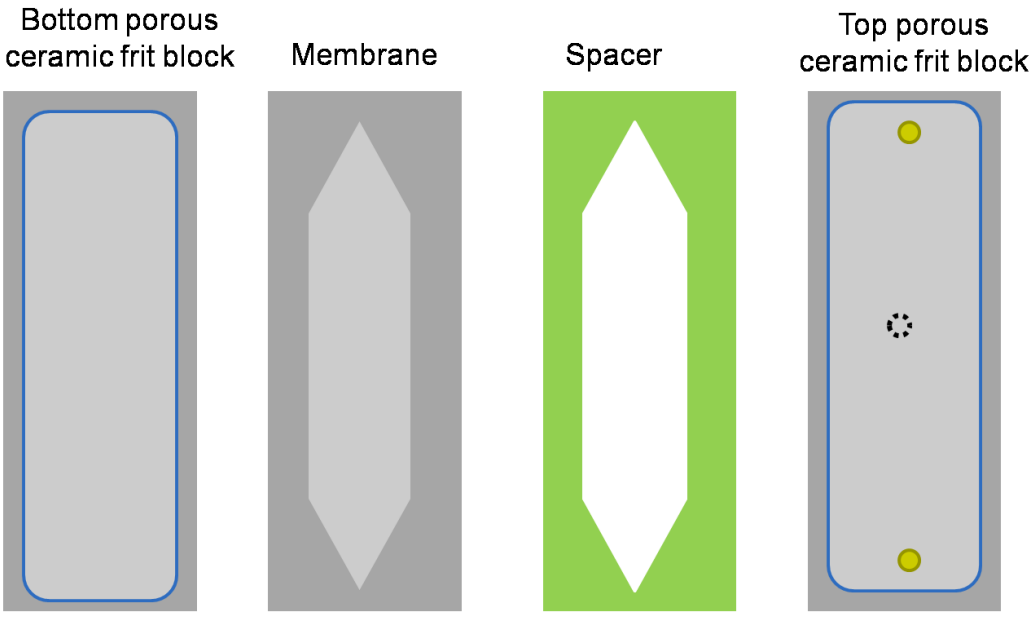

Figure 1.02. a) Channel design of F4. b) The main components of the AF4 channel.

Separation Theory

After injection into the channel, the separation enters the relaxation time in which the axial-flow bypasses the channel and only the cross-flow is entering the channel.[10] The relaxation time allows for the analytes to concentrate and equilibrate onto the accumulation wall. After the relaxation time, the axial-flow is redirected into the channel and carries the analytes down the channel. The axial-flow forms a laminar type flow profile with a faster flow velocity in the center and the slowest at the walls. This means that analytes that spend longer periods of time towards the center of the channel will elute faster from the system.

F3 has two main modes of separation: normal and steric. Normal mode, also known as Brownian mode, occurs when the analytes have a diameter smaller than 1 μm. In this mode, the analytes are pushed against the accumulation wall during the relaxation time. Then, as they are carried through the channel via the axial-flow, the analytes diffuse back towards the center of the channel. The analytes will equilibrate into a position based on their diffusion and the opposing cross-flow force. Smaller analytes have greater diffusional forces and will migrate further towards the channel's center. Due to the laminar flow profile, this results in an elution order of small to large analytes. The retention time in normal mode may be used directly to calculate the hydrodynamic radius of the analytes using Equation 1.01 where t_r is retention time, η is the solution viscosity, w is the channel thickness, d is the particle diameter, V_c is the cross-flow, k is the Boltzmann's constant, T is temperature of the solution and V is the axial-flow. Typically,

F4 is run at room temperature. If using the same carrier solution composition and flow rates, the retention time is directly proportional to the particle diameter.[11]

$$t_r = \frac{\pi \eta w^2 d V_c}{2kTV} \qquad \text{Equation 1.01}$$

This equation assumes no interactions between the analyte and membrane. Typically, the membrane is made of an inert material; one of the most popular materials for biological molecules being regenerated cellulose. Several papers on optimization of the carrier solution have been reported to examine how different variables affect separation and recovery including ionic strength, pH, and surfactant type/concentration.[12-14] In chapter two, I will discuss a comprehensive study on the effect of carrier solution composition on nanoparticles, both neutral and charged, and proteins.

The second separation mode is steric mode which occurs with analytes greater than 1 μm in diameter. Once a molecule becomes larger, the diffusion forces are too small to play a role in the separation. In this case, an opposing force caused by the rebounding cross-flow from the accumulation wall "lifts" the particles away from the wall. The greater the diameter the more area the "lift" force has to push the particle back towards the center of the channel. This results in an elution order of large to small particles. An additional separation mode can occur in the F4 system called hyperlayer mode. This mode is conditional on the use of particularly high cross-flow rates with micron-sized particles and can be difficult to differentiate from steric mode. Neither of these modes can be used to calculate the hydrodynamic diameter of the particles directly.[5] However, the use of known standards within the expected size range may be used in order to estimate the size of an unknown particle.

Asymmetric Field Flow Fractionation

The original design of F4 was formed with a symmetrical channel (Figure 1.02a). In the early 2000s, the system was redesigned to simplify both the instrument setup and membrane manufacturing to reduce cost. The redesign has only one porous wall compared to F4's two porous walls. The top porous wall was replaced with a transparent solid top wall which allows facile flow (both flow stream and focusing) performance observation with the use of simple colored dyes. The cross-flow pump draws the fluid out of the channel through the bottom porous wall. In order to maintain a constant pressure, the channel was redesigned in an asymmetrical figure, reducing the width of the channel gradually to compensate for the reduced volume as the carrier solution passes through the channel (Figure 1.03). The redesigned system is referred to as asymmetric flow field flow fractionation or AF4. Since there is no longer a cross-flow introduced from the top frit, a third flow, the focus-flow, has been introduced into the configuration for the purposes of equilibrating and focusing the sample immediately after injection. This is called the focusing period. After the sample is injected into the channel, the axial-flow and the focus-flow meet opposing each other, concentrating the sample into a small area on the membrane.[5]

AF4 has found significantly more favor in the scientific community compared to F4. The design simplified the assembly and disassembly of the channel. In addition, the

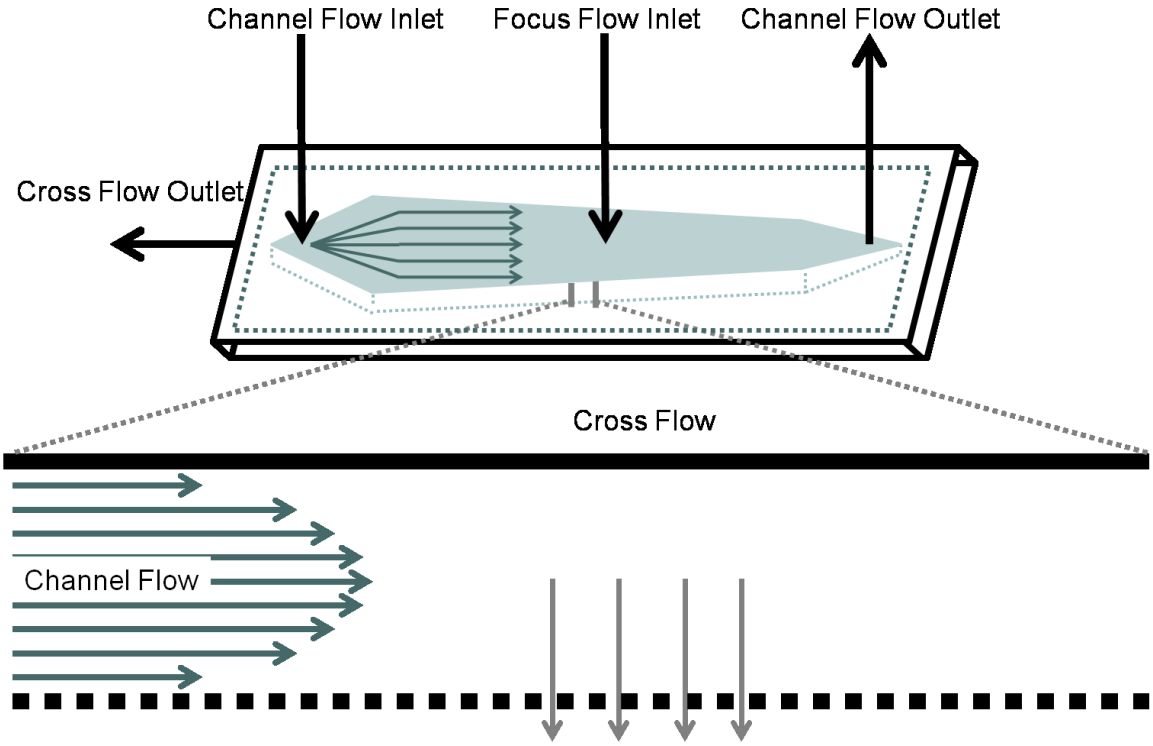

Figure 1.03. Schematic for AF4.

new channel structure of the AF4 included a rubber seal that prevents leaks. The F4 channel design lacked this seal, requiring the membrane to have a special silica sealant. The sealant increases the cost of the membranes by as much as a factor of ten. The less expensive membranes in the AF4 allow frequent replacement of the part. An important factor when contemplating biological investigations is sample carryover. Therefore, the ability to replace the membrane frequently, which is the part most likely to interact and retain any sample analytes, is a huge benefit to the application of the AF4 in bioanalysis.

Applications

F4 has been applied to a wide range of biological and non-biological analytes. Due to the ability to run a wide variety of carrier solutions including organics and salty aqueous buffers, F4 can be applied to a diverse number of analytes including nano- and micro- particles, polymers, proteins, viruses, and cells.[15-25] With output flow rates from 0.2-5 mL/min, F4 is compatible with many different types of detectors. Typically, any detector that can be attached to an HPLC column, may be used with F4.

Nanoparticle separation and characterization has been a popular application of F4. The hydrodynamic radius (R_h) can be calculated from the F4 elution time although the theory applies the Stokes relationship which assumes the analyte of interest is a hard sphere. In addition, complex samples may be too complicated for accurate sizing. Thus, a second detector should be used for complementary size determination.[23] The most popular methods of nanoparticle analysis are transmission electron microscope (TEM) for absolute size measurements and dynamic light scattering (DLS) for hydrodynamic size

measurements as no prior separation mechanism is required. The lack of separation means that samples have much higher polydispersity.[23] One restriction with DLS is that the measurement gives an average diameter for all the analytes present in the solution. If the sample is polydisperse, DLS sizes are not an accurate representation of the entire population as it will skew the measured sizes towards the larger particles. This can be particularly problematic when aggregation is present. Multi-angled light scattering (MALS) is more popular than DLS for on-line detection because, in addition to size, it can also calculate the radius of gyration (Rg) which can be used for absolute molar mass determination. F4-MALS can be used to determine a particle's shape factor (ρ) using Equation 1.02. A sphere's shape factor is 0.755 and the value increases as the particle deviates from a sphere.[23]

$$\rho = \frac{R_g}{R_h} \qquad \text{Equation 1.02}$$

Many types of nanoparticles have been analyzed on F4-MALS including gold, silver, titanium oxide, and carbon nanotubes.[20-22, 26-37] Size characterization and/or particle stability under different solution conditions including ionic strength and pH have been investigated. F4 has been extensively used in the analysis of both environmental and manufactured NPs.[12, 28] Environmental NPs are those that occur naturally in the environment. The main parameter to describe NPs is their size as this will determine their behavior in interactions, aggregation, biological and environmental uptake, and production of reactive oxygen species.[38]

Beyond size fractionation, the other parameter of interest in environmental NPs is metal speciation. To determine the metal species and concentration, inductively coupled

plasma atomic emission spectroscopy or mass spectrometry (ICP-AES or ICP-MS) are the most commonly employed online detectors for F4. In environmental studies, ICP-MS provides a method to investigate natural nanoparticles and understand their size dependent compositions.[39-42] ICP-MS allows the simultaneous detection of up to 45 elements which, when combined with F4's fractionation, can give valuable information regarding trace-element concentrations and colloidal size distributions.[23] Some examples are studies tracking the amount of uranium, lead, copper, phosphorus, manganese, iron, and zinc taken up by organic colored material and iron oxide nanoparticles in river (Mississippi River) and coastal waters (Mississippi Bright, USA).[23] Interestingly, F4 was also used to study atmospheric particles. When compared with an on-line scanning mobility particle sizer (SMPS), the F4 results indicated smaller sized particles. This suggested a disaggregation of the atmospheric particles as they were transferred to aqueous phase, which more likely mimics what occurs when the particles are wetted in lung fluid or surface waters.[43] For manufactured NPs, F4 has been widely applied to study NPs size, composition, aggregation behavior, determination of surface coating thickness, and to monitor NP growth.[20-22, 30, 32, 33, 37, 44-47] Also, by changing the carrier solution, such as the ionic strength or pH, one can determine manufactured NPs stability in a variety of solutions.[12, 21, 28]

Protein aggregation is important to both the pharmaceutical and food industries. This aggregation can be an indicator of protein destabilization.[16, 19, 48-51] A common separation method for protein analysis is SEC. However, the SEC packed channel can be harsh due to the sheer stress the protein aggregates undergo. This stress can break apart

aggregates to form the monomer. In fact, some protein dimers and trimers have only been observed in F4, as they typically represent a small fraction of the entire amount of protein. One study investigated a series of environmental factors on the behavior of bovine serum albumin (BSA).[49] Protein Denaturation could be studied by increasing the temperature prior to injection into the F4. As BSA denatures, its overall size increases. Therefore, by tracking the elution time of the BSA, the authors were able to indicate that the denaturation temperature for BSA was 66 °C, which was in agreement with literature. The authors also tracked the formation of the BSA dimer as a function of sodium chloride concentration. They found that sodium chloride was necessary for dimer formation by reducing the electrostatic repulsion between the monomers. This study shows the applicability of using F4 to understand the effects of environmental factors for protein stability relevant to food and vaccine storage.

Bacterial cells are another system that has been analyzed on F4. As dead gram negative bacteria can disassemble and release endotoxins, a method to separate the live and dead cells is necessary.[52] Flow cytometry has been the instrument of choice for cell separations, but has limited application to smaller cells, with a lower size limit of 200 nm.[53] F4, SdF3, and electrical F3 (EF3) were applied to separate four different bacteria, each obtaining separation within 15 minutes.[54] Dead cells are differentiated from live cells due to earlier elution times. As most cells are in complex matrices, such as food, blood, or soil, the separation power of F4 is useful. Using F4-ICP-MS, Shewanella oneidensis strain MR-1 were separated from exopolymers in the cell suspension and analyzed to determine the amount of uranium taken up as a function of pH.[55] It was found

that the maximum asdosprtion of uranium occurred at pH 5.0 where uranium exists as the UO_2^{2+} cation and interacts with the negative carboxylates on the cell surface. The experiment was the first to show the presence of an exopolymer from the cell which binds the uranium. The exopolymer had low UV adsorption and was only visible by ICP-MS due to the bound uranium.

Biological Cleanup Tool

Beyond the standard separation of analytes, the F4/AF4 systems can be used as a biological cleanup tool. The cross-flow can act not only as a separating force, but it can also remove non-specific binding. Non-specific bindings are weak and unstable, so when the cross-flow acts upon the complexes, the weak bond is broken and separated from the more stable complexes resulting in a "cleaning" phenomenon. This was previously explored in our group using an immunoglobulin G (IgG) conjugated polystyrene magnetic microparticles with a diameter of 5.28 um that had been incubated in cell lysate. IgG will bind specifically to proteins A and G naturally found in the cell lysate. Nonspecific protein absorption could also occur in this matrix. It was shown that the F4 had superior washing capabilities when compared to a standard centrifugation wash or magnetic pulldown while preserving the specific IgG-Protein A interactions (Figure 1.04).[56]

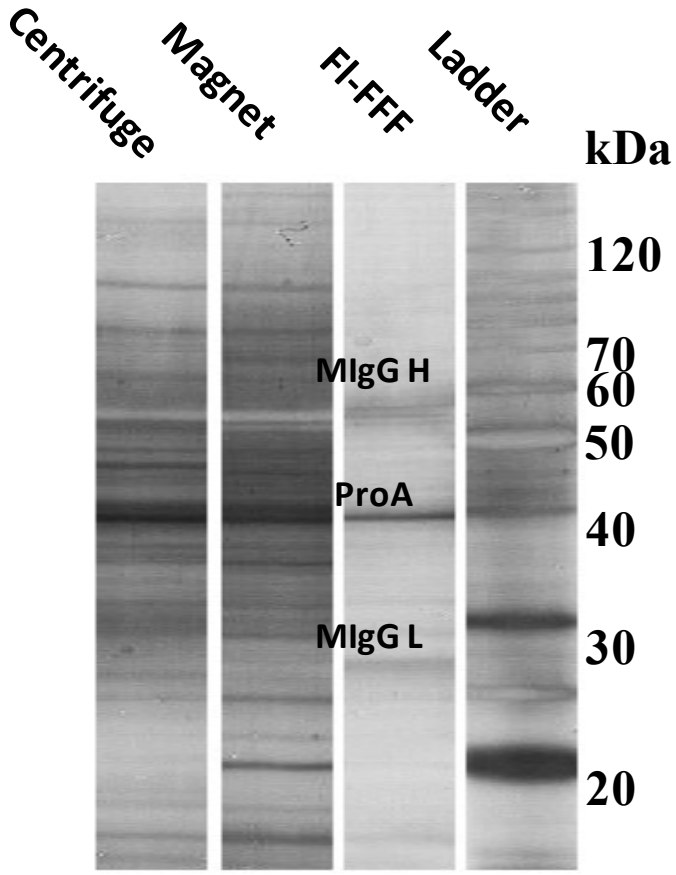

Figure 1.04. SDS-PAGE gel comparing magnetic microparticles conjugated with protein G and incubated in cell lysate. The F4 (here labeled as Fl-FFF) wash had significantly reduced non-specific binding while maintaining the specific protein A-G binding compared with centrifugation and magnetic pull-down washing methods. Reprinted with permission. [56] Copyright 2008 American Chemical Society.

The main focus of this dissertation was to develop a fundamental understanding on how to apply F4 and AF4 for bioanalysis. As nanomaterials become applied increasingly in biological systems it becomes necessary to develop methods to study the complex matrices that are created. In chapter two, we investigated how different carrier solutions in F4 effect the recovery of proteins and nanoparticles in order to find an optimum condition for simultaneous analysis. In chapter three, we continued the carrier solution investigation to AF4 to understand the effect both the carrier solution and the incubation buffer had on the binding of an immunoglobulin E (IgE) specific aptamer to IgE. We were able to apply the separation of the free aptamer from the labeled aptamer/protein complex to detect protein as low as 33 nM. In chapter four we expanded the AF4 study to the kinetics of the aptamer/protein complexation and work to understand how short segments of DNA behave in the channel. The final chapter will discuss the future outlook of AF4 in bioanalytical chemistry.

References

1. Liu, J.; Demeule, B.; Shire, S. J. In *Separation-based analytical methods for measuring protein aggregation*, John Wiley & Sons, Inc.: pp 11-36.

2. Hong, P.; Koza, S.; Bouvier, E. S. P., A review size-exclusion chromatography for the analysis of protein biotherapeutics and their aggregates. *J. Liq. Chromatogr. Relat. Technol.* 35, (20), 2923-2950.

3. Bhushan, R.; Dixit, S., Application of HPLC, gel electrophoresis and size exclusion chromatography for separation and characterization of storage proteins of soybean and peanut. *Acta Chromatogr.* 24, (3), 323-349.

4. Sekhon, B. S., An overview of capillary electrophoresis: pharmaceutical, biopharmaceutical and biotechnology applications. *J. Pharm. Educ. Res.* 2, (2), 2-36.

5. Giddings, J. C.; Schimpf, M. E.; Caldwell, K., *Field-Flow Fractionation Handbook*. John Wiley & Sons, Inc.: New York, 2000.

6. Kanai, Y., Review of analytical methods (observation, separation) of colloidal materials. *Chishitsu Nyusu* **2007,** 631, 19-23.

7. Chianea, T.; Assidjo, N. E.; Cardot, P. J. P., Sedimentation field-flow-fractionation: emergence of a new cell separation methodology. *Talanta* **2000,** 51, (5), 835-847.

8. Giddings, J. C.; Williams, P. S., Multifaceted analysis of 0.01- to 100-Î¼m particles by sedimentation field-flow fractionation. *Am. Lab. (Shelton, Conn.)* **1993,** 25, (16), 88, 90-5.

9. Arner, E. C.; Kirkland, J. J. In *Sedimentation field flow fractionation*, 1992; Royal Soc. Chem.: 1992; pp 208-27.

10. Giddings, J. C.; Yang, F. J.; Myers, M. N., Flow-field-flow fractionation: a versatile new separation method. *Science* **1976,** 193, (4259), 1244-1245.

11. Giddings, J. C.; Yang, F. J.; Myers, M. N., Theoretical and experimental characterization of flow field-flow fractionation. *Analytical Chemistry* **1976,** 48, (8), 1126-1132.

12. Cumberland, S. A.; Lead, J. R., Particle size distributions of silver nanoparticles at environmentally relevant conditions. *J. Chromatogr., A* **2009,** 1216, (52), 9099-9105.

13. Neubauer, E.; v.d. Kammer, F.; Hofmann, T., Influence of carrier solution ionic strength and injected sample load on retention and recovery of natural nanoparticles using Flow Field-Flow Fractionation. *Journal of Chromatography A* In Press, Corrected Proof.

14. Benincasa, M.-A.; Caldwell, K. D., Flow field-flow fractionation of poly(ethylene oxide): effect of carrier ionic strength and composition. *Journal of Chromatography A* **2001,** 925, (1-2), 159-169.

15. Rebolj, K.; Pahovnik, D.; Zagar, E., Characterization of a Protein Conjugate Using an Asymmetrical-Flow Field-Flow Fractionation and a Size-Exclusion Chromatography with Multi-Detection System. *Anal. Chem. (Washington, DC, U. S.)* 84, (17), 7374-7383.

16. Glantz, M.; Haakansson, A.; Lindmark, M. H.; Paulsson, M.; Nilsson, L., Revealing the Size, Conformation, and Shape of Casein Micelles and Aggregates with Asymmetrical Flow Field-Flow Fractionation and Multiangle Light Scattering. *Langmuir* 26, (15), 12585-12591.

17. Johann, C.; Ramage, P.; Hemmig, R., Asymmetric flow field-flow fractionation (AF4) with multi-angle light scattering (MALS) for high-throughput protein refolding. *LC-GC Eur.* **2005,** 18, (10), 532,536,538.

18. Jiang, Y.; Miller, M. E.; Li, P.; Hansen, M. E., Characterization of water-soluble polymers by flow FFF-MALS. *Am. Lab. (Shelton, Conn.)* **2000,** 32, (3), 98, 101-106, 108.

19. Silveira, J. R.; Hughson, A. G.; Caughey, B., Fractionation of prion protein aggregates by asymmetrical flow field-flow fractionation. *Methods Enzymol.* **2006,** 412, (Amyloid, Prions, and Other Protein Aggregates, Part B), 21-33.

20. Reschiglian, P.; Rambaldi, D. C.; Zattoni, A., Flow field-flow fractionation with multiangle light scattering detection for the analysis and characterization of functional nanoparticles. *Anal. Bioanal. Chem.* 399, (1), 197-203.

21. Cho, T. J.; Hackley, V. A., Fractionation and characterization of gold nanoparticles in aqueous solution: asymmetric-flow field flow fractionation with MALS, DLS, and UV-Vis detection. *Anal. Bioanal. Chem.* 398, (5), 2003-2018.

22. Cho, T. J.; Zheng, J.; Clogston, J. D.; Hackley, V. A.; Patri, A. K., Characterization of Gold Nanoparticles In Aqueous Solution: Asymmetric-Flow Field-Flow Fractionation with MALS, PCS and UV-Vis Detection. *Mater. Res. Soc. Symp. Proc.* **2007,** 1019E, (Engineered Nanoscale Materials for the Diagnosis and Treatment of Disease), No pp. given, Paper #: 1019-FF04-04.

23. Baalousha, M.; Stolpe, B.; Lead, J. R., Flow field-flow fractionation for the analysis and characterization of natural colloids and manufactured nanoparticles in environmental systems: A critical review. *Journal of Chromatography A* 1218, (27), 4078-4103.

24. Tsuruta, E., Separation of polymers and microparticle and online light scattering measurement. *Kagaku Sochi* **2006,** 48, (7), 94-96.

25. Bolea, E.; Laborda, F.; Castillo, J. R., Metal associations to microparticles, nanocolloids and macromolecules in compost leachates: Size characterization by asymmetrical flow field-flow fractionation coupled to ICP-MS. *Anal. Chim. Acta* 661, (2), 206-214.

26. Loeschner, K.; Navratilova, J.; Legros, S.; Wagner, S.; Grombe, R.; Snell, J.; von, d. K. F.; Larsen, E. H., Optimization and evaluation of asymmetric flow field-flow fractionation of silver nanoparticles. *J. Chromatogr. A* 1272, 116-125.

27. Dutz, S.; Kuntsche, J.; Eberbeck, D.; Mueller, R.; Zeisberger, M., Asymmetric flow field-flow fractionation of superferrimagnetic iron oxide multicore nanoparticles. *Nanotechnology* 23, (35), 355701/1-355701/7.

28. Delay, M.; Dolt, T.; Woellhaf, A.; Sembritzki, R.; Frimmel, F. H., Interactions and stability of silver nanoparticles in the aqueous phase: Influence of natural organic matter (NOM) and ionic strength. *J. Chromatogr. A* 1218, (27), 4206-4212.

29. Schaedlich, A.; Rose, C.; Kuntsche, J.; Caysa, H.; Mueller, T.; Goepferich, A.; Maeder, K., How Stealthy are PEG-PLA Nanoparticles? An NIR In Vivo Study Combined with Detailed Size Measurements. *Pharm. Res.* 28, (8), 1995-2007.

30. Schmidt, B.; Loeschner, K.; Hadrup, N.; Mortensen, A.; Sloth, J. J.; Bender, K. C.; Larsen, E. H., Quantitative Characterization of Gold Nanoparticles by Field-Flow Fractionation Coupled Online with Light Scattering Detection and Inductively Coupled Plasma Mass Spectrometry. *Anal. Chem. (Washington, DC, U. S.)* 83, (7), 2461-2468.

31. Melucci, M.; Zambianchi, M.; Barbarella, G.; Manet, I.; Montalti, M.; Bonacchi, S.; Rampazzo, E.; Rambaldi, D. C.; Zattoni, A.; Reschiglian, P., Facile tuning from blue to white emission in silica nanoparticles doped with oligothiophene fluorophores. *J. Mater. Chem.* 20, (44), 9903-9909.

32. Rambaldi, D. C.; Zattoni, A.; Reschiglian, P.; Melucci, M.; Zambianchi, M.; Barbarella, G.; Bonacchi, S.; Montalti, M.; Rampazzo, E. In *Analysis and characterization of multifunctional oligothiophene-silica hybrid nanomaterials by AF4-MALS-FD*, CRC Press: pp 183-186.

33. Lohrke, J.; Briel, A.; Maeder, K., Characterization of superparamagnetic iron oxide nanoparticles by asymmetrical flow-field-flow fractionation. *Nanomedicine (London, U. K.)* **2008,** 3, (4), 437-452.

34. Guan, X.; Cueto, R.; Russo, P.; Qi, Y.; Wu, Q., Asymmetric Flow Field-Flow Fractionation with Multiangle Light Scattering Detection for Characterization of Cellulose Nanocrystals. *Biomacromolecules* 13, (9), 2671-2679.

35. Gigault, J.; Grassl, B.; Le, H. I.; Lespes, G., Accurate determination of the length of carbon nanotubes using multi-angle light scattering. *Microchim. Acta* 175, (3-4), 265-271.

36. Gigault, J.; Grassl, B.; Lespes, G., Multi-wall carbon nanotube aqueous dispersion monitoring by using A4F-UV-MALS. *Anal. Bioanal. Chem.* 401, (10), 3345-3353.

37. Zattoni, A.; Rambaldi, D. C.; Reschiglian, P.; Melucci, M.; Krol, S.; Garcia, A. M. C.; Sanz-Medel, A.; Roessner, D.; Johann, C., Asymmetrical flow field-flow fractionation with multi-angle light scattering detection for the analysis of structured nanoparticles. *J. Chromatogr., A* **2009,** 1216, (52), 9106-9112.

38. Dubascoux, S.; Von, D. K. F.; Le, H. I.; Gautier, M. P.; Lespes, G., Optimization of asymmetrical flow field flow fractionation for environmental nanoparticles separation. *J. Chromatogr., A* **2008,** 1206, (2), 160-165.

39. Lesher, E. K.; Ranville, J. F.; Honeyman, B. D., Analysis of pH Dependent Uranium(VI) Sorption to Nanoparticulate Hematite by Flow Field-Flow Fractionation - Inductively Coupled Plasma Mass Spectrometry. *Environ. Sci. Technol.* **2009,** 43, (14), 5403-5409.

40. Prestel, H.; Schott, L.; Niessner, R.; Panne, U., Characterization of sewage plant hydrocolloids using asymmetrical flow field-flow fractionation and ICP-mass spectrometry. *Water Research* **2005,** 39, (15), 3541-3552.

41. Siripinyanond, A.; M. Barnes, R., Flow field-flow fractionation-inductively coupled plasma mass spectrometry and metal speciation in proteins: A feasibility study. *Journal of Analytical Atomic Spectrometry* **1999,** 14, (9), 1527-1531.

42. Contado, C.; Blo, G.; Conato, C.; Dondi, F.; Beckett, R., Experimental approaches for size-based metal speciation in rivers. *J. Environ. Monit.* **2003,** 5, (6), 845-851.

43. Kim, W.-S.; Park, Y. H.; Shin, J. Y.; Lee, D. W.; Lee, S., Size Determination of Diesel Soot Particles Using Flow and Sedimentation Field-Flow Fractionation. *Analytical Chemistry* **1999,** 71, (15), 3265-3272.

44. Ehrhart, J.; Mingotaud, A.-F.; Violleau, F., Asymmetrical flow field-flow fractionation with multi-angle light scattering and quasi elastic light scattering for characterization of poly(ethyleneglycol-b-Ïµ-caprolactone) block copolymer self-assemblies used as drug carriers for photodynamic therapy. *J. Chromatogr., A* 1218, (27), 4249-4256.

45. Schmidt, B.; Petersen, J. H.; Bender, K. C.; Plackett, D.; Johansen, N. R.; Katiyar, V.; Larsen, E. H., Combining asymmetrical flow field-flow fractionation with light-scattering and inductively coupled plasma mass spectrometric detection for characterization of nanoclay used in biopolymer nanocomposites. *Food Addit. Contam., Part A* **2009,** 26, (12), 1619-1627.

46. von, d. K. F.; Legros, S.; Hofmann, T.; Larsen, E. H.; Loeschner, K., Separation and characterization of nanoparticles in complex food and environmental samples by field-flow fractionation. *TrAC, Trends Anal. Chem.* 30, (3), 425-436.

47. Calzolai, L.; Gilliland, D.; Garcìa, C. P.; Rossi, F., Separation and characterization of gold nanoparticle mixtures by flow-field-flow fractionation. *Journal of Chromatography A* 1218, (27), 4234-4239.

48. Hawe, A.; Romeijn, S.; Filipe, V.; Jiskoot, W., Asymmetrical flow field-flow fractionation method for the analysis of submicron protein aggregates. *J. Pharm. Sci.* 101, (11), 4129-4139.

49. Yohannes, G.; Wiedmer, S. K.; Elomaa, M.; Jussila, M.; Aseyev, V.; Riekkola, M.-L., Thermal aggregation of bovine serum albumin studied by asymmetrical flow field-flow fractionation. *Anal. Chim. Acta* 675, (2), 191-198.

50. Cao, S.; Pollastrini, J.; Jiang, Y., Separation and characterization of protein aggregates and particles by field flow fractionation. *Curr. Pharm. Biotechnol.* **2009,** 10, (4), 382-390.

51. Samontha, A.; Nipattamanon, C.; Shiowatana, J.; Siripinyanond, A., Toward better understanding of salt-induced hen egg white protein aggregation using field-flow fractionation. *J. Agric. Food Chem.* **2008,** 56, (19), 8809-8814.

52. Shenep, J. L.; Mogan, K. A., Kinetics of Endotoxin Release during Antibiotic Therapy for Experimental Gram-Negative Bacterial Sepsis. *The Journal of Infectious Diseases* **1984,** 150, (3), 380-388.

53. Nebe-von-Caron, G.; Stephens, P. J.; Hewitt, C. J.; Powell, J. R.; Badley, R. A., Analysis of bacterial function by multi-colour fluorescence flow cytometry and single cell sorting. *Journal of Microbiological Methods* **2000,** 42, (1), 97-114.

54. Saenton, S.; Lee, H.; Gao, Y.-S.; Ranville, J. F.; Williams, S. K. R., Evaluation of Different Field-Flow Fractionation Techniques for Separating Bacteria. *Separation Science and Technology* **2000,** 35, (11), 1761 - 1775.

55. Jackson, B. P.; Ranville, J. F.; Neal, A. L., Application of flow field flow fractionation-ICPMS for the study of uranium binding in bacterial cell suspensions. *Anal. Chem.* **2005,** 77, (5), 1393-1397.

56. Li, J.; Ge, J.; Yin, Y.; Zhong, W., Multiplexed Affinity-Based Protein Complex Purification. *Analytical Chemistry* **2008,** 80, (18), 7068-7074.

Chapter Two

Impact of Carrier Fluid Composition on the Recovery of Nanoparticles and Proteins in Flow Field Flow Fractionation

Originally published in the Journal of Chromatography A[1]

Samantha Schachermeyer, Jonathan Ashby, MinJung Kwon, Wenwan Zhong*

1. INTRODUCTION

Flow field flow fractionation (F4) uses an axial channel-flow and a perpendicular cross-flow to separate analytes based on their hydrodynamic radius. Since its invention by Calvin Giddings, F4 has found applications in environmental studies[2-5], nanomaterials characterization[6-8], food analysis[3, 9-11], and drug carrier development[12-18], owing to its superior compatibility with analytes larger than a few nanometers. A variety of large substances have been analyzed by F4, including bacterial cells[19], particles, nanocolloids[20], and proteins[21]. Employment of on-line detectors that are able to measure the size and molecule mass of the eluted molecules further enhances the applicability of F4 [14, 19, 22-26]. Moreover, F4 has proved to be an effective tool for purification of protein complexes before bioassays or downstream analysis [27, 28].

One problem often encountered in F4, however, is analyte-membrane interactions which can result in significant sample loss. Accurate quantitation is then hampered, and after-column collection for subsequent analysis becomes difficult. Extensive sample optimization is needed to minimize sample loss in F4 while maintaining adequate size

resolution, by optimizing flow rates and carrier fluid compositions. Typically, DI water with surfactants added is used for separating particles; and salted buffers are employed for protein analysis, to ensure high sample recovery. However, rapid development of nanotechnology makes it more and more frequent to have both nanoparticles (NPs) and proteins simultaneously present in the sample. Some examples include using bioconjugated NPs for specifically recognizing and labeling proteins [29-31]; and studying protein adsorption on NPs for better understanding of nanotoxicity [32-34]. Although F4 is good at handling biocomplexes with minimum disturbance to complex structure, for it to be applied to the aforementioned samples containing the protein-NP complexes, its capability to manage NPs in a protein-friendly environment with negligible sample loss should be evaluated.

Impacts on sample adsorption from the carrier fluid's ionic strength and membrane surface polarity were investigated briefly for bacteria as well as standard polystyrene latex particles with sizes ranging from 0.43 to 8 μm [25, 35, 36]. These previous studies used only up to10 mM KCl or NaCl for the effect of ionic strength, and focused more on the impact from membrane properties [25, 35]. A recent study of using asymmetrical F4 to analyze Ag nanoparticles with sizes around 25-30 nm also provided insights on how both nanoparticle surface charge and membrane zeta-potential would impact on particle adsorption on the membrane[37].

In the present work, we studied membrane adsorption of polystyrene NPs that occurred in F4 when the carrier fluid (CF) contained various types of anion and cation at high concentrations, and compared the adsorption behaviors between NPs and proteins.

We also measured the zeta-potential and hydration size of the NPs in the corresponding CF for better interpretation of our results. Our study aims to find out the carrier fluid compositions that are suitable for studying NPs present in biomolecule-friendly environments.

2. MATERIAL AND METHODS

2.1 Chemicals

The majority of this investigation was carried out on polystyrene NPs (46 ± 2, 102 ± 3, and 199 ± 6 nm) purchased from Thermo Scientific (NIST traceable particle size standards, 3000 series; Waltham, MA, USA). Based on the manufacturer, these polystyrene particles were produced by emulsion polymerization using an anionic surfactant and had surface sulfate groups which arose from the polymerization initiator. They are called "unfunctionalized NPs" in the following text because their surface groups were not specifically added after synthesis. Polybead® carboxylated polystyrene NPs (42.0 ± 6.3 and 85.1 ± 6.5 nm) were obtained from Polysciences, Inc. (Warrington, PA, USA). These particles were functionalized to carry carboxyl groups on the surface, and thus were referred to "the carboxylate NPs" below. Human serum albumin (HSA) and immunoglobulin (IgG) were obtained from Sigma Aldrich (St. Louis, MO, USA) in the form of lyophilized powders.

All chemicals used in this study, such as hydrogen chloride (HCl), sodium hydroxide (NaOH), sodium dihydrogen phosphate (NaH_2PO_4), disodium hydrogen phosphate (Na_2HPO_4), the chloride salts of sodium, potassium, cesium, and magnesium

(NaCl, KCl, CsCl, $MgCl_2$), and the 1 M HEPES stock solution (pH 7.3), were acquired from Fisher Scientific (Pittsburgh, PA, USA). The phosphate buffers were prepared from mixing the mono- and dibasic- phosphates at ratios calculated with the buffer design tool available on http://www.currentprotocols.com/WileyCDA/CurPro3Tool/toolId-3.html, to achieve the desired pH and phosphate concentration. The HEPES buffer was diluted from stock to reach the desired 10 mM concentration. Salts were added to 10 mM phosphate or HEPES at corresponding concentrations to prepare solutions with different ionic strengths.

2.2 F4 conditions

The F1000 series from Postnova Analytics (Salt Lake City, UT, USA) was used in our study. In this symmetrical F4 system, the cross-flow is delivered to the channel by a separate pump than the channel flow. The cross-flow enters from the center of the top channel wall, goes across the channel, passes through the membrane, and finally exits via the bottom channel block. This flow mode is called the open mode in F1000. The F1000 can also run in a recirculating mode, in which the cross flow runs in a closed circle without going to the outlet. Recirculating mode is recommended for separation, as it has a more consistent backpressure and channel flow rate. In F1000, sample injection is done in a stop-flow manner (or called equilibrium or relaxation in other places) which allows each sample component to form a steady state zone near the accumulation wall. During the stop-flow mode, the cross-flow continues but the channel stream is bypassing the

column. Without the channel flow to carry it further into the channel and being stopped by the cross-flow stream, the sample settles down toward the accumulation wall.

A 254 μm spacer was used to generate the channel thickness, and a 30 kDa MWCO regenerated cellulose (RC) membrane served as the accumulation wall. A UV detector, set at 280 nm, was used as the primary means of detection. Membranes were replaced at least every 14 days or as needed. CFs were prepared daily and filtered with 0.2 μm filters before usage. The CF composition used for each individual study and the corresponding flow rates were listed in Table 1. All CFs contained 0.025% Fl-70. The flow rates used were optimized using the CF of 10 mM phosphate at pH 7.4 to deliver the best resolution of all three unfunctionalized polystyrene NPs, or a symmetrical peak of HSA within a reasonable time. Each CF was allowed to equilibrate in the system for 1 h at the separation flow rates in the open mode before sample injection. Separation was performed in the recirculating mode to maintain stable flow conditions. Instrument control, data acquisition, and initial data analysis were carried out with software provided by Postnova. The fractograms and analysis plots were prepared by OriginPro 8.0 (OriginLab Corporation, Northampton, MA, USA).

Samples were injected with a fixed volume of 20 μL. The NPs were diluted to either 0.25 % (for the 42-nm carboxylate and the 46-nm unfunctionalized NPs) or 0.125% (for the larger sizes) (w/v) in Milli-Q water (resistivity18.2 MΩ.cm, Billerica, MA, USA). Proteins were prepared at 5 mg/mL freshly on a daily basis in water and kept at 4 ºC between injections.

Table 2.01. List of F4 running conditions used in this study.

Effect/phenomenon being investigated		**Carrier fluid**	**Flow rates (channel, cross)**
Unfunctionalized Polystyrene nanoparticles, diameter of 46-, 102-, 199-nm	Sample adsorption assessment within the same day or on consecutive days	10 mM phosphate with 0.025% FL70, pH 7.4	2.75 , 0.75 $mL \cdot min^{-1}$
	Increasing ionic strength in solutions with different anions	10, 20, and 50 mM phosphate with 0.0025% FL-70, pH 7.4	
		10 mM HEPES with 25, 50, and 100 mM NaCl, 0.0025% FL-70, pH 7.3	
	Increasing ionic strength in solutions with different cations	1, 5, 10, 25 mM NaCl, KCl, CsCl in 10 mM phosphate, 0.0025% FL-70, pH 7.4	
		1, 5, 10 mM $MgCl_2$ in 10 mM phosphate, 0.0025% FL-70, pH 7.4	
Comparison of 102-nm unfunctionalized polystyrene and 85-nm Carboxylate NP		10 mM HEPES with 5, 25, 50, 100, 150 mM NaCl, 0.0025% FL-70, pH 7.3	
Brief study on proteins			
HSA and IgG	Ionic strength	10 mM phosphate with 0.025% FL-70, with 0, 50, 100, 150 mM NaCl, pH 7.4	0.75 and 3 $mL \cdot min^{-1}$

2.2 Zeta potential and hydration size measurements

Zeta potential and hydration size measurements were taken with a Brookhaven Zetaplus system (Holtsville, NY, USA). All particles were diluted to 0.25% (w/v) in the corresponding buffer before the measurement. Each measurement was the mean value of 50 cycles.

2.3 Circular Dichroism spectroscopy of IgG and HSA

All circular dichroism(CD) measurements were taken on a Jasco J-815 CD instrument, using a quartz cuvette with a 1-mm path-length. IgG and HSA were prepared in the buffers of interest with a final protein concentration of 0.5 mg/mL. CD spectra were collected from 190 to 260 nm, with a step of 1 nm and a scan rate of 100 nm/min. Only data points from 200-260 nm were retained due to buffer interference at lower wavelengths. The spectra were plotted and analyzed using Origin.

3. CALCULATION OF RELATIVE RECOVERY

We tested diverse types of CF, most of which had high ionic strength and caused sample adsorption onto the channel membrane. As a result, membrane performance deteriorated rapidly. The retention time for the same type of NPs was elongated and very poor particle recovery was observed, if the fractograms of the three unfunctionalized NPs in 10 mM phosphate (pH 7.4) obtained over a period of 6 days were compared (Figure 2.01a and 2.01b). The peak area decreased about 15% on day 6, compared to day 1, for the 46- and 102-nm NPs, and more than 60% for the 199-nm NPs. However, no

significant peak area reduction for all sizes was observed within one day, if repeated injections were performed over a 10-hour period in the same CF (Figure 2.01c and 2.01d). To take into account of the day-to-day deterioration of the membrane when comparing sample recovery in different CFs tested on different days, the first run of the day was done in 10 mM phosphate at pH 7.4, and the relative recovery (RR) of NPs in various CFs examined on that day was calculated using the following equation:

$$RR = (A/A^*) \times 100\% \quad (1)$$

in which A was the peak area of the NP in the investigated CF and A* was peak area from the first CF of the day, which was always 10 mM phosphate, pH 7.4. The peak areas were the average of two consecutive runs.

4. RESULTS

4.1.1 pH effect

Since biological samples could be stable at a pH varied slightly from the physiological pH of 7.4, we first tested sample adsorption in CFs with pH of 6.2, 7.4, and 8.2, while keeping the total phosphate ion concentration to be 10 mM. The NPs were well separated under these pH values, with almost identical peak areas except for pH 6.2

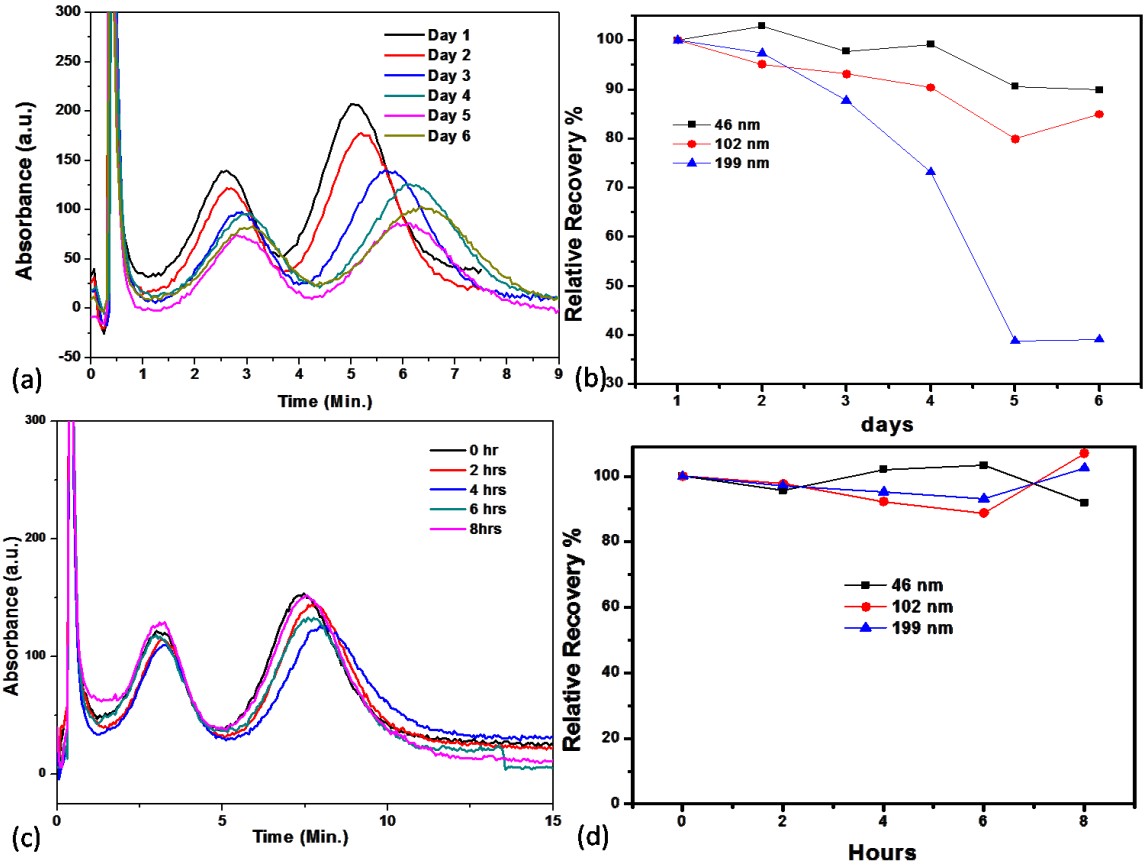

Figure 2.01. (a) Separation profile tracked over 6 consecutive days to show the change of the membrane condition due to sample adsorption. (b) Percent recovery over 6 consecutive days to show the decrease of the 199 nm nanoparticle recovery indicating the membrane deterioration. (c) Separation profile tracked over 8 consecutive hours to show minimal change in membrane condition. (d) Percent recovery over 8 consecutive hours to show that under the same CS the nanoparticles maintain their recovery, indicating any change of recovery may be attributed to changes in the CS.

(Figure 3.02a), in which the peak area of the 199 nm NPs dropped by half (Figure 2.02b). The 199 nm NPs still carried a large negative zeta-potential of -61.65±0.97 mV in this slightly acidic buffer, and neither the zeta-potential or the particle hydration size of the unfunctionalized NPs changed significantly within the small pH range we investigated (Figure 2.02c).

4.1.2 Increasing anion concentration in carrier fluid

The effect of CF ionic strength on membrane adsorption was then investigated. A series of phosphate buffers were prepared to contain a total phosphate concentration of 10, 20, and 50 mM at pH 7.4. Similar to the phenomenon observed above, the 199 nm NPs were influenced most significantly. Its relative recovery (RR) dropped below 30% with 20 mM phosphate and the peak completely disappeared with 50 mM phosphate (Figure 2.03a and 2.03b). The absolute value of the negative zeta-potential of the 199-nm NPs decreased almost linearly with increase of phosphate concentration, but had no significant change in hydration size (Figure 2.03c).

We also compared the impact from the type of anions, i.e. $H_2PO_4^-$ -HPO_4^{2-} and Cl^-, with increasing ionic strength in CF. NaCl was added to the 10 mM HEPES buffer (pH 7.3) at concentrations of 25, 50, and 100 mM NaCl. HEPES is a zwitterionic organic buffering agent, and 10 mM HEPES only contributed to an ionic strength of 0.003 M, and the dominant anion in these solutions was Cl^-. Since it is not meaningful to compare RR if no peak could be seen, this step of investigation was focused on the 102-nm NPs. The relative recovery, RR, of the 102-nm NPs in the corresponding CF, was plotted against

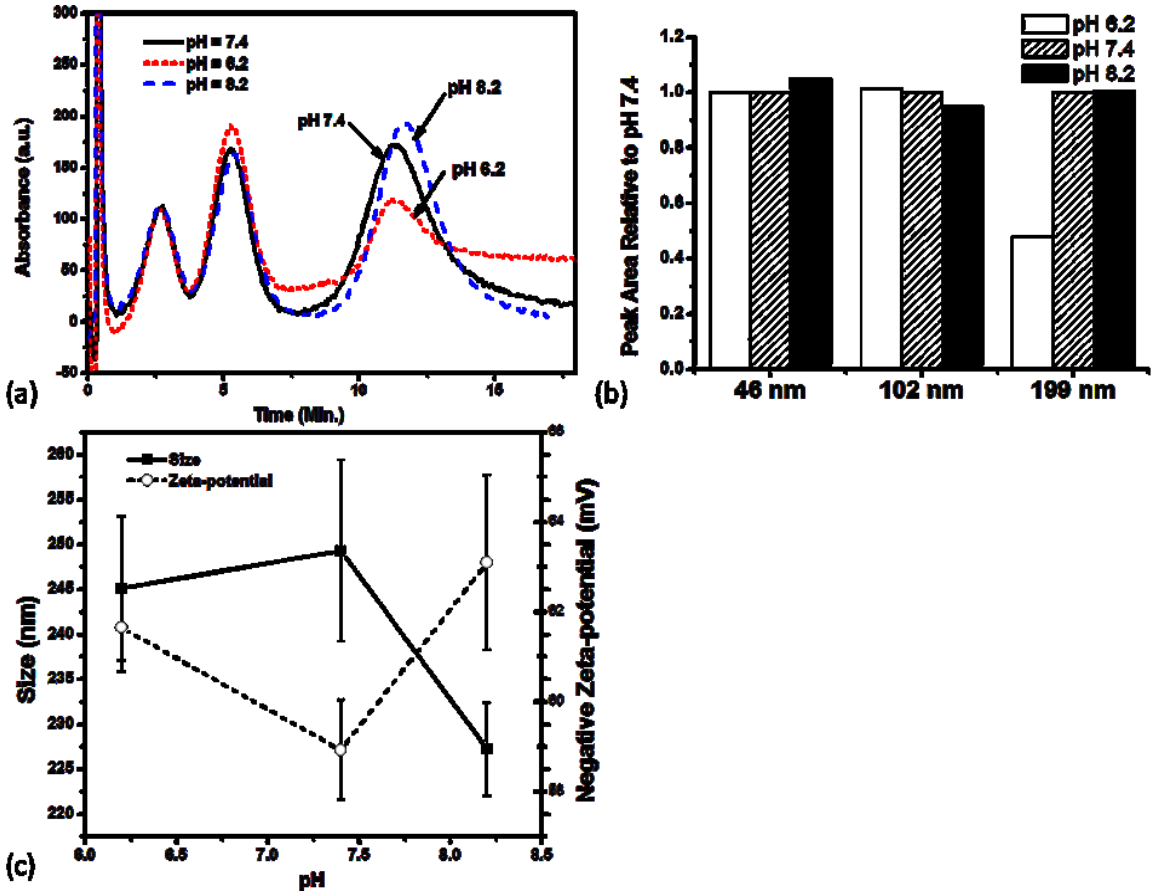

Figure 2.02. (a) Fractograms, (b) the area of particles relative to pH 7.4 area on the three unmodified NPs and (c) the zeta-potential and hydration size plot of the 199 nm unfunctionalized NP in CFs with different pH of 6.2, 7.4, and 8.2.

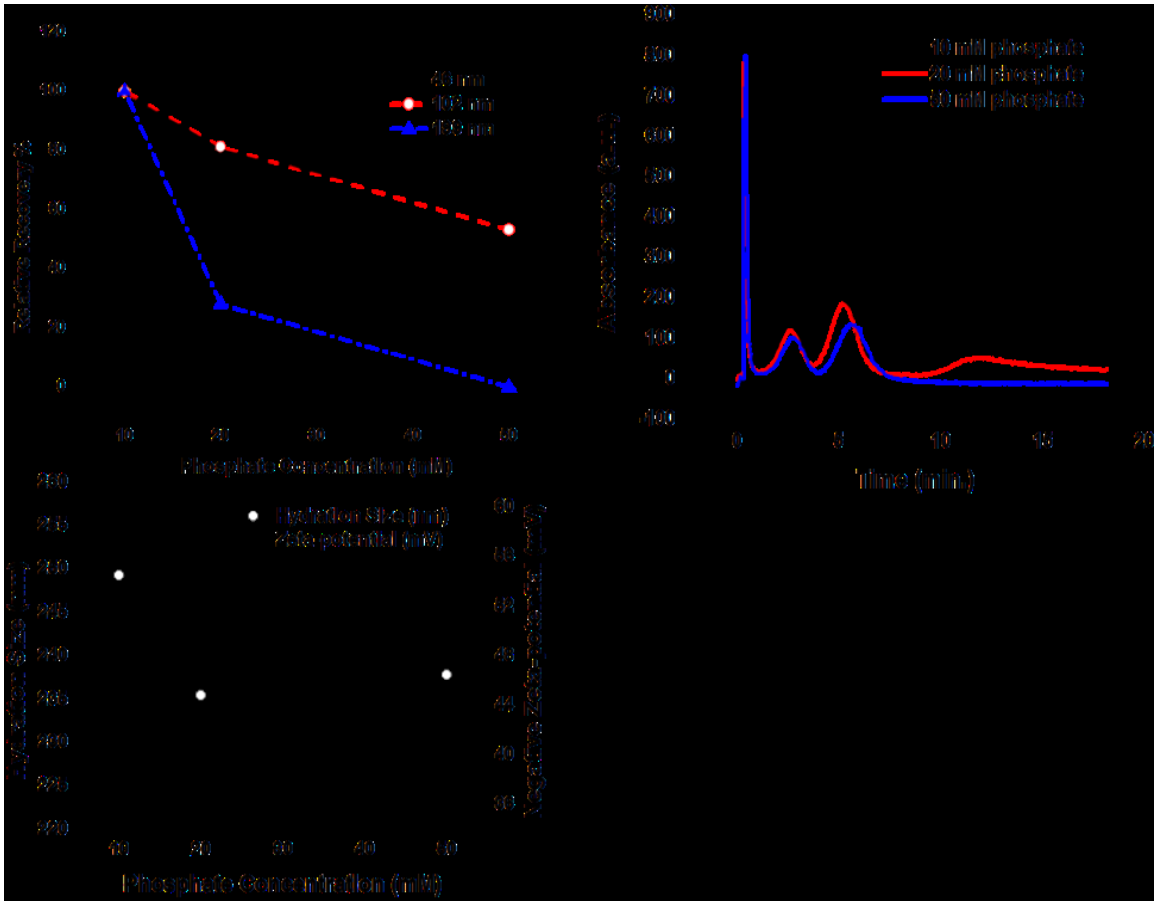

Figure 2.03. (a) Relative recovery, (b) separation profile of three unmodified NPs with increasing phosphate concentration and (c) zeta potential plot of the 199-nm unfunctionalized NP with increasing phosphate concentration in CF.

the ionic strength, I, of the phosphate or HEPES-NaCl CFs. It was discovered that, with a comparable I, Cl^- seemed to induce bigger decrease in RR compared to the $H_2PO_4^-$ - HPO_4^{2-} system (Figure 3.04a). With 50 mM phosphate (I = 0.115 M), the RR was around 53.2%, but the RR in HEPES-100 mM NaCl (I = 0.103 M) was only 25.7%. This was consistent with the zeta-potential relationship of the NPs in these two series CFs: the NP zeta-potential was more negative in phosphate buffers than in HEPES-NaCl buffers (Figure 2.04b). The hydration size change had no obvious trend with small increments of around 4-8 nm, compared to the actual size of the NPs, following variation in ionic strength or anion types (Figure 2.04c).

4.1.3 Cation type

Subsequently, impact on particle RR from the type of counter ions in CF was studied. Sodium, potassium, cesium, and magnesium chlorides were added to the base solution of 10 mM sodium hydrogen- and dihydrogen-phosphate at pH 7.4, the function of which was to maintain pH stability. The fractograms were shown in Figure 2.05a-d. Among the three monovalent alkali metals, no obvious change in peak area for the two smaller particles was observed with increasing cation concentrations in CF. The RR plot vs. salt concentration for the 102-nm NP can be found in Figure 2.06a. However, consistent RR reduction for the 199-nm NPs was seen (Figure 2.06b); and RR was lower with cations having higher atomic numbers, i.e. in the order of $Cs^+ < K^+ < Na^+$: RR of the 199-nm NPs was 90% in CF with Na^+, dropped to 60% with K^+ and 50% with Cs^+. Figure 2.06c compared the absolute value of the negative zeta-

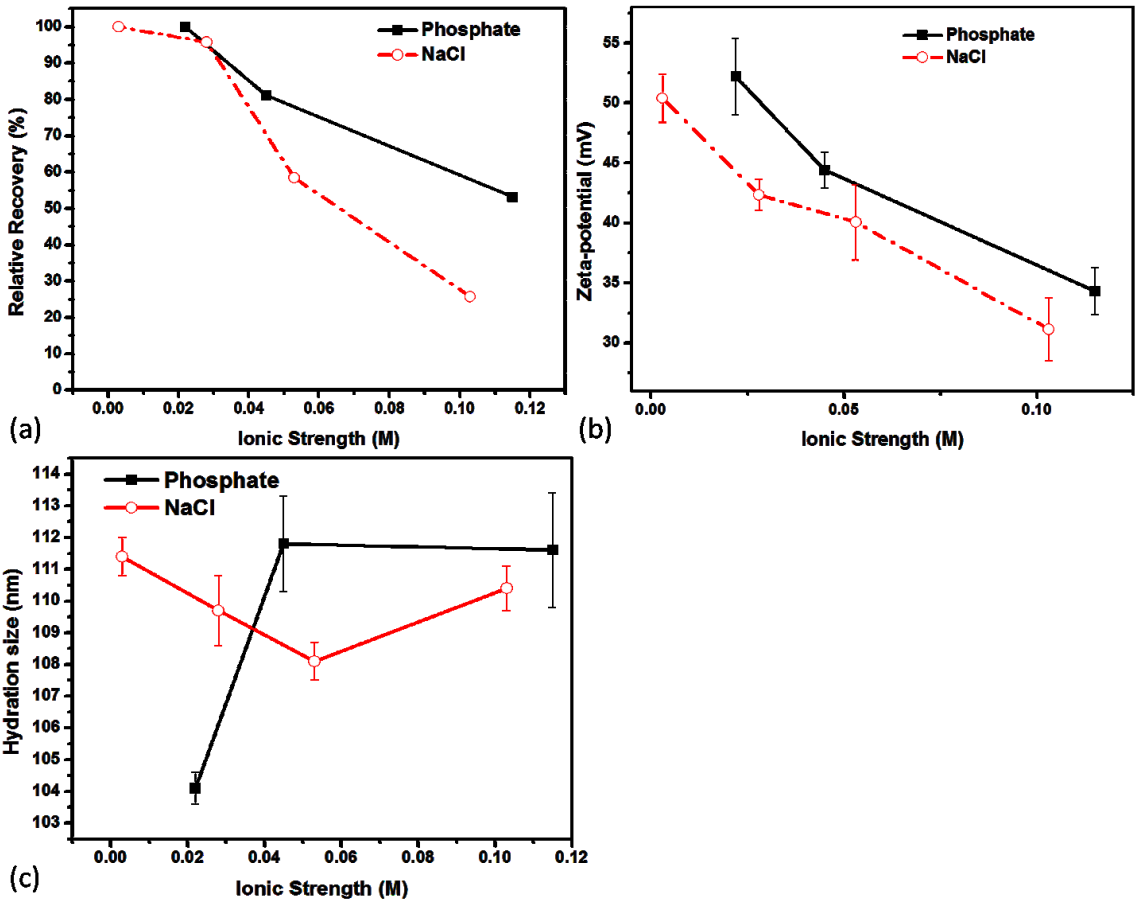

Figure 2.04. (a) Relative recovery, (b) Zeta potential plot, (c) and Hydration size of the 102-nm unfunctionalized NP with increasing phosphate or chloride concentration in CF.

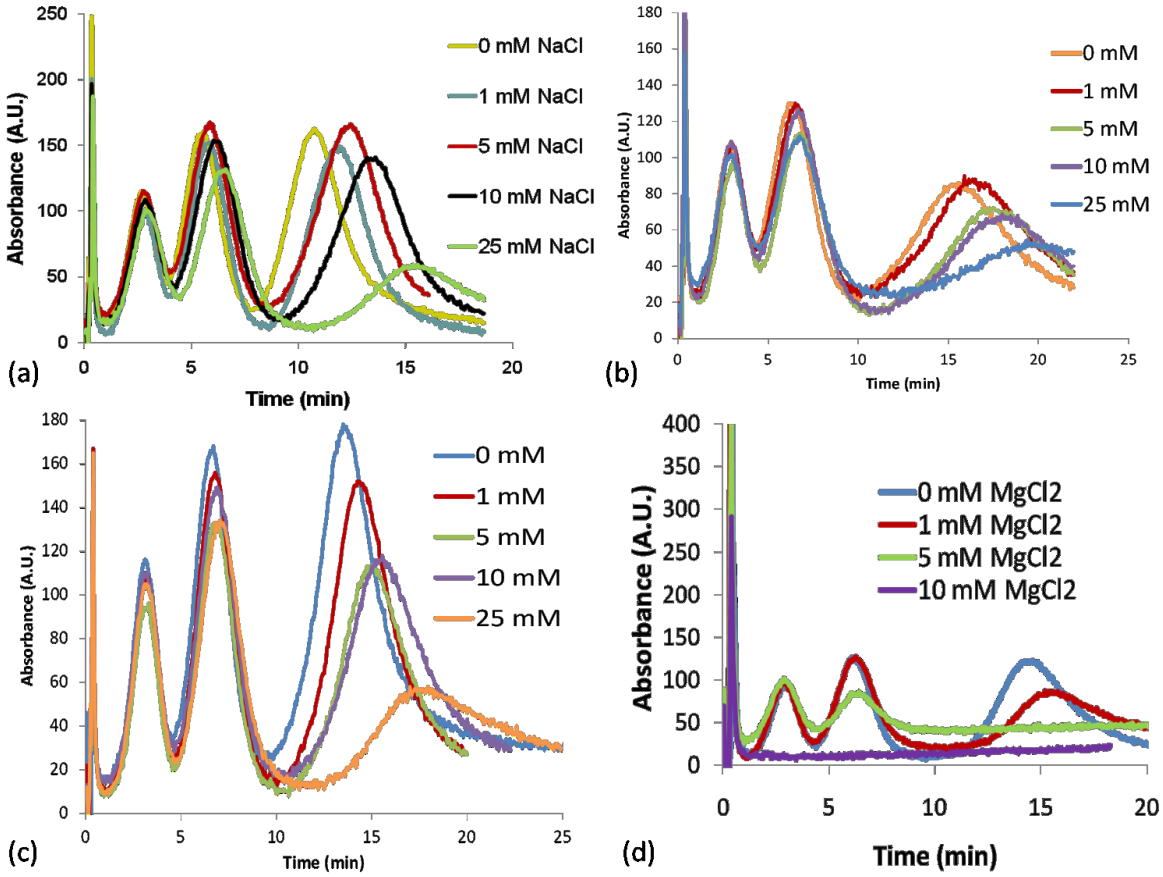

Figure 2.05 Separation profile of three unmodified NPs with increasing (a) NaCl (b) KCl (c) CsCl and (d) $MgCl_2$ concentrations in 10 mM sodium phosphate buffer, pH 7.4.

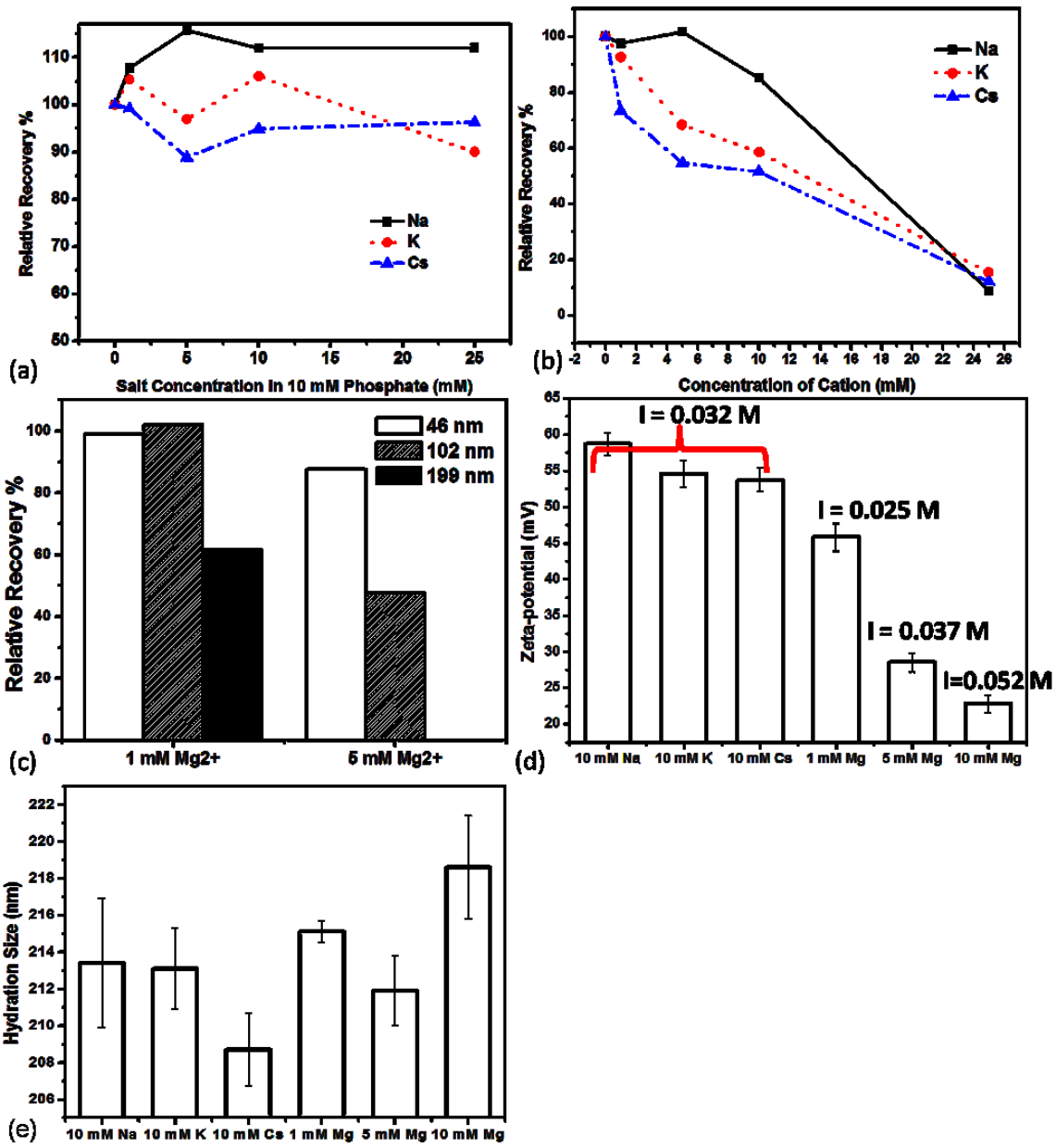

Figure 2.06. (a) RR of the 102-nm and (b) 199-nm unfunctionalized NPs vs. the alkali salt concentration in 10 mM phosphate CF. (c) RR of three unfunctionalized NPs in 10 mM phosphate with 1 or 5 mM $MgCl_2$ added. (d) Zeta potential of the 199-nm unfunctionalized NP in 10 mM sodium phosphate buffer, pH 7.4, with 10 mM Na^+, K^+, and Cs^+, or with 1, 5, and 10 mM Mg^{2+}. (e) Hydration size of the 203 nm unmodified NP in 10 mM sodium phosphate buffer, pH 7.4, with either 10 mM monovalent cation (Na, K, Cs) or $MgCl_2$ at different concentrations (1, 5, and 10 mM).

potential of the NPs in 10 mM alkali salt solutions, but little difference, < 5 mV, was detected among Na^+, K^+, and Cs^+, even though the zeta-potential was more negative in Na^+ than in K^+ and Cs^+ (Figure 2.06d). Hydration size change was also not large, with that in the Cs^+ solution about 4-nm smaller than in the Na^+ and K^+ solutions (Figure 2.06e).

Particle adsorption was more severe in CF containing Mg^{2+}. When the Mg^{2+} concentration increased from 1 to 5 mM, more than 50% peak area reduction was observed for the 102-nm NPs, and no particles could be eluted out of the column with 10 mM Mg^{2+} (Figure 2.06d). The divalent Mg^{2+} led to a much lower zeta-potential on the NPs even at a comparable ionic strength to the monovalent cations (Figure 2.06d), but did not significantly influence the particle hydration size (Figure 2.06e).

4.2 Comparison of unfunctionalized and carboxylated nanoparticles

As mentioned in the experiment section, the unfunctionalized polystyrene NPs carried sulfate groups on the surface which was originated from the polymerization initiator. The sulfate groups gave sufficient surface potential for the particles to be stably suspended in aqueous solutions. We also tested the NPs specially functionalized with carboxyl groups to incorporate surface groups for bioconjugation in our study, and compared their adsorption behavior with the unfunctionalized NPs having a comparable size in the salted carrier fluids of F4. Membrane adsorption of the carboxylate 85-nm NPs was much less than the unfunctionalized NPs in CFs with high ionic strength (Figure

2.07a). Larger than 90% RR was obtained for the carboxylate NPs, in CFs with 5 to 150 mM NaCl; while the RR of the unfunctionalized NPs dropped rapidly to 26% with only 100 mM NaCl. The CFs in this step of study were prepared by adding NaCl to 10 mM HEPES, and the main anion in the solution was Cl^-. Correspondingly, the zeta-potential of the unfunctionalized NPs decreased much faster than that on the carboxylate NPs when the ionic strength increased (Figure 3.07b), with little change observed in hydration size (Figure 2.07c).

4.3 Proteins

Unlike the solid spherical NPs, proteins have more flexible structures and contain both hydrophobic and hydrophilic residues, the display of which on the protein surface depends on the environment. In addition, proteins have high diffusion coefficients compared to NPs, and higher cross flow rates than in NP separation are often used to improve resolution. Therefore, adsorption of protein on the channel membrane in F4 could be different than that of the solid particles. Previous attempts of separating proteins by F4 typically used I close to 0.1 M [38-41] to match the physiological condition. In this study, salt effects on protein adsorption was investigated, using two representative proteins: human serum albumin (HSA, Mw 65 kDa, pI 4.7) and human immunoglobulin G (IgG, Mw 150 kDa, pI 5.5~9.1). They are considered to be "soft" proteins with low structural stability, and are generally found to adsorb on a variety of surfaces regardless of surface hydrophobicity [42, 43]. Ionic strength was controlled by adding NaCl to 10 mM phosphate, in which the zeta-potentials of both proteins were

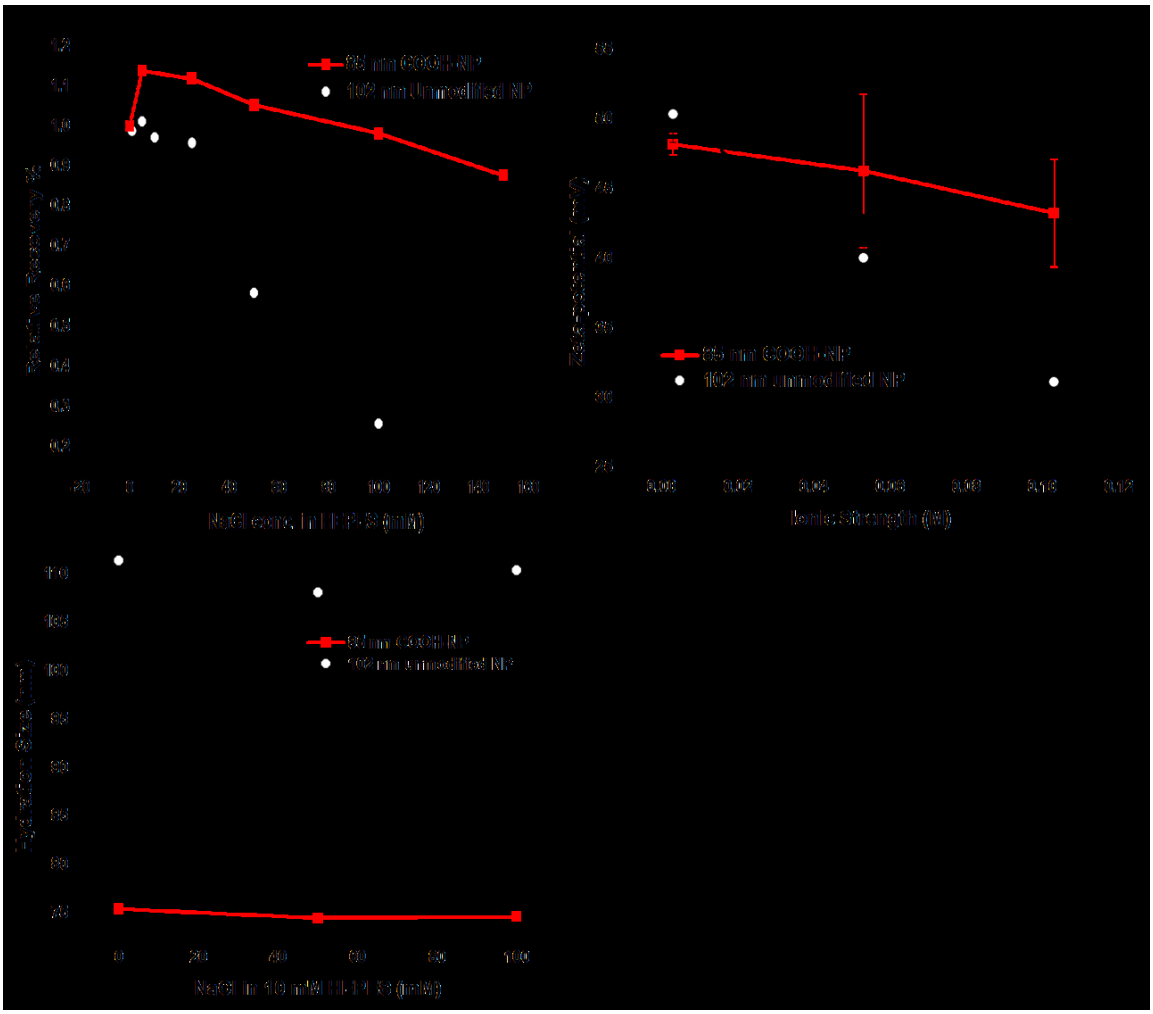

Figure 2.07 (a) RR (b) zeta-potential and (c) hydration size of the 85-nm carboxylate NPs and the 102-nm unfunctionalized NPs in CFs with increasing ionic strength obtained by adding NaCl to 10 mM HEPES (pH 7.3).

measured to be around - 40 mV. Though both carried negative surface charges, HSA and IgG behaved differently in salted CFs. The shape and area of the HSA peak were not affected by either the salt content or the pH (6.2, 7.4, and 8.2) in CF (Figure 2.08a and b). In contrast, IgG was strongly adsorbed onto the membrane without NaCl in CF, but the peak resumed with 50 mM NaCl, and stabilized at above 100 mM NaCl (Figure 2.09). This completely opposite adsorption trend to that of the NPs points out that the cause of protein adsorption on the accumulation wall could be different from that of the NPs.

5. DISCUSSIONS

5.1 Particle adsorption

Particle adsorption on the accumulation wall in F4 is governed by particle-wall interaction that is balanced by two forces: the attractive van der Waals force and the electrostatic repulsion between particles or between particle and membrane surface [9, 44-46]. If the repulsive force dominates, an energy barrier is to be overcome for particles to adsorb, which will give out high sample recovery at the end of the column. Accordingly, if the attractive force is stronger, particle aggregation and surface adsorption would be significant. The attractive van der Waals force, F_{vdW}, is proportional to $R^3/l^2(2R+l)^2$, R being particle radius and l representing the surface-surface distance between particle and membrane[37, 47, 48]. Since the regenerated cellulose (RC) membrane has a pKa ~ 3.5 owing to ionization of its carboxyl groups [49], the negatively charged NPs were repelled from the membrane surface via a repulsion force, $F_{el.}$ This force can be calculated from the following equation:

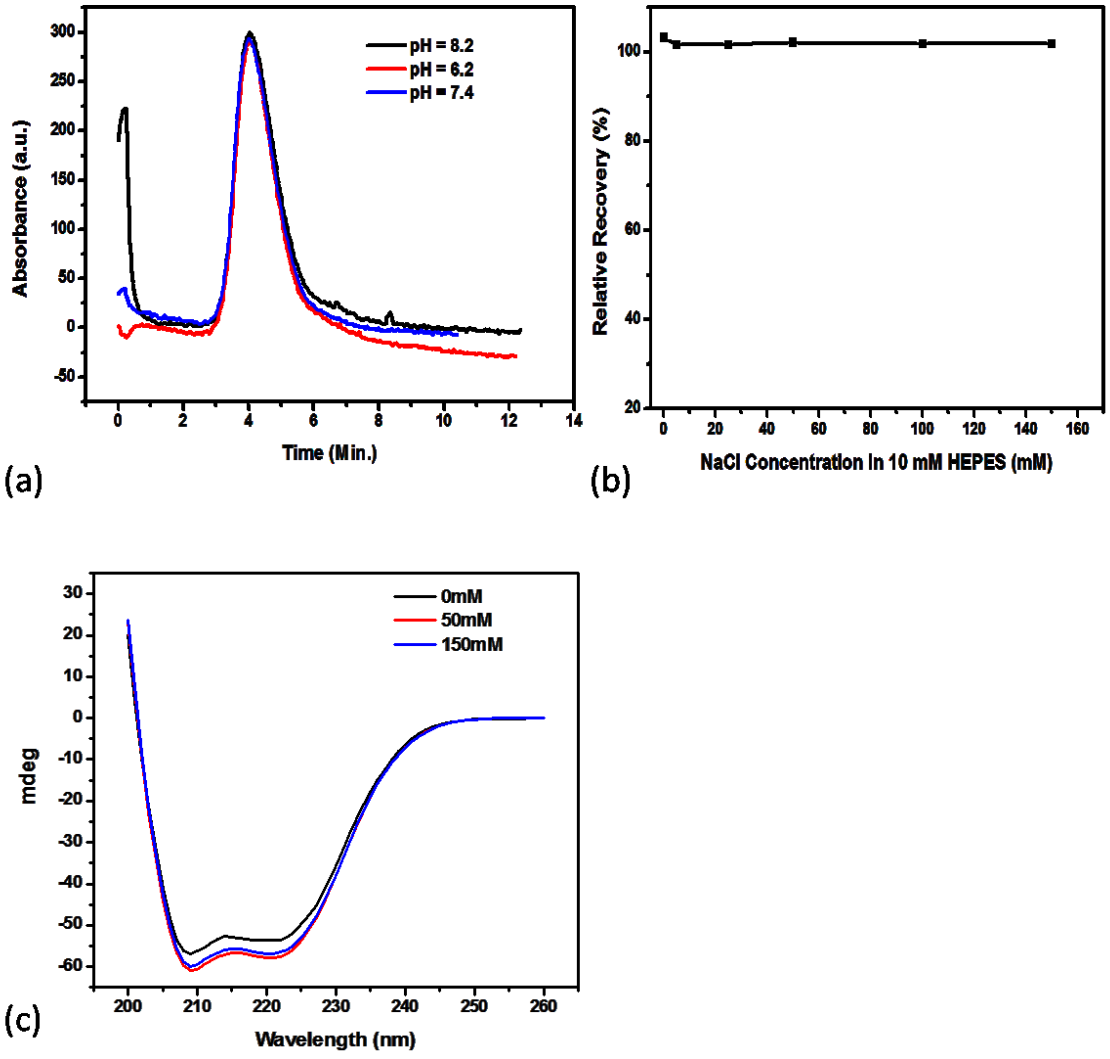

Figure 2.08. (a) HSA (5 mgmL^{-1}) profile under different pH conditions in phosphate buffered solution. (b) HSA (5 mgmL^{-1}) recovery with increasing NaCl concentration in 10 mM HEPES, pH 7.3. (c) CD spectra of HSA in 10 mM phosphate with 0, 50, and 150 mM NaCl.

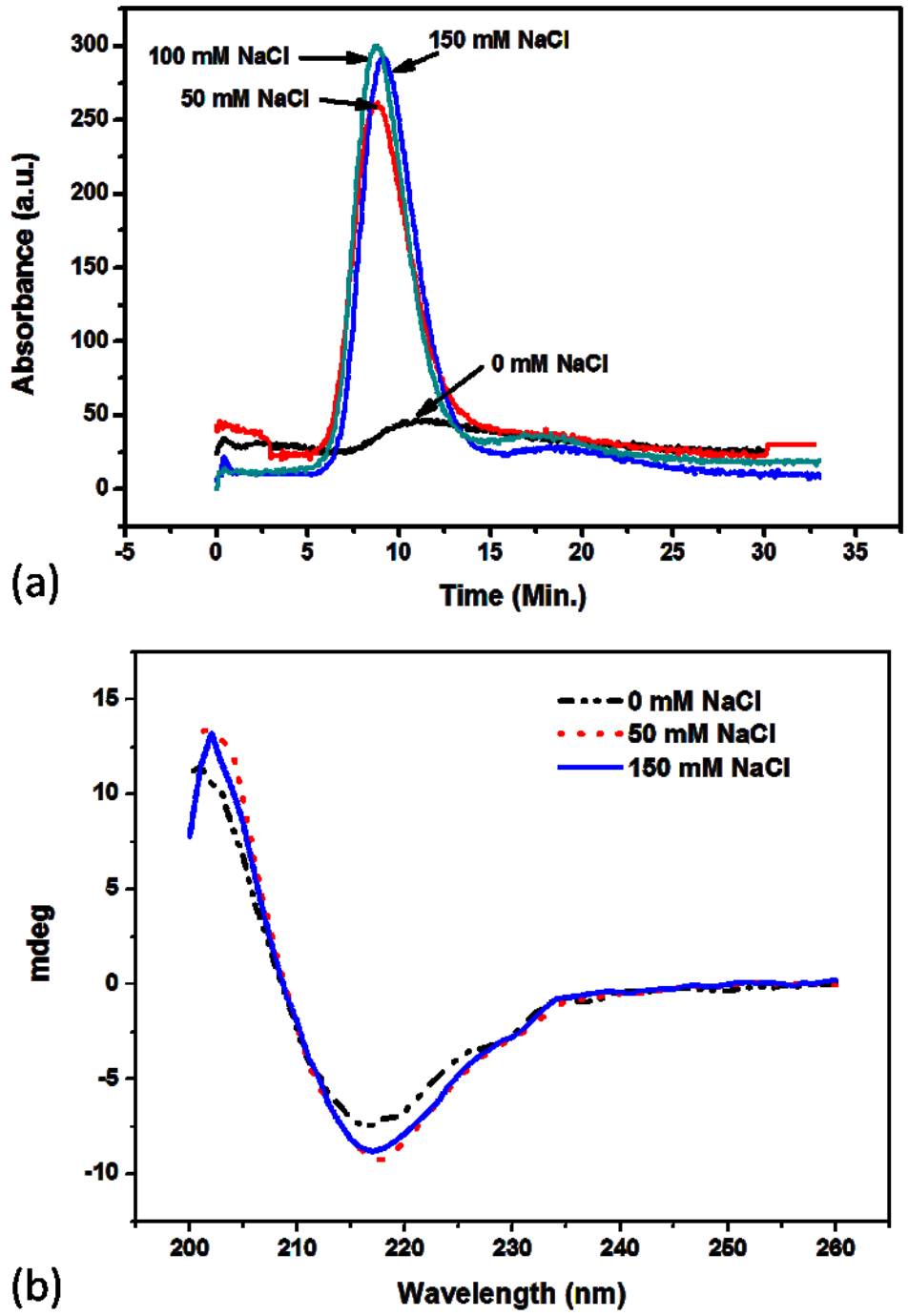

Figure 2.09. (a) Fractograms and (b) CD spectra of IgG in CF containing10 mM sodium phosphate plus 0, 50, or 150 mM NaCl.

$$F_{el} = 16\pi kRT\rho\delta\, e^{l/\delta} \tanh(z_i e\zeta_1/4kT) \tanh(z_i e\zeta_2/4kT) \quad (2)$$

in which k is the Boltzmann constant, R and l are the same as in F_{vdW}, and T is the temperature, ρ is density of the media, δ is the thickness of the double-layer, ζ is the zeta-potential of the substance[37, 47]. The repulsion force is also dependent on the membrane property. Any change in CF should induce change on the membrane, the contribution of which cannot be ignored. Unfortunately, we do not have access to instruments that can measure membrane zeta-potential and could not evaluate this side of the adsorption theory. Therefore, our discussion was focused on changes on NPs caused by variations in CF composition.

Most of the adsorption observed in our study for the unfunctionalized NPs can be explained by the above theory. With increasing ionic strength, the absolute value of the zeta-potential of the particles dropped rapidly (Figure 2.04b). The high ionic strength also led to smaller double-layer thickness, δ. Both reductions could lower F_{el}, and more adsorption was thus observed. The largest particles were in general more affected than the smaller ones by variation in pH and ionic strength (Figures 2.02a, 2.03a, and 2.06a & b). This is mainly because of their close location to the membrane surface, i.e. smaller particle-membrane distance, l; and large particle radius, R. Thus, they were subjected to a higher attractive van de Waals force, F_{vdW}, than the 46- and 102-nm NPs; and their interaction with the membrane was more sensitive to change in F_{el} (Equation 2) even when the variation in particle zeta-potential was small. For example, in the case of CFs with different pH, significant peak reduction for the 199-nm NPs was observed at pH 6.2 with small difference detected in particle zeta-potential (Figures 2.02a and c). Based on

the work conducted by A. Ulrich *et al*., the zeta-potential of the RC 30kDa membrane would change from -20 mV to -15 mV when pH dropped from 8 to 6 [37]. Therefore, small reduction in F_{el} could have occurred due to such change in the membrane zeta-potential, leading to significant adsorption of the largest particles.

The effect from counter ion valency and size largely exerts by changing the zeta-potential and by affecting the thickness of the diffuse double layer[50]. In our study, no significant variation in NP zeta-potential was detected for the three alkali ions, but higher RR was observed with Na^+, compared to K^+ and Cs^+. This could be attributed to the hydrated radius of the alkali ions that decreases in the order of $Na^+ > K^+ > Cs^+$. The more hydrated cation results in a larger stern layer thickness, the first layer of the double-layer that lies on the surface and is dictated by the size of the counter ion. This enlarged F_{el}, as well as the distance between particle and membrane, which decreased the attractive van der Waals force. The sum effect was then a higher RR in Na^+ than the other two alkali cations. Mg^{2+} has higher valency, yielding more compression to the diffuse double-layer. Additionally, higher reduction in zeta potential with higher valency ions was reported as compared to lower valency ions [50], matching with our zeta-potential measurement results. Hence, lower RR was found with Mg^{2+} in the CF compared to the monovalent alkali cations.

Besides electrostatic repulsion and van der Waals attraction, comparison of effects from phosphate and Cl^- (Figure 2.04), or between NPs with sulfate and carboxylate surface groups (Figure 2.07), suggests that Donnan exclusion may take place and contribute to NPs adsorption. The polystyrene NPs had a porous structure, and could

retain certain amounts of solution, called the occluded liquid phase. When the phosphate and chloride anions are in the solution, they would be repelled from the particle surface by the negatively charged sulfate groups, in accordance with the Donnan exclusion effect. The Cl^- ions were permanently charged, and not retained by the NPs. However, the phosphate anions were weakly ionized, and could penetrate the charged layer in their molecular forms and be retained inside the polystyrene particles. The retained phosphate ions provided a larger ion pool to counter-balance the higher concentration of the counter ions in the solution at higher salt concentration and resulted in a smaller drop in the zeta-potential of the NP surface, leading to better particle recovery in the phosphate buffer at high ionic strength (Figure 2.04). Similarly, the carboxylate NPs yielded higher recovery than the unfunctionalized NPs with sulfate groups on the surface in CF with high NaCl concentration (Figure 2.07). The sulfate groups were permanently charged; but the carboxylate groups were rapidly exchanging between the molecular and ionic forms. While the carboxyl groups were in the neutral, molecular form, the Cl^- was able to penetrate the carboxylate layer and become trapped inside the porous polystyrene NPs. In contrast, total ion exclusion occurred on the sulfate-decorating surface, and very little Cl^- could be retained.

5.2 Protein adsorption

Proteins have much smaller sizes, i.e. R, than the ≥50 nm NPs, and thus experience smaller attractive van der Waals force. The negative zeta-potential of HSA and IgG also supported that they should be electrostatically repelled from the RC membrane.

However, protein adsorption on surface is highly complicated, and have been concluded in previous studies to rely on the three-dimensional protein structure and structure stability, and be governed more by hydrophobic interaction than electrostatic forces [43, 51, 52]. Different structure conformation in buffers with varied salt concentrations could be accounted for the adsorption behaviors of IgG in CFs with or without salt. We analyzed the secondary structure of IgG under the different buffer conditions used in this study by Circular Dichoism (CD) spectroscopy (Figure 2.09b). IgG has primarily antiparallel β-pleated sheets (β-helices), characterized by negative bands at 218 nm [53]. With 50- or 150-mM salt, this peak was clearly observable. There was no significant difference between the CD spectra of IgG in 50 and 150 mM sodium chloride, which was in agreement with what was seen in the F4 fractograms. However, it was reduced about 24% when there was no salt present. The CD spectra of HSA in the same solutions (Figure 2.08c) showed the typical, negative signals at distinct wavelengths of 208 and 222 nm for α-helical proteins[53]. A small, ~7% signal reduction at both wavelengths with no salt indicated slight decrease in the α-helical content. Additionally, the normalized (against signal at 207 nm) signal at 211 nm, a wavelength commonly used in calculation of both helix and sheet structure in CD spectrum analysis[54], increased with the increasing salt concentration for IgG, while it remained constant for HSA (Figure 2.08d). This result is indicative of the secondary structure changing from the more organized beta-sheet to a more random distribution. The structural change implies that, without salt, IgG lost some of its rigidity, making it easier to adapt to the membrane surface via hydrophobic interaction, and thus more susceptible to adsorption onto the F4 membrane.

In contrast, HSA structure experienced smaller change in CFs with salt or without salt, and the repulsion between HSA and RC could have contributed to the high recovery of HSA in F4.

6. CONCLUSIONS

In this study, adsorption of the unfunctionalized NPs onto the channel membrane in F4 with different types of CFs was investigated. Maintaining high electrostatic repulsion is the key to obtain high sample recovery when using F4 to separate NPs in buffers with high ionic strength. Owing to the Donnan exclusion effect, another possible way to improve recovery of porous particles at high ionic strength is by using the weakly dissociated anions, or by using particles having weak anion as the surface functional groups. Since the Donnan exclusion effect is related to the retention volume of liquid inside the NP structure, we could confirm the contribution of Donnan exclusion to NP adsorption by comparing the adsorption behaviors of NPs with different crosslinking degrees in future studies. NPs with higher crosslinking degrees have higher occluded liquid phase inside, and should be more resistant to adsorption in CF with high ionic strength induced by weakly ionized anions.

While electrostatic or hydrophobic interaction with membrane still plays an important role to protein adsorption on the membrane, our brief study on two selective proteins supported that protein conformation should also be taken into account. Previous knowledge on protein adsorption behavior on surface could guide the effort of

minimizing protein adsorptions in F4. A more systematic investigation of a series of proteins with different structure stability is needed to test our hypothesis.

From the results of this study, we propose that selection of F4conditions when analyzing NPs carrying proteins on the surface needs to consider protein-membrane interaction more, since protein determines the surface property and thus the electrostatic or hydrophobic interaction with the membrane. Additionally, the size of particle is an important factor to be considered because it affects how close the particles are to the membrane and how strong the attractive van der Waals force is. This concept has been guiding us in our on-going study of NP-protein interaction and investigation of the bioconjugated NPs.

ACKNOLOWDGEMENT

All CD data was obtained by Jonathan Ashby. Min Kwon worked on solution preparation.

REFERENCES

1. Schachermeyer, S.; Ashby, J.; Kwon, M.; Zhong, W., Impact of carrier fluid composition on recovery of nanoparticles and proteins in flow field flow fractionation. *J. Chromatogr. A* **2012,** 1264, 72-79.

2. Gimbert, L. J.; Andrew, K. N.; Haygarth, P. M.; Worsfold, P. J., Environmental applications of flow field-flow fractionation (FIFFF). *TrAC, Trends Anal. Chem.* **2003,** 22, (9), 615-633.

3. Kammer, F. v. d.; Legros, S.; Hofmann, T.; Larsen, E. H.; Loeschner, K., Separation and characterization of nanoparticles in complex food and environmental samples by field-flow fractionation. *Trends Anal. Chem.* **2011,** 30, (3), 425-436.

4. Bolea, E.; Laborda, F.; Castillo, J. R., Metal associations to microparticles, nanocolloids and macromolecules in compost leachates: Size characterization by asymmetrical flow field-flow fractionation coupled to ICP-MS. *Anal. Chim. Acta* **2010,** 661, (2), 206-214.

5. Baalousha, M.; Stolpe, B.; Lead, J. R., Flow field-flow fractionation for the analysis and characterization of natural colloids and manufactured nanoparticles in environmental systems: A critical review. *Journal of Chromatography A* 1218, (27), 4078-4103.

6. Benincasa, M.-A.; Caldwell, K. D., Flow field-flow fractionation of poly(ethylene oxide): effect of carrier ionic strength and composition. *Journal of Chromatography A* **2001,** 925, (1-2), 159-169.

7. Messaud, F. A.; Sanderson, R. D.; Runyon, J. R.; Otte, T.; Pasch, H.; Williams, S. K. R., An overview on field-flow fractionation techniques and their applications in the separation and characterization of polymers. *Progress in Polymer Science* **2009,** 34, (4), 351-368.

8. Kim Ratanathanawongs, S.; Shiundu, P. M.; Calvin Giddings, J., Size and compositional studies of core-shell latexes using flow and thermal field-flow fractionation. *Colloids and Surfaces A: Physicochemical and Engineering Aspects* **1995,** 105, (2-3), 243-250.

9. Farmakis, L.; Koliadima, A.; Karaiskakis, G.; Zattoni, A.; Reschiglian, P., Study of the influence of surfactants on the size distribution and mass ratio of wheat starch granules by sedimentation/steric field-flow fractionation. *Food Hydrocolloids* **2008,** 22, (6), 961-972.

10. Wittgren, B.; Wahlund, K.-G., Effects of flow-rates and sample concentration on the molar mass characterisation of modified celluloses using asymmetrical flow field-flow fractionation-multi-angle light scattering. *J. Chromatogr. A* **1997,** 791, (1-2), 135-149.

11. Modig, G.; Nilsson, L.; Bergenståhl, B.; Wahlund, K.-G., Homogenization-induced degradation of hydrophobically modified starch determined by asymmetrical flow field-flow fractionation and multi-angle light scattering. *Food Hydrocolloids* **2006,** 20, (7), 1087-1095.

12. Madörin, M.; van Hoogevest, P.; Hilfiker, R.; Langwost, B.; Kresbach, G. M.; Ehrat, M.; Leuenberger, H., Analysis of Drug/Plasma Protein Interactions by Means of Asymmetrical Flow Field-Flow Fractionation. *Pharmaceutical Research* **1997,** 14, (12), 1706-1712.

13. Reschiglian, P.; Zattoni, A.; Roda, B.; Casolari, S.; Moon, M. H.; Lee, J.; Jung, J.; Rodmalm, K. r.; Cenacchi, G., Bacteria Sorting by Field-Flow Fractionation. Application to Whole-Cell Escherichia coli Vaccine Strains. *Anal. Chem.* **2002,** 74, (19), 4895-4904.

14. Citkowicz, A.; Petry, H.; Harkins, R. N.; Ast, O.; Cashion, L.; Goldmann, C.; Bringmann, P.; Plummer, K.; Larsen, B. R., Characterization of virus-like particle assembly for DNA delivery using asymmetrical flow field-flow fractionation and light scattering. *Analytical Biochemistry* **2008,** 376, (2), 163-172.

15. Arifin, D. R.; Palmer, A. F., Determination of Size Distribution and Encapsulation Efficiency of Liposome-Encapsulated Hemoglobin Blood Substitutes Using Asymmetric Flow Field-Flow Fractionation Coupled with Multi-Angle Static Light Scattering. *Biotechnology Progress* **2003,** 19, (6), 1798-1811.

16. Kratochwil, N. A.; Huber, W.; Müller, F.; Kansy, M.; Gerber, P. R., Predicting plasma protein binding of drugs: a new approach. *Biochemical Pharmacology* **2002,** 64, (9), 1355-1374.

17. Park, I.; Paeng, K.-J.; Yoon, Y.; Song, J.-H.; Moon, M. H., Separation and selective detection of lipoprotein particles of patients with coronary artery disease by frit-inlet asymmetrical flow field-flow fractionation. *Journal of Chromatography B* **2002,** 780, (2), 415-422.

18. Fraunhofer, W.; Winter, G., The use of asymmetrical flow field-flow fractionation in pharmaceutics and biopharmaceutics. *European Journal of Pharmaceutics and Biopharmaceutics* **2004,** 58, (2), 369-383.

19. Jackson, B. P.; Ranville, J. F.; Neal, A. L., Application of flow field flow fractionation-ICPMS for the study of uranium binding in bacterial cell suspensions. *Anal. Chem.* **2005,** 77, (5), 1393-1397.

20. Stolpe, B.; Guo, L.; Shiller, A. M.; Hassellöv, M., Size and composition of colloidal organic matter and trace elements in the Mississippi River, Pearl River and the northern Gulf of Mexico, as characterized by flow field-flow fractionation. *Marine Chem.* **2010,** 118, (3-4), 119-128.

21. Siripinyanond, A.; M. Barnes, R., Flow field-flow fractionation-inductively coupled plasma mass spectrometry and metal speciation in proteins: A feasibility study. *Journal of Analytical Atomic Spectrometry* **1999,** 14, (9), 1527-1531.

22. Nebe-von-Caron, G.; Stephens, P. J.; Hewitt, C. J.; Powell, J. R.; Badley, R. A., Analysis of bacterial function by multi-colour fluorescence flow cytometry and single cell sorting. *Journal of Microbiological Methods* **2000,** 42, (1), 97-114.

23. Augsten, C.; Mäder, K., Characterizing molar mass distributions and molecule structures of different chitosans using asymmetrical flow field-flow fractionation combined with multi-angle light scattering. *International Journal of Pharmaceutics* **2008,** 351, (1-2), 23-30.

24. Rambaldi, D. C.; Reschiglian, P.; Zattoni, A.; Johann, C., Enzymatic determination of cholesterol and triglycerides in serum lipoprotein profiles by asymmetrical flow field-flow fractionation with on-line, dual detection. *Anal. Chim. Acta* **2009,** 654, (1), 64-70.

25. Lim, S.; Lee, S.; Choi, S.; Moon, J.; Hong, S., Evaluation of biofouling potential of microorganism using flow field-flow fractionation (Fl-FFF). *Desalination* **2010,** 264, (3), 236-242.

26. Melucci, D.; Guardigli, M.; Roda, B.; Zattoni, A.; Reschiglian, P.; Roda, A., A new method for immunoassays using field-flow fractionation with on-line, continuous chemiluminescence detection. *Talanta* **2003,** 60, (2-3), 303-312.

27. Li, J.; Zhong, W., A two-dimensional suspension array system by coupling field flow fractionation to flow cytometry. *J. Chromatogr. A* **2008,** 1183, (1-2), 143-149.

28. Li, J.; Ge, J.; Yin, Y.; Zhong, W., Multiplexed Affinity-Based Protein Complex Purification. *Anal. Chem.* **2008,** 80, (18), 7068-7074.

29. Chan, C. P.-y., Ingenious nanoprobes in bioassays. *Bioanalysis* **2009,** 1, (1), 115-133.

30. Song, S.; Qin, Y.; He, Y.; Huang, Q.; Fan, C.; Chen, H.-Y., Functional nanoprobes for ultrasensitive detection of biomolecules. *Chem. Soc. Rev.* **2010,** 39, (11), 4234-4243.

31. JanÄa, J.; Berneron, J.-F. o.; Boutin, R., Micro-thermal field-flow fractionation: new high-performance method for particle size distribution analysis. *Journal of Colloid and Interface Science* **2003,** 260, (2), 317-323.

32. Lynch, I.; Dawson, K. A., Protein-nanoparticle interactions. *Nano Today* **2008,** 3, (1-2), 40-47.

33. Karmali, P. P.; Simberg, D., Interactions of nanoparticles with plasma proteins: Implication on clearance and toxicity of drug delivery systems. *Expert Opin. Drug Delivery* **2011,** 8, (3), 343-357.

34. Mahmoudi, M.; Lynch, I.; Ejtehadi, M. R.; Monopoli, M. P.; Bombelli, F. B.; Laurent, S., Protein-Nanoparticle Interactions: Opportunities and Challenges. *Chem. Rev.* **2011,** 111, (9), 5610-5637.

35. Lee, E.; Shon, H. K.; Cho, J., Biofouling characteristics using flow field-flow fractionation: Effect of bacteria and membrane properties. *Biores. Technol.* **2010,** 101, (5), 1487-1493.

36. Park, N.; Kwon, B.; Kim, I. S.; Cho, J., Biofouling potential of various NF membranes with respect to bacteria and their soluble microbial products (SMP): Characterizations, flux decline, and transport parameters. *Journal of Membrane Science* **2005,** 258, (1-2), 43-54.

37. Ulrich, A.; Losert, S.; Bendixen, N.; Al-Kattan, A.; Hagendorfer, H.; Nowack, B.; Adlhart, C.; Ebert, J.; Lattuadae, M.; Hungerb€uhler, K., Critical aspects of sample handling for direct nanoparticle analysis and analytical challenges using asymmetric field flow fractionation in a multi-detector approach. *J. Anal. Atom. Spectrom.* **2012,** 27, 1120-1130.

38. Liu, M.-K., Li, P. and Giddings, J. C., Rapid protein separation and diffusion coefficient measurement by frit inlet flow field-flow fractionation. *Protein Science* **1993,** 2, 1520-1531.

39. Reschiglian, P.; Zattoni, A.; Roda, B.; Michelini, E.; Roda, A., Field-flow fractionation and biotechnology. *Trends in Biotechnology* **2005,** 23, (9), 475-483.

40. Song, J. H.; Kim, W.-S.; Park, Y. H.; Yu, E. K.; Lee, D. W., Retention characteristics of various proteins in flow field-flow fractionation: effects of pH, ionic strength, and denaturation. *Bull. Korean Chem. Soc.* **1999,** 20, (10), 1159-1164.

41. Yohannes, G.; Wiedmer, S. K.; Elomaa, M.; Jussila, M.; Aseyev, V.; Riekkola, M.-L., Thermal aggregation of bovine serum albumin studied by asymmetrical flow field-flow fractionation. *Anal. Chim. Acta* **2010,** 675, (2), 191-198.

42. Rankl, M.; Ruckstuhl, T.; Rabe, M.; Artus, G. R. J.; Walser, A.; Seeger, S., Conformational reorientation of immunoglobulin G during nonspecific interaction with surfaces. *ChemPhysChem* **2006,** 7, (4), 837-846.

43. NAKANISHI, K.; SAKIYAMA, T.; IMAMURA, K., On the Adsorption of Proteins on Solid Surfaces, a Common but Very Complicated Phenomenon. *J. Biosci. Bioeng.* **2001,** 91, 233-244.

44. Lioris, N.; Farmakis, L.; Koliadima, A.; Karaiskakis, G., Estimation of the particle-wall interaction energy in sedimentation field flow fractionation. *J. Chromatogr., A* **2005,** 1087, (1-2), 13-19.

45. Mori, Y.; Kimura, K.; Tanigaki, M., Influence of particle-wall and particle-particle interactions on retention behavior in sedimentation field-flow fractionation. *Anal. Chem.* **1990,** 62, (24), 2668-72.

46. Pasol, L.; Martin, M.; Ekiel-Jezewska, M. L.; Wajnryb, E.; Blawzdziewicz, J.; Feuillebois, F., Motion of a sphere parallel to plane walls in a Poiseuille flow. Application to field-flow fractionation and hydrodynamic chromatography. *Chem. Eng. Sci.* **2011,** 66, (18), 4078-4089.

47. Parsegian, V. A., *A Handbook for Biologists,Chemists, Engineers, and Physicists*. Cambridge University Pr.: 2006.

48. Hong, J. H.; Kim, W.-S.; Lee, D. W., Comparison of Retention behavior of various polystyrene latex particles and gold colloids on different channel walls in flow-field flow fractionation. *J. liquid chromatogr. relat. technol.* **2003,** 26, 3003-3035.

49. Patel, K.; Angelos, S.; Dichtel, W. R.; Coskun, A.; Yang, Y.-W.; Zink, J. I.; Stoddart, J. F., Enzyme-Responsive Snap-Top Covered Silica Nanocontainers. *Journal of the American Chemical Society* **2008,** 130, (8), 2382-2383.

50. Pratt, E. D.; Huang, C.; Hawkins, B. G.; Gleghorn, J. P.; Kirby, B. J., Rare cell capture in microfluidic devices. *Chem. Eng. Sci.* **2011,** 66, (7), 1508-1522.

51. Gray, J. J., The interaction of proteins with solid surfaces. *Curr. Opin. Struct. Biol.* **2004,** 14, (1), 110-115.

52. Lu, J. R., Protein adsorption and interactions at interfaces. *Neutron Scattering Biol.* **2006**, 265-282.

53. Greenfield, N. J., Using circular dichroism spectra to estimate protein secondary structure. *Nat. Protoc.* **2006,** 1, 2876-2890.

54. Raussens, V.; Ruysschaert, J. M.; Goormaghtigh, E., Protein concentration is not an absolute prerequisite for the determination of secondary structure from circular dichroism spectra: a new scaling method. *Anal. Biochem.* **2003,** 319, 114-121.

Chapter Three

Aptamer-Protein Binding Detected by Asymmetric Flow Field Flow Fractionation

Originally published in the Journal of Chromatography A[1]

Samantha Schachermeyer, Jonathan Ashby, Wenwan Zhong*

1. Introduction

Aptamers are short, single-stranded DNAs or RNAs that bind to their targets with high affinity and specificity. Through systematic evolution by exponential enrichment (SELEX), aptamers can be selected from DNA or RNA libraries containing 10^{13}-10^{15} random sequences. They offer several advantages in comparison to antibodies for detection, including convenient modification, high sequence versatility, superior stability, and lack of immunogenicity.[2] In the past two decades, aptamers for a large variety of targets - such as metal ions, small molecules, proteins, viruses, and bacteria - have been reported,[3-8] and many of them have found applications in diverse areas.[9-14] For instance, cell-binding aptamers have been applied to enrich target cells from body fluids and enabled biomarker discovery.[6, 15, 16] Additionally, inhibitory aptamers that, upon binding, can block the subsequent interaction of their targets with membrane receptors, enzyme substrates, or host cells, are promising drug candidates.[17-19]

The most popular application of aptamers is in the area of molecular sensing.[9-11, 13, 20, 21] Aptamers can be conveniently immobilized on sensor surfaces for specific target recognition.[22] Aptamer-based protein arrays have been constructed for specific capture and detection of biomarkers in biological samples.[23] Alternatively, homogeneous assays have also been designed without aptamer immobilization.[21] For example, molecular

beacons containing aptamer sequences can be switched from a closed to an open state by aptamer-target interaction.[24] Although simple, such methods rely on the availability of multiple fluorophores without spectral overlaps to enable multiplex detection and highly effective quenchers to reduce detection background, due to the co-existence of the target-bound and free aptamers in solution.[25] To solve such difficulties, separation-enabled sensing has been employed, taking advantage of the high resolving power of capillary electrophoresis (CE). The open separation channel utilized by CE imposes minimum damage to the aptamer-target complex, and CE-based detection of multiple proteins and small molecules using aptamers labeled with the same fluorescent tag has been demonstrated.[26-30] Good separation efficiency, quick turn-around time, high simplicity, and low sample consumption make CE an effective tool not only for detection of aptamer-target binding, but also for aptamer selection.[31]

Effective aptamer-based sensors depend on the achievement of stable aptamer-target interaction. Aptamers need to fold into an appropriate three-dimensional structure to yield optimal affinity and specificity to their targets.[32, 33] There are four types of secondary structures: hairpin stem-loops, symmetric and asymmetric bulges flanked by helical regions, pseudo-knots, and G-quadruplexes.[34] Formation of these secondary structures is strongly affected by the incubation conditions such as ionic strength, cation type, and pH.[35] For example, Mg^{2+} can generally enhance the folding energy and thus stability of aptamer folding;[32] but G-quadruplex prefers K^{+} over divalent ions.[35-37] Diverse selection of buffers have been used, with different types of buffer ions, such as phosphate, Tris, HEPES, and a wide range of divalent cation concentrations from 1 – 10

mM Mg^{2+}. Applying the same buffer composition as used in the SELEX selection process should be the best way to obtain optimal binding, but this could be constrained by the measurement technique employed or the application. For instance, to maintain the appropriate folding of aptamers in CE, salts like NaCl can be added to the running buffers but only up to 50 mM, otherwise significant increase of Joule heating and deterioration of separation performance could occur.[30] The other buffer employed in CE is tris-glycine buffer with K^+ or Mg^{2+},[28, 29] which is commonly used in native gel electrophoresis and electrophoretic-mobility shift assays.

Similar to CE, flow field flow fractionation (F4) is a separation technique suitable for analysis of biological complexes owing to its open channel, i.e. a channel without any packing materials. Unlike the packed channels that can induce sheer force stress and break up the binding, the open channel is gentle on complexes and well maintains their native structure. While CE that separate things based on charge-to-size ratios, F4 relies on molecular diffusion to obtain size-based separation of analytes with dimensions from 0.001 to 50 μm. It has been employed for rapid isolation of protein complexes from the unbound background proteins as well as for measurement of the binding between IgG and Fc receptor.[38-40] Asymmetrical F4 (AF4) is a sub-family of F4 that has higher simplicity in instrumentation than the traditional symmetrical F4; and has been widely applied for protein analysis nowadays. Since the separation is independent of buffer composition, as long as the buffer keeps analyte membrane adsorption low, AF4 permits the usage of a wide range of buffers as the carrier solution to better accommodate different targets.[41] This feature represents an advantage of AF4 over CE in the study of

aptamer-target binding, because buffers with high or low ionic strength, or with various divalent cations and buffering anions, can be employed to achieve the optimal binding environment, even when the complex is inside the separation channel. In addition, the larger channel used by AF4 (the smallest dimension of AF4 channel is its thickness which is 350 μm in our system) can accommodate higher amounts of samples (the maximum sample loading is between 10 and 100 μg, based on the manufacturer) and thus it is more suitable for after-channel collection when needed. In spite of these unique features, only few reports can be found about application of AF4 in study of protein interaction, in which shift of the protein peak as an indication of size change was observed, with the target protein bound to a small molecule,[42] a lipid,[43] or a receptor protein.[44] A brief demonstration of ssDNA-protein binding was shown by the Moon group in their frit-inlet AF4 system, where the ssDNA peak acquired to a later migration time with the protein.[45] However, to our knowledge, no previous report was found to analyze aptamer-target binding using AF4, neither how the elution conditions would affect the biomolecular interaction has been investigated.

Herein, in the present report, we explored if indeed AF4 was suitable for detection of aptamer-target interaction. We studied how incubation and AF4 running conditions would affect the binding between human immunoglobulin E (IgE) and its aptamer; and several factors were found important for stabilizing the complex during separation. Our study has established the viability of using AF4 for protein detection in homogenous solution with aptamers carrying fluorescent tags, which will also be useful for detection

of multiple targets if they have significant size difference, as well as for study of aptamer-target binding in different buffers.

2. Materials and Methods

2.1 Chemicals

All chemicals used in this study, including tris base, glycine, potassium dihydrogen phosphate (KH_2PO_4), disodium hydrogen phosphate (Na_2HPO_4) and the chloride salts of sodium, potassium, and magnesium (NaCl, KCl, $MgCl_2$) were purchased from Fisher Scientific (Pittsburgh, PA, USA). Phosphate buffered saline (1×PBS) was prepared by mixing 1.44 g Na_2HPO_4 (anhydrous), 0.24 g KH_2PO_4, 0.20 g KCl, and 8.0 g NaCl in 1.0 L deionized (DI) water and adjusting the pH to 7.40 (± 0.03) with 6 N HCl. The resultant solution had a final concentration of 137 mM NaCl, 10 mM phosphate, and 2.7 mM KCl. Up to 1 mM Mg^{2+} (0.20 g $MgCl_2 \cdot 6H_2O$) could be added to this 1×PBS. The NaCl concentrations were changed to 50 or 100 mM, based on the type of study to be conducted. A 1×TGK buffer was made, containing 25 mM tris, 182 mM glycine, and 5 mM KH_2PO_4, at an adjusted pH of 8.34. All buffers were filtered with 0.20 µm nitrocellulose filter (Whatman, Piscataway, NJ), and used within 48 hours.

The DNA aptamer for IgE (5'- /6-FAM/ ggg gCA CgT TTA TCC gTC CCT CCT AgT ggC gTg CCC CA -3') was purchased from IDT technologies (Coralville, Iowa, USA). Human immunoglobulin E (IgE) was obtained from Athens Research and Technology (Athens, Georgia, USA). Stock protein solutions (1.145 mg/mL) were stored

in small aliquots at -20 °C and underwent only one freeze-thaw cycle to preserve protein quality. The IgE stock was diluted tenfold in 1×PBS with 1 mM Mg^{2+}, unless otherwise stated, and stored at 4 °C. The diluted IgE solutions were used for up to 7 days. The data used for side-by-side comparison were taken from the same diluted aliquot, in case small changes in protein quality induced by storage condition would affect binding. Stock DNA solutions (10 μM) were prepared in the same 1×PBS unless otherwise indicated and kept at room temperature (RT).

2.2 AF4 conditions

An AF2000 asymmetrical flow field flow fractionation system manufactured by Postnova Analytics (Salt Lake City, UT, USA) was used in this study. The separation channel had a depth of 350 μm, and the injection loop volume was 20 μL. All separations were done with a 10 kDa MWCO regenerated cellulose membrane, an input (tip) flow (the flow entering the channel from the top) of 3.3 mL/min and a cross flow (the flow exiting the channel through the membrane) of 3 mL/min, for a detector output flow rate of 0.3 mL/min. (NOTE: for more details about tip and cross flow directions, please refer to Figure 3.04 and Sec. 3.2.) The carrier solution (CS) was 1×PBS with or without Mg^{2+}, as specified in Results and Discussion. In most of the study, during injection, a focusing time of 6 min was used, with a tip and cross flow at 0.2 mL/min and 3 mL/min, respectively. These conditions were only varied when studying the effects of the focusing flow rates and duration. The eluent from the AF4 system was monitored by the SPD-20A Prominence UV/Vis detector at 280 nm, and also by the Waters™ 474

scanning fluorescence detector with an excitation wavelength of 495 nm and an emission wavelength of 525 nm (Milford, MA, USA). The UV absorption signal was obtained for survey purpose, i.e. confirming stable baseline and successful injection of the DNA and the protein; and only the fluorescent signals were used for calculation of the protein-bound aptamer fraction attained under different experimental conditions. Prior to injection, 1 μM aptamer was mixed with varying concentrations of IgE in 50 μL 1×PBS containing 0, 0.5, or 1 mM Mg^{2+}, and incubated for 30 minutes at RT to ensure sufficient binding. The incubation step was done for all samples except for the incubation vs non-incubation experiment.

The AF4 conditions and buffer compositions used in all the studies reported here were summarized in Table 3.01.

2.3 Binding ratio calculations

In our study**,** the protein-bound aptamer fraction, A*, obtained under different experimental conditions was calculated by dividing the protein-bound aptamer peak area (A) over the area sum of the free (F) and bound aptamer peaks:

$$A^* = A/(A+F) \qquad \text{(Equation 3.01)}$$

The relative standard deviation (RSD) for A* from repeated injections was normally around or below 5%, showing good run-to-run reproducibility. However, the A* values measured using the recombinant IgE from different manufacture batches could vary by more than 10%, probably due to difference in protein expression. Therefore, data used for comparison were obtained with the same protein aliquot. We also normalized the A*

value against that acquired using 1×PBS with 1 mM Mg^{2+} as both the incubation buffer (IB) and carrier solution, and focusing the sample with a tip and cross flow rate of 0.20 mL/min and 3.00 mL/min, respectively, for 6 minutes. This set of running condition was referred as the "standard running condition" in the following text. The normalized A* values were compared to show the true difference among experimental conditions. All measurements reported were conducted in triplicate.

3. Results and Discussion

3.1 Composition and pH of the incubation buffer and carrier solution

Unlike homogeneous binding assays, separation-based analysis of molecular interaction would expose the interactive molecules to two surroundings: the buffer used for pre-injection incubation, and the separation buffer. Therefore, we first investigated how the compositions of these two buffers would affect the fraction of the protein-bound aptamer measured by AF4.

3.1.1 Incubation Buffer (IB)

The IgE-binding aptamers, including the one chosen in our study, share a common stem-loop structure.[46, 47] Previous studies have revealed that, while the loop sequence is very critical for the binding, increasing the stem stability could improve binding affinity.[47, 48] It has been well known that the structure and stability of nucleic acid folding is governed substantially by cation type and ionic strength.[49-51] Changing

these conditions should then affect binding affinity owing to variation in the stability of the stem-loop structure. The common buffer used for aptamer-protein binding is 1×PBS containing Mg^{2+}. Therefore, we prepared a series of phosphate buffers (10.1 mM Na_2HPO_4 and 1.76 mM KH_2PO_4) with a constant [Mg^{2+}] of 1 mM but varied concentrations of NaCl (100 or 137 mM); and studied their impact on aptamer binding (Table 3.01). We also adjusted the Mg^{2+} concentration in the regular 1×PBS (i.e. with 137 mM NaCl) to be 0, 0.5, and 1 mM (Table 3.01). One micromolar aptamer was incubated with 50 nM IgE in these buffers for 30 minutes, a duration allowing binding to reach equilibrium based on our preliminary investigation. The resulted samples were analyzed by AF4 using 1×PBS with 1 mM $MgCl_2$ as the CS; and the protein-bound aptamer fraction (A*) was measured, normalized against that acquired using 1×PBS with 1 mM Mg^{2+} as the IB, and plotted in Figure 3.01a. For better estimation of the stability of the folded, stem-loop aptamer, we also computed its folding free energy change (ΔG) at 25 °C in these solutions using Mfold[52], and listed them along with the A* plot in **Figure 3.01a**.

From the ΔG values, we can see that, increasing NaCl and Mg^{2+} concentrations would yield more negative ΔG values, with the lowest ΔG, -10.95 kcal/mol, achieved with the highest NaCl and Mg^{2+} concentrations. Yet, Mg^{2+} seemed to impose higher influence on ΔG than NaCl. For instance, decreasing the NaCl concentration to 100 mM raises the ΔG to -10.79 kcal/mol; but removal of 1 mM Mg^{2+} could increase it to a higher value of -10.49 kcal/mol. The more negative ΔG corresponds to a higher aptamer folding stability, so we expected to see lower bound ratios in the IBs with lower NaCl or Mg^{2+}

Table 3.01: A summary of AF4 experimental details including IB, CS, focusing time, and flow rates.

Study	Incubation Buffer Employed	Carrier Solution Employed	Focusing time	Flow rates during focusing (tip, cross)
Composition of Incubation Buffer (IB)	**Ionic Strength:** 10 mM Phosphate, 2.7 mM KCl, 1 mM $MgCl_2$, pH 7.40, **plus 50, 100, or 137 mM NaCl**	10 mM Phosphate, 2.7 mM KCl, 137 mM NaCl (1xPBS); 1 mM $MgCl_2$, pH 7.4	6 minutes	0.2 and 3.0 mL/min
	Divalent cation concentration: 10 mM Phosphate, 2.7 mM KCl, 137 mM NaCl, pH 7.40 (1xPBS); **plus 0, 0.5, or 1 mM $MgCl_2$**			
	pH: 10 mM Phosphate, 2.7 mM KCl, 137 mM NaCl, 1 mM $MgCl_2$, **with pH 6.20, 7.40, or 8.20**			
	A different buffer system: **1xTGK, pH 8.34**			
Composition of Carrier Solution (CS)	10 mM Phosphate, 2.7 mM KCl, 137 mM NaCl, pH 7.40 (1xPBS); **no $MgCl_2$**	**Divalent cation concentration:** 1xPBS; **plus 0 or 1 mM $MgCl_2$**		
	10 mM Phosphate, 2.7 mM KCl, 137 mM NaCl, pH 7.40 (1xPBS); **1 mM $MgCl_2$**	**Divalent cation concentration:** 1xPBS; **plus 0 or 1 mM $MgCl_2$**		
		Ionic Strength: 10 mM Phosphate, 2.7 mM KCl, 1 mM MgCl2, pH 7.4, **plus 100 or 137 mM NaCl**		
		pH: 1xPBS plus 1 mM $MgCl_2$, **pH 8.20**		
		A different buffer system: **1xTGK, pH 8.34**		
Conditions used during on-column focusing	10 mM Phosphate, 2.7 mM KCl, 137 mM NaCl, pH 7.40 (1xPBS); 1 mM $MgCl_2$	10 mM Phosphate, 2.7 mM KCl, 137 mM NaCl, pH 7.40 (1xPBS); 1 mM $MgCl_2$	**3, 6, or 12 minutes**	0.2 and 3.0 mL/min
			6 minutes	**0.2 and 3.0 mL/min**
				0.3 and 4.5 mL/min
				0.4 and 6.0 mL/min

a)

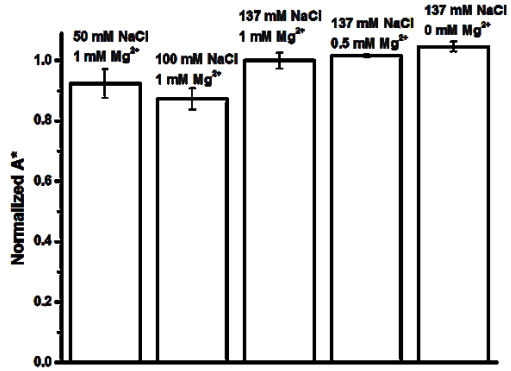

IB Compositions	ΔG (kcal/mol) at 25 °C
50 mM NaCl in PBS, 1 mM Mg^{2+}	-10.58
100 mM NaCl in PBS, 1 mM Mg^{2+}	-10.79
137 mM NaCl in PBS, 1 mM Mg^{2+}	-10.95
137 mM NaCl in PBS, 0.5 mM Mg^{2+}	-10.85
137 mM NaCl in PBS, 0 mM Mg^{2+}	-10.49

b)

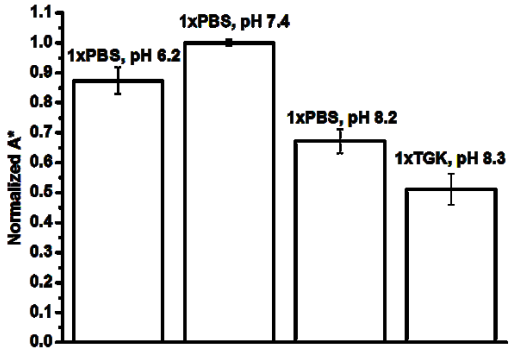

Figure 3.01. Comparison of the normalized IgE-bound aptamer ratios obtained with an IB with varied a) NaCl or $MgCl^{2+}$ concentrations, and b) pH values, while keeping the CS to be 1×PBS with 1 mM Mg^{2+}. The table shown in a) listed the calculated free energy change when the aptamer folded in the corresponding solutions. The final Na^{+} concentration in the solutions used in calculation included 20 mM Na^{+} originated from the phosphate salts plus that from NaCl.

concentrations. Contrary to our prediction, no significant variations in aptamer binding were detected among this set of IBs, the normalized A* values ranging from 0.872±0.036 to 1.05±0.017 (Figure 3.01a). It is possible that the CS used, which contained 137 mM NaCl and 1 mM Mg^{2+} and yielded the lowest ΔG among all situations, stabilized the aptamer structure once it entered the AF4 channel.

Subsequently, we investigated how buffer pH could impact aptamer binding. We measured the A* for the aptamer/protein mixtures incubated in 1×PBS with 1 mM Mg^{2+} at pHs of either 6.20, 7.40, or 8.20. The binding in another basic buffer, 1×TGK at pH 8.3, was also tested. This buffer is widely used in the electrophoresis-based aptamer studies.[53-56] This time significantly lower A* values were detected in the not-neutral solutions, with the basic pH being more devastating to the binding than the acidic condition. The normalized A* was 0.87±0.04 and 0.67±0.04 in the 1×PBS at pH of 6.2 and 8.2, respectively. The bound aptamer ratio in 1×TGK was only half of that in the neutral 1×PBS. Small changes in pH around 7.4 should have a negligible impact on DNA folding, because the ionization states of the phosphate group and the groups participating in base-pairing are not affected. However, it has been reported that pH would affect the secondary structure of IgE (pI 4.5-9.3).[57] Change in protein conformation can also be devastating to aptamer-protein interaction due to the loss of binding epitopes on protein surface. Protein damage was not shown in the IBs tested in Figure 3.01a, because the secondary structure of immunoglobulin should remain unchanged with a NaCl concentration higher than 50 mM, as found in our previous study.[41]

By evaluating the results shown in Figure 3.01b, we concluded that, influence from the IBs on aptamer folding was alleviated by a favorable CS, but change to protein conformation caused by the IB was not recoverable on channel. The larger size and higher structure complexity of IgE compared to the aptamer may make it more difficult for the protein to resume to the proper folding state after being damaged. In all of the IBs tested, no influence was observed on the elution time of either the DNA or the DNA-protein complex, with DNA eluted at 5.03± 0.22 min and the complex at 13.82± 0.33 min (n=12) for analysis during the same day. As the membrane aged, the retention time increased up to a minute for both peaks due to sample adsorption, but same day RSD values were always less than 5%.

3.1.2 Carrier solution

Our above study revealed that, the composition and pH of the IB could affect aptamer-protein binding, but the changes might be reversed by a judiciously selected CS in AF4, hinting higher influence from the CS to the interaction. This is reasonable because the aptamer-protein complex would be exposed to the CS during the separation course. Herein, we studied aptamer binding in CS with different compositions and pH values, while keeping the IB the same (1×PBS with 1 mM Mg^{2+} at pH 7.4). We have known from free energy calculation that Mg^{2+} is more important than NaCl in stabilizing the folded aptamer. Therefore, we first looked into the binding situation in CS containing 1 or 0 mM Mg^{2+}. Without Mg^{2+} in the CS, no binding was seen between the aptamer and protein, even though the IB contained 1 mM Mg^{2+} (Figure 3.02). The complex peak

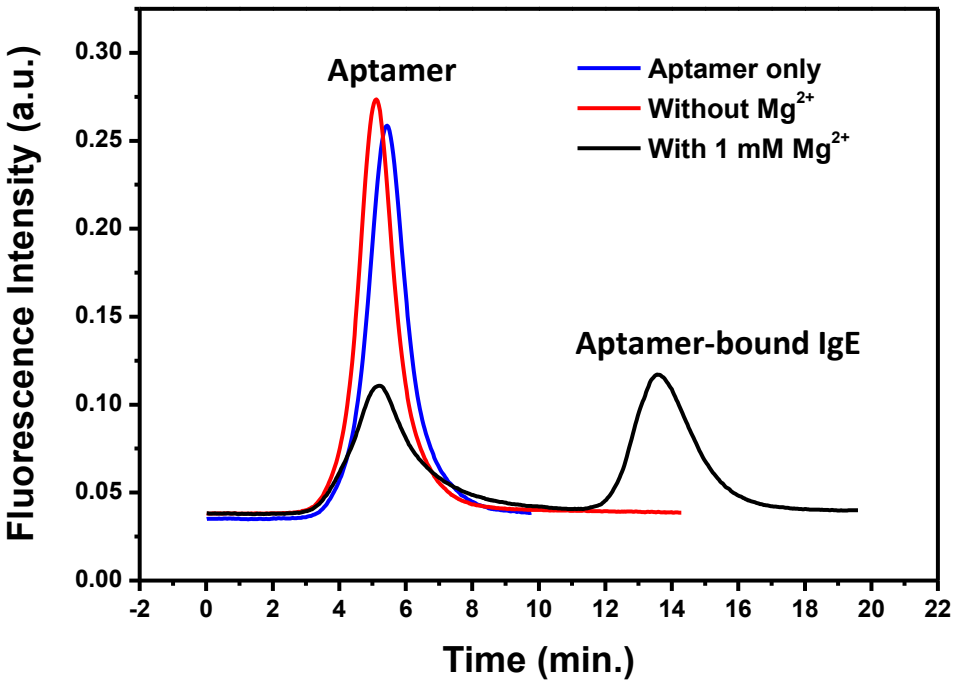

Figure 3.02. Fractograms of aptamer only, and aptamer incubated with IgE with or without Mg^{2+} in the carrier solution. Without the presence of Mg^{2+} in the CS, the free aptamer peak was shown to be of similar size for both the aptamer only and the aptamer incubated with IgE, indicating that no binding occurred. The IB for all three runs was 1xPBS with 1 mM $MgCl^{2+}$.

only appeared with the addition of $MgCl_2$ to the CS. This result clearly states that, during the separation, the aptamer must be kept in an environment that maintains its appropriate secondary structure. Even though the calculated folding ΔGs only differ by 0.46 kcal/mol with or without Mg^{2+} (-10.95 vs. -10.49 kcal/mol), the aptamer with the less stable folding would dissociate from the aptamer-protein complex more rapidly. Once dissociated, the unfolded DNA would be separated from the protein due to its smaller size (12.17 kDa), leave the sample zone, and not be able to bind the protein again and reform the complex. Eventually, no detectable amount of the bound aptamer was eluted at the end of the channel.

The depletion of aptamer from the sample zone can be supported by looking at the diffusion distance of aptamer during the separation time course. We first calculated the gravity center distance from the accumulation wall, *l*, of each peak, using the equation shown below:

$$l = \lambda * w = t_0/(6 * t_r) * w \qquad \text{(Equation 3.02)}$$

In this equation, λ is the retention parameter; t_0 is the void time and calculated to be 0.86 min by our channel dimensions and the cross/output flow rates used in the study;[58] t_r is the retention time, and w is the channel thickness, which is 0.350 mm in our system. The average t_r of DNA and the protein complex under our standard running conditions were 5.03 min for DNA and 13.82 min for the complex. The *l* of the DNA and the complex was calculated to be 10 and 3.6 μm, respectively. Because the gravity center of the sample is governed by the ratio of diffusion coefficient and the linear cross flow velocity at the membrane surface u_o, i.e.

$$l = D/u_o \qquad \text{(Equation 3.03)}$$

we can estimate the diffusion coefficient of DNA. With a cross volume flow rate of 3 mL/min and a channel surface area of 3160 mm^2 in our system, D of the DNA was calculated to be 1.6 x 10^{-6} cm^2/s. Thus, for the DNA to diffuse out of the complex zone with a gravity center at 3.6 μm above the accumulation wall, it would take only 4.1 x 10^{-2} sec. This short time supports that, once dissociated from the protein, the aptamer would be separated from the protein immediately, preventing reformation of the complex.

We next looked at the effects from NaCl concentration (representing ionic strength), pH, and buffer composition in CS. We kept the NaCl concentration at 100 mM and beyond to ensure minimum adsorption of IgE to the membrane in the neutral PBS, as reported in our previous study.[41] The results are shown in Figure 3.03. A more basic CS still exhibited lower bound aptamer ratios, while changes in NaCl concentration with the presence of Mg^{2+} did not significantly affect binding. Interestingly, the TGK buffer behaved much better than in the IB study, delivering a higher normalized ratio (0.84±0.05) than that (0.59±0.01) in 1×PBS at pH 8.2, even without the addition of Mg^{2+}. TGK is commonly used in mobility shift assays for study of DNA-protein binding, meaning that DNA could fold into favorable secondary structures for protein binding in this buffer and Mg^{2+} is not needed in this case.[53-56] As mentioned above, pH variation would affect IgE conformation, and thus interfere with aptamer binding. However, the relatively small drop in the bound ratio observed in Figure 3 in comparison to that shown in Figure 3.01 indicated that, the time IgE spent inside the channel might be too short to induce any significant structure change in the protein due to its large size and

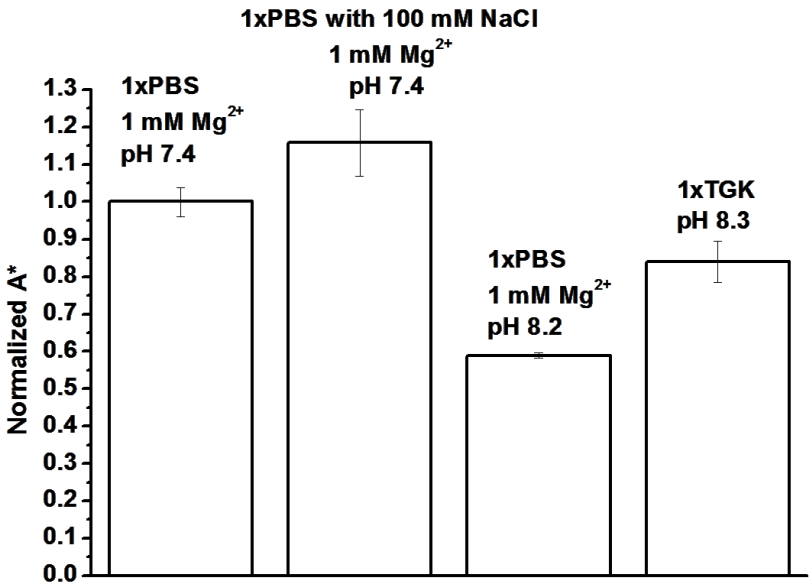

Figure 3.03. Comparison of the normalized IgE-bound aptamer ratios obtained with varying CS compositions as labeled. The IB for all the runs was 1xPBS with 1 mM $MgCl^{2+}$.

rigid structure. The lower bound ratio detected in the basic PBS than with the TGK could be attributed to protein adsorption on the channel membrane with this CS. Since this solution contained 1 mM Mg^{2+}, and both the regenerated cellulose membrane and IgE carried high negative charges at pH 8.2, the Mg^{2+} could serve as a bridge to attract more IgE molecules to the membrane surface, causing lower protein recovery in AF4. Lower sample recovery with the divalent Mg^{2+} than with the monovalent alkali cations has also been reported previously.[41]

We have learned from the above study that, when using AF4 to study aptamer-protein binding, an aptamer-friendly CS should be employed to maintain complex integrity on channel; and selection of IB should pay more attention to its influence on protein structure than on aptamer folding. Once the protein structure is damaged in the IB, it would not be recovered soon enough inside the separation channel, and weak binding will be observed. In addition, selection of CS should avoid significant sample adsorption on the channel membrane to achieve accurate binding measurement.

3.2 Focusing time and flow-rates

Another reason that renders the CS a higher influencing power than the IB over aptamer binding is the unique focusing step required by AF4. This step would quickly eliminate the IB components in the sample zone right after the sample being loaded on the channel. The focusing step confines the injected molecules into a narrow zone and is done by two opposing flows, a tip flow going in from the channel inlet and a focus flow entering from the outlet end. These two flows meet at a focusing position that is

determined by the ratio of their flow rates and concentrate the sample in a narrow stripe across the breadth axis of the channel (Figure 3.04). During this step, IB would leave the channel through the membrane and be replaced by CS; and the aptamer-protein complex could be dissociated or reformed, depending on the compatibility of CS with aptamer folding and/or protein conformation. In our study, we used a focusing time of 6 minutes, which is recommended by the manufacturer for the flow conditions used to achieve baseline resolution of the aptamer and IgE. Compared to the overall separation time of 16 minutes, this was not a short period. Therefore, impacts of the focusing conditions, i.e. the focusing time and flow rates, on complex integrity should be investigated.

We first tested three sets of tip and cross flow rates, while maintaining a constant tip-to-cross flow ratio. This would focus the sample at the same channel position, so that identical separation conditions could be employed post focusing. With higher flow rates, the sample injected should be focused into a narrower and more concentrated zone. Increasing the concentrations of the interacting components should enhance binding. Indeed, compared to the ratio obtained with a tip flow rate of 0.2 mL/min, the bound aptamer ratio consistently increased by 5±1% and 11±3% with the tip flow rate going up to 0.3 and 0.4 mL/min (Figure 3.05a). Further increasing the focusing rates could lead to higher binding ratios, but high flow rates also put too much mechanical stress on the pumps and are impractical.

Focusing duration can also affect the total amount of complex detected at the end of the channel. Longer focusing time may help to form more complexes, if the reaction has not yet reached equilibrium; or even permit on-channel incubation for complexes that

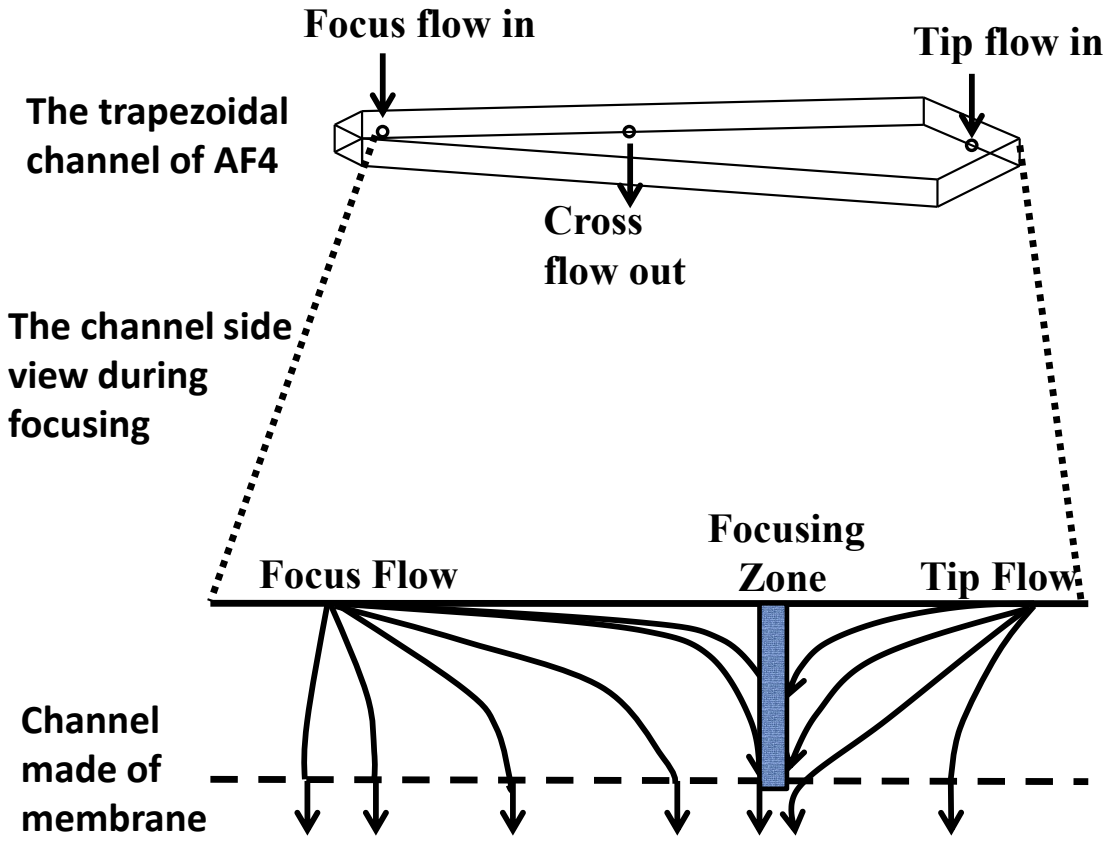

Figure 3.04. Schematic of AF4 during the focusing step.

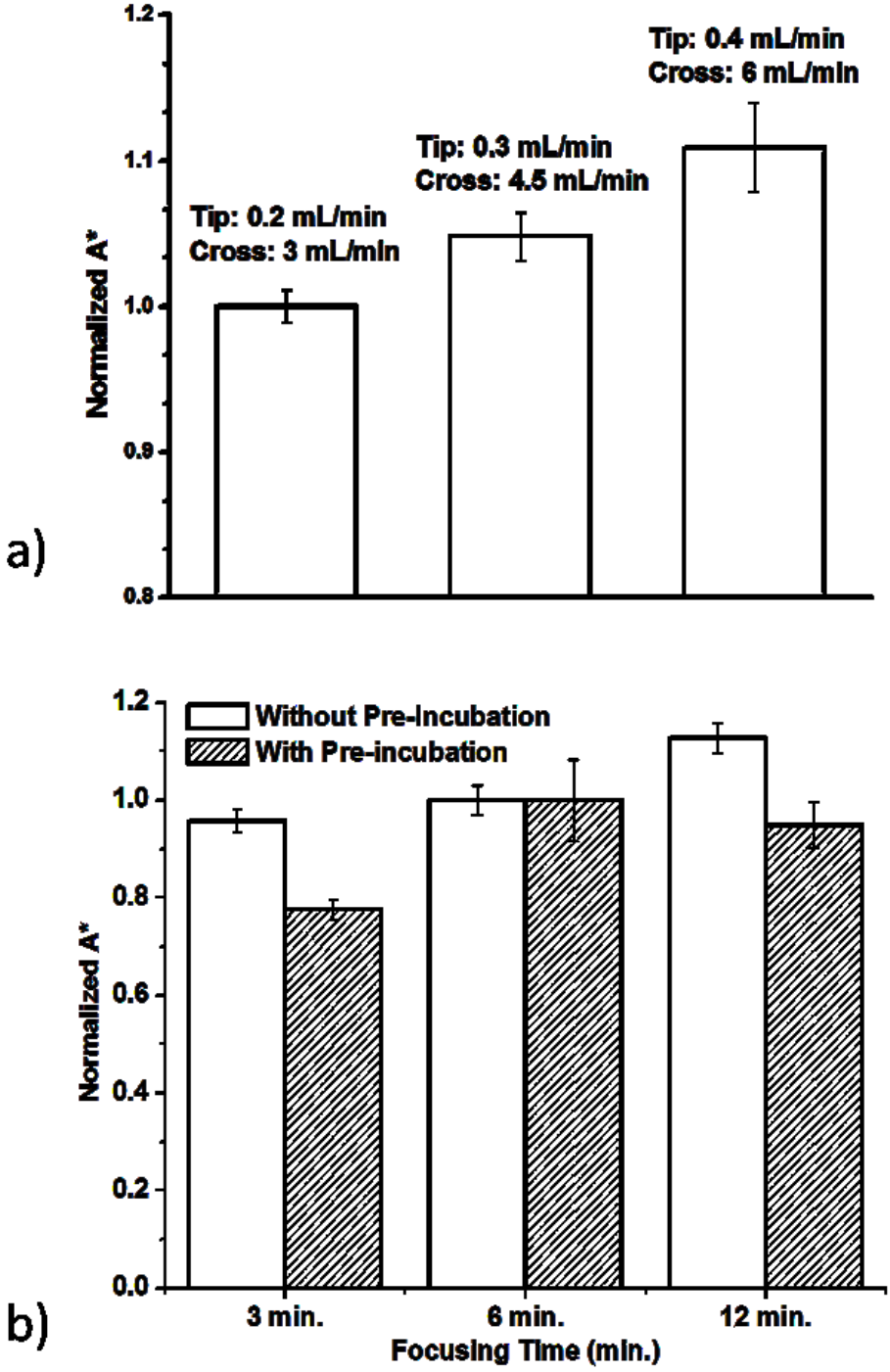

Figure 3.05. Comparison of the normalized IgE-bound aptamer ratios under a) increasing flow rates with constant ratio between tip and focus flows; and b) increasing focusing time with constant tip and focus flows. Both the IB and the CS for all the runs was 1xPBS with 1 mM $MgCl^{2+}$.

can be assembled rapidly, to eliminate the need of pre-incubation and shorten the overall analysis time. Three focusing times were investigated: 3 min, 6 min, and 12 min, accompanied with or without a 30-min preincubation. The results were shown in Figure 3.05b. Without preincubation, a focusing time of 3 minutes was enough to reach 96±2% of the bound ratio obtainable with a 6-minute focusing step. Further increasing the focusing time to 12 minutes would raise the bound ratio by 13±3%. This result clearly indicates the complex could be formed during the focusing step inside the AF4 channel. Focusing time shorter than 3 minutes or longer than 12 minutes was not tested. Too lengthy of a focusing time definitely induces more sample adsorption on the channel membrane; and further reduction of the focusing duration could result in more peak broadening and longer elution time. Dropping the focusing duration from 6 to 3 minutes, the full width at half maximum (FWHM) of the aptamer peak increased from 2.20 to 2.64 minutes with the retention time elongated from 6.31 to 7.41 minutes (Figure 3.06), leading to poorer separation efficiency.

It is also noteworthy that, no significant difference was detected between the bound ratios obtained with or without pre-incubation when the focusing time was 6 minutes. This supports that either a 30-minute pre-incubation or a 6-minute on-channel incubation could yield comparable aptamer binding. The ability to reach an equivalent bound ratio in a shorter time period during sample focusing in AF4 could be attributed to the increased analyte concentration at the focused zone, since the injected sample plug was compressed at this region. We estimated the height of the sample zone by injecting a blue dye to the system, which was smaller than 1 mm. The focused position was near the

bottom of the inlet triangle of the trapezoid channel, which was about 1.5 cm. The channel thickness was 0.35 mm in our system. Taking all these dimensions into consideration, and assuming the focused sample take the shape of a rectangular cube, we estimated the sample volume to be V = 1.5 mm x 1 mm x 0.35 mm = 0.525 μL. We injected 20 μL so the compression factor was about 38 fold. Moreover, more frequent molecule interactions could occur when the two opposing flows, the tip and focus flows, collide at the focusing position. Both factors may also be responsible for the higher normalized A value observed in Figure 3.05b for the without-pre-incubation sample with a focusing time of 12 minutes. Even though the same trend was found with a 3-min focusing step, the difference should probably be attributed more to the decomposition of the pre-formed complex due to the larger volume with insufficient focusing, as indicated by the wider peaks in Figure 3.06. Still, more investigation should be carried out in the future to obtain better understanding of the formation and fate of the aptamer-protein complex inside the AF4 channel.

Nevertheless, a focusing step that can be utilized for on-channel incubation with enhanced binding efficiency represents another advantage of AF4 in analysis of aptamer-target binding in addition to convenient selection of carrier solution.

3.3 Detection of IgE by the fluorescently labeled aptamer using AF4

At last, we detected IgE by AF4 using the fluorescently labeled aptamer. One micromolar aptamer was pre-incubated with IgE at various protein concentrations. The total amount of aptamer was in excess to ensure sufficient protein binding. The area of

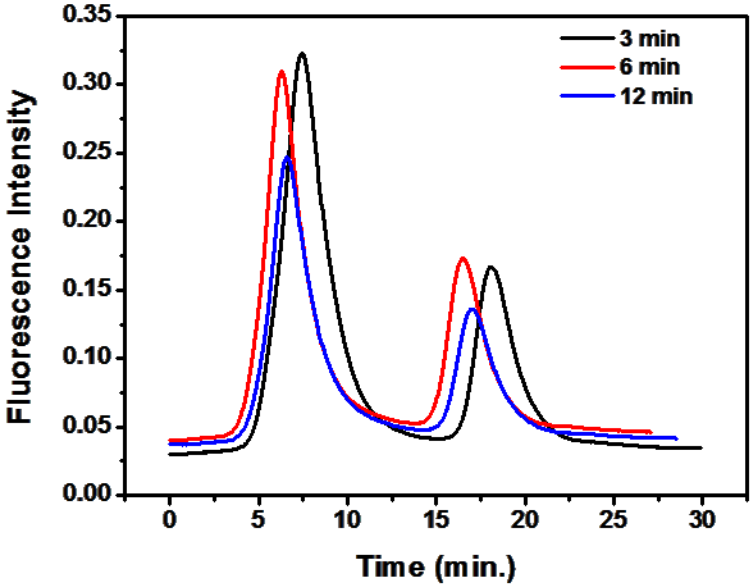

3.06. Fractograms with various focusing times, showing broader peak with a shorter focusing time and delayed elution of the aptamer and the protein.

the complex peak was plotted against IgE concentration (Figure 3.07). As low as 33 nM IgE in the 20-μL injection volume was detected experimentally. As was seen in the IB study, the presence or absence of Mg^{2+} in the IB did not affect aptamer binding measured by AF4, since the two calibration curves obtained with IBs with or without 1 mM Mg^{2+} almost overlapped with each other (Figure 3.08). The detection limit in the present system was not very low, mainly due to the inadequate fluorescence emitted by the FITC probe. It can be further improved by using a fluorophore with higher quantum yields, such as the Alexa dyes, or using fluorescent nanoparticles like quantum dots. Like other separation-enabled sensing techniques, AF4 can resolve the target from the interfering components present in the sample matrix, providing the advantage of background reduction and sample clean-up elimination.

4. Conclusions

In this study, we have demonstrated the feasibility of using AF4 for detection of aptamer-protein interaction. The carrier solution, rather than the incubation buffer, was found to be the most critical factor in preserving the aptamer complex during separation. The sample focusing step was adequate for on-channel incubation to form the stable aptamer-protein complex. Successful detection of IgE at a reasonably low concentration was achieved with the aptamer labeled with a relatively not-so-bright dye.

Our study also highlights the advantages offered by AF4 for analysis of aptamer binding compared to the existing separation-based techniques. These advantages include good compatibility with diverse carrier solutions and simplicity in performing on-channel

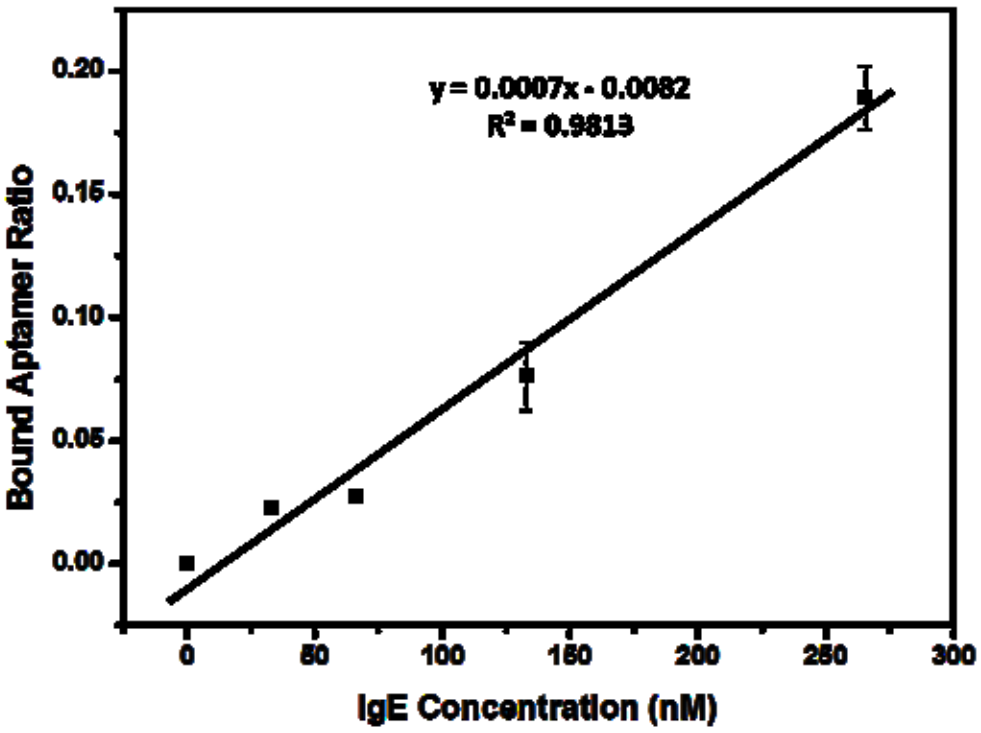

Figure 3.07. Calibration curve obtained by incubating IgE with 1 μM aptamer. The protein-bound aptamer ratio was plotted against IgE concentration. For all injections, the IB and CS was 1xPBS with 1 mM $MgCl^{2+}$.

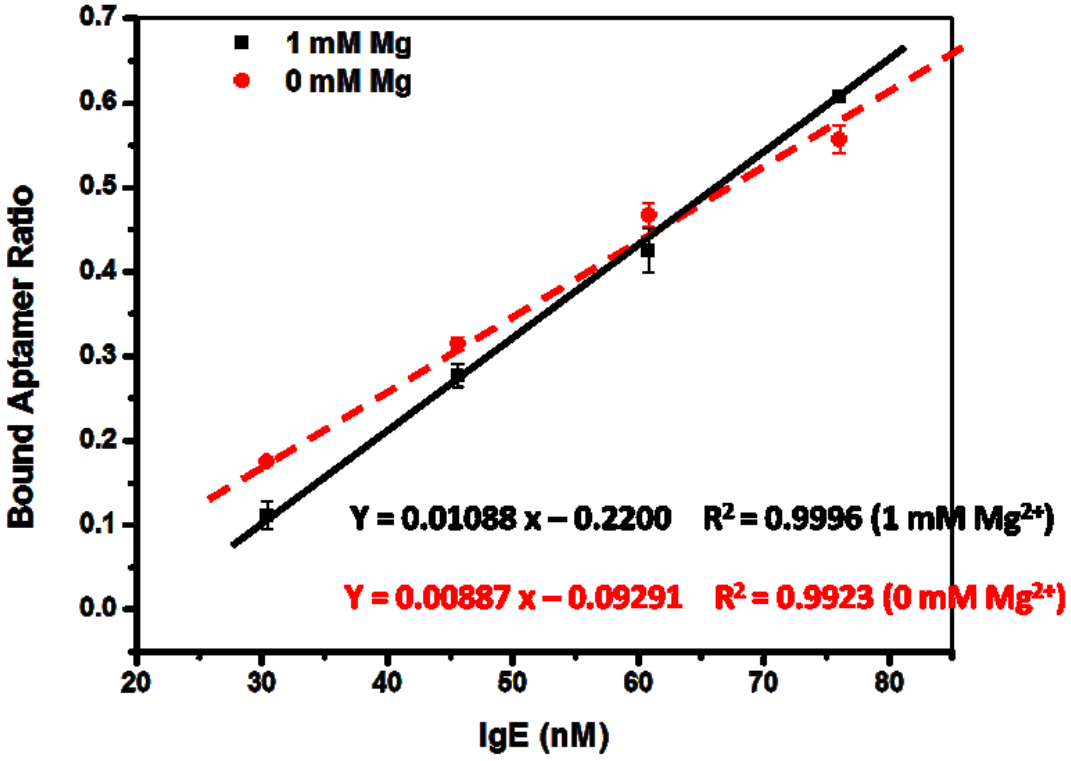

Figure 3.08. Calibration curves of IgE incubated with 1 μM aptamer in buffers IB with and without Mg^{2+}.

incubation. The capability to accommodate different buffers can provide the optimal binding environment for the interaction system during analysis, and also facilitate comparison of aptamer-target binding strength under different conditions for better understanding of the relationship between aptamer folding and solution environment. On-channel incubation can simplify the procedure and shorten the overall time. Since F4 has a different separation mechanism than CE, it is a nice complementary tool to CE in affinity measurement and detection of biomolecules, if separation of aptamer and complex was not easily achieved by CE. Nonetheless, it is more suitable than CE in applications that involve large or neutral biological particles, require after-channel collections, or demand CE-incompatible interaction environments. Moreover, AF4 can handle higher sample loads per injection and thus permit easier after-channel collection, compared to CE.

Acknowledgements

The work was supported by National Science Foundation CAREER CHE-1057113. Jonathan Ashby contributed with solution preparation and was supported by the National Science Foundation Graduate Research Fellowship under Grant Number DGE-0813967.

References.

1. Schachermeyer, S.; Ashby, J.; Zhong, W., Aptamerâ€“protein binding detected by asymmetric flow field flow fractionation. *Journal of Chromatography A*, (0).

2. Ruigrok, V. J. B.; Levisson, M.; Eppink, M. H. M.; Smidt, H.; van der Oost, J., Alternative affinity tools: more attractive than antibodies? *Biochem. J.* **2011,** 436, (1), 1-13.

3. Binning, J. M.; Leung, D. W.; Amarasinghe, G. K., Aptamers in virology: recent advances and challenges. *Front. Virol.* **2012,** 3, 29.

4. Georgianna, W. E.; Young, D. D., Development and utilization of non-coding RNA-small molecule interactions. *Org. Biomol. Chem.* **2011,** 9, (23), 7969-7978.

5. Silverman, S. K., Selective functionalization: Shields for small molecules. *Nat. Chem.* **2012,** 4, (10), 774-775.

6. Dua, P.; Kim, S.; Lee, D.-k., Nucleic acid aptamers targeting cell-surface proteins. *Methods* **2011,** 54, (2), 215-225.

7. Hamula, C. L. A.; Zhang, H.; Li, F.; Wang, Z.; Le, X. C.; Li, X.-F., Selection and analytical applications of aptamers binding microbial pathogens. *TrAC, Trends Anal. Chem.* **2011,** 30, (10), 1587-1597.

8. Shamah, S. M.; Healy, J. M.; Cload, S. T., Complex Target SELEX. *Accounts of Chemical Research* **2008,** 41, (1), 130-138.

9. Famulok, M.; Mayer, G., Aptamer Modules as Sensors and Detectors. *Acc. Chem. Res.* **2011,** 44, (12), 1349-1358.

10. Iliuk, A. B.; Hu, L.; Tao, W. A., Aptamer in Bioanalytical Applications. *Anal. Chem.* **2011,** 83, (12), 4440-4452.

11. Kong, R.-M.; Zhang, X.-B.; Chen, Z.; Tan, W., Aptamer-Assembled Nanomaterials for Biosensing and Biomedical Applications. *Small* **2011,** 7, (17), 2428-2436.

12. Tan, W.; Wang, H.; Chen, Y.; Zhang, X.; Zhu, H.; Yang, C.; Yang, R.; Liu, C., Molecular aptamers for drug delivery. *Trends Biotechnol.* **2011,** 29, (12), 634-640.

13. Teller, C.; Willner, I., Functional nucleic acid nanostructures and DNA machines. *Curr. Opin. Biotechnol.* **2010,** 21, (4), 376-391.

14. Zhu, G.; Ye, M.; Donovan, M. J.; Song, E.; Zhao, Z.; Tan, W., Nucleic acid aptamers: an emerging frontier in cancer therapy. *Chem. Commun.* **2012,** 48, (85), 10472-10480.

15. Liu, J.; You, M.; Pu, Y.; Liu, H.; Ye, M.; Tan, W., Recent developments in protein and cell-targeted aptamer selection and applications. *Curr. Med. Chem.* **2011,** 18, (27), 4117-4125.

16. Pratt, E. D.; Huang, C.; Hawkins, B. G.; Gleghorn, J. P.; Kirby, B. J., Rare cell capture in microfluidic devices. *Chem. Eng. Sci.* **2011,** 66, (7), 1508-1522.

17. Bunka, D. H. J.; Platonova, O.; Stockley, P. G., Development of aptamer therapeutics. *Curr. Opin. Pharmacol.* **2010,** 10, (5), 557-562.

18. Ng, E. W. M.; Shima, D. T.; Calias, P.; Cunningham, E. T., Jr.; Guyer, D. R.; Adamis, A. P., Pegaptanib, a targeted anti-VEGF aptamer for ocular vascular disease. *Nat. Rev. Drug Discovery* **2006,** 5, (2), 123-132.

19. Pendergrast, P. S.; Marsh, H. N.; Grate, D.; Healy, J. M.; Stanton, M., Nucleic acid aptamers for target validation and therapeutic applications. *J Biomol Tech* **2005,** 16, (3), 224-34.

20. Citartan, M.; Gopinath, S. C. B.; Tominaga, J.; Tan, S.-C.; Tang, T.-H., Assays for aptamer-based platforms. *Biosens. Bioelectron.* **2012,** 34, (1), 1-11.

21. Sassolas, A.; Blum, L. J.; Leca-Bouvier, B. D., Homogeneous assays using aptamers. *Analyst* **2011,** 136, (2), 257-274.

22. Balamurugan, S.; Obubuafo, A.; Soper, S. A.; Spivak, D. A., Surface immobilization methods for aptamer diagnostic applications. *Anal. Bioanal. Chem.* **2008,** 390, (4), 1009-1021.

23. Mok, W.; Li, Y., Recent progress in nucleic acid aptamer-based biosensors and bioassays. *Sensors* **2008,** 8, (11), 7050-7084.

24. Jiang, Y.; Fang, X.; Bai, C., Signaling Aptamer/Protein Binding by a Molecular Light Switch Complex. *Anal. Chem.* **2004,** 76, (17), 5230-5235.

25. Zeng, X.; Zhang, X.; Yang, W.; Jia, H.; Li, Y., Fluorescence detection of adenosine triphosphate through an aptamer-molecular beacon multiple probe. *Anal. Biochem.* 424, (1), 8-11.

26. Janssen, K. P. F.; Knez, K.; Spasic, D.; Schrooten, J.; Lammertyn, J., Multiplexed protein detection using an affinity aptamer amplification assay. *Anal. Bioanal. Chem.* **2012,** 404, (6-7), 2073-2081.

27. Song, M.; Zhang, Y.; Li, T.; Wang, Z.; Yin, J.; Wang, H., Highly sensitive detection of human thrombin in serum by affinity capillary electrophoresis/laser-induced fluorescence polarization using aptamers as probes. *J. Chromatogr., A* **2009,** 1216, (5), 873-878.

28. Zhang, H.; Li, X.-F.; Le, X. C., Tunable Aptamer Capillary Electrophoresis and Its Application to Protein Analysis. *J. Am. Chem. Soc.* **2008,** 130, (1), 34-35.

29. Zhang, H.; Li, X.-F.; Le, X. C., Differentiation and detection of PDGF isomers and their receptors by tunable aptamer capillary electrophoresis. *Anal. Chem. (Washington, DC, U. S.)* **2009,** 81, (18), 7795-7800.

30. Zhu, Z.; Ravelet, C.; Perrier, S.; Guieu, V.; Roy, B.; Perigaud, C.; Peyrin, E., Multiplexed Detection of Small Analytes by Structure-Switching Aptamer-Based Capillary Electrophoresis. *Anal. Chem.* **2010,** 82, (11), 4613-4620.

31. Mosing, R. K.; Bowser, M. T., Isolating aptamers using capillary electrophoresis-SELEX (CE-SELEX). *Methods Mol. Biol.* **2009,** 535, (Nucleic Acid and Peptide Aptamers), 33-43.

32. Ruff, K. M.; Snyder, T. M.; Liu, D. R., Enhanced Functional Potential of Nucleic Acid Aptamer Libraries Patterned to Increase Secondary Structure. *J. Am. Chem. Soc.* **2010,** 132, 9453–9464.

33. Mayer, G., The Chemical Biology of Aptamers. *Angew. Chem., Int. Ed.* **2009,** 48, 2672-2689.

34. Eaton, B. E.; Gold, L.; Zichi, D. A., Let's get specific: the relationship between specificity and affinity. *Chem. Biol.* **1995,** 2, 633-638.

35. Baldrich, E.; Restrepo, A.; O'Sullivan, C. K., Aptasensor Development: Elucidation of Critical Parameters for Optimal Aptamer Performance. *Anal. Chem.* **2004,** 76, (23), 7053-7063.

36. Hianik, T.; OstatnÃ¡, V.; Sonlajtnerova, M.; Grman, I., Influence of ionic strength, pH and aptamer configuration for binding affinity to thrombin. *Bioelectrochemistry* **2007,** 70, (1), 127-133.

37. Kankia, B. I.; Marky, L. A., Folding of the Thrombin Aptamer into a G-Quadruplex with Sr^{2+}: Stability, Heat, and Hydration. *Journal of the American Chemical Society* **2001,** 123, (44), 10799-10804.

38. Li, J.; Ge, J.; Yin, Y.; Zhong, W., Multiplexed Affinity-Based Protein Complex Purification. *Analytical Chemistry* **2008,** 80, (18), 7068-7074.

39. Li, J.; Zhong, W., A two-dimensional suspension array system by coupling field flow fractionation to flow cytometry. *Journal of Chromatography A* **2008,** 1183, (1-2), 143-149.

40. Pollastrini, J.; Dillon, T. M.; Bondarenko, P.; Chou, R. Y. T., Field flow fractionation for assessing neonatal Fc receptor and FcÎ³ receptor binding to monoclonal antibodies in solution. *Analytical Biochemistry* **2011,** 414, (1), 88-98.

41. Schachermeyer, S.; Ashby, J.; Kwon, M.; Zhong, W., Impact of carrier fluid composition on recovery of nanoparticles and proteins in flow field flow fractionation. *J. Chromatogr. A* **2012,** 1264, 72-79.

42. Muhonen, J.; Vidgren, J.; Helle, A.; Yohannes, G.; Viitala, T.; Holopainen, J. M.; Wiedmer, S. K., Interactions of fusidic acid and elongation factor G with lipid membranes. *Anal. Biochem.* **2008,** 374, (1), 133-142.

43. Yohannes, G.; Wiedmer, S. K.; Tuominen, E. K. J.; Kinnunen, P. K. J.; Riekkola, M.-L., Cytochrome c-dimyristoylphosphatidylglycerol interactions studied by asymmetrical flow field-flow fractionation. *Anal. Bioanal. Chem.* **2004,** 380, (5-6), 757-766.

44. Pollastrini, J.; Dillon Thomas, M.; Bondarenko, P.; Chou Robert, Y. T., Field flow fractionation for assessing neonatal Fc receptor and Fcγ receptor binding to monoclonal antibodies in solution. *Anal Biochem* **2011,** 414, (1), 88-98.

45. Kang, D.; Moon, M. H., Miniaturization of frit inlet asymmetrical flow field-flow fractionation. *Anal. Chem.* **2004,** 76, (13), 3851-3855.

46. Fischer, N. O.; Tok, J. B. H.; Tarasow, T. M., Massively parallel interrogation of aptamer sequence, structure and function. *PLoS One* **2008,** 3, (7), No pp given.

47. Katilius, E.; Flores, C.; Woodbury, N. W., Exploring the sequence space of a DNA aptamer using microarrays. *Nucleic Acids Research* **2007,** 35, 7626-7635.

48. Wiegand, T. W.; Williams, P. B.; Dreskin, S. C.; Jouvin, M. H.; Kinet, J. P.; Tasset, D., High-affinity oligonucleotide ligands to human IgE inhibit binding to Fc epsilon receptor I. *J Immunol* **1996,** 157, (1), 221-230.

49. Duckett, D. R.; Murchie, A. I. H.; Lilley, D. M. J., The role of metal ions in the conformation of the four-way DNA junction. *Embo J.* **1990,** 9, (2), 583-90.

50. Granot, J.; Kearns, D. R., Interactions of DNA with divalent metal ions. II. Proton relaxation enhancement studies. *Biopolymers* **1982,** 21, (1), 203-18.

51. McFail-Isom, L.; Shui, X.; Williams, L. D., Divalent Cations Stabilize Unstacked Conformations of DNA and RNA by Interacting with Base Π Systems. *Biochemistry* **1998,** 37, (49), 17105-17111.

52. Zuker, M., Mfold web server for nucleic acid folding and hybridization prediction. *Nucleic Acids Res.* **2003,** 31, 3406-3415.

53. Cann, J. R., Theory and practice of gel electrophoresis of interacting macromolecules. *Anal. Biochem.* **1996,** 237, (1), 1-16.

54. Fried, M. G.; Bromberg, J. L., Factors that affect the stability of protein-DNA complexes during gel electrophoresis. *Electrophoresis* **1997,** 18, (1), 6-11.

55. Roder, K.; Schweizer, M., Running-buffer composition influences DNA-protein and protein-protein complexes detected by electrophoretic mobility-shift assay (EMSA). *Biotechnol. Appl. Biochem.* **2001,** 33, (3), 209-214.

56. Ronai, Z.; Wang, Y.; Khandurina, J.; Budworth, P.; Sasvari-Szekely, M.; Wang, X.; Guttman, A., Transcription factor binding study by capillary zone electrophoretic mobility shift assay. *Electrophoresis* **2003,** 24, (1-2), 96-100.

57. Silton, R. P.; FernÃ¡ndez-Caldas, E.; Trudeau, W. L.; Swanson, M. C.; Lockey, R. F., Prevalence of specific IgE to the storage mite, Aleuroglyphus ovatus. *Journal of Allergy and Clinical Immunology* **1991,** 88, (4), 595-603.

58. Wahlund, K.-G.; Nilsson, L., Flow FFF -- Basics and Key Applications. In *Field-Flow Fractionation in Biopolymer Analysis*, Williams, S. K. R.; Caldwall, K. D., Eds. Springer-Verlag/Wien: 2012; pp 1-21.

Chapter Four

AF4 Analysis for use of ssDNA Affinity Tags

1. Introduction

Open channel separation methods are excellent techniques to explore intermolecular interactions. The absence of channel packing creates minimal disturbance to molecules allowing for a more native environment while separating bound complexes from unbound molecules. One of the more popular open channel separation methods for bioanalysis is capillary electrophoresis (CE).[1, 2] A small sampling volume on the nanoliter scale and a fast analysis time make CE a very attractive separation tool. CE has been applied to a wide range of bioanalysis including protein-NP separation, affinity measurements, and aptamer selection.[1, 3-8] However, despite its many advantages and applications, CE is limited on the ability to use biologically suitable buffers as high ionic strength leads to Joule heating and poorer separation. Asymmetric field flow fractionation (AF4) is another open channel separation instrument. The separation force in AF4 is a perpendicular crossflow to the channel flow resulting in a hydrodynamic size separation compared to CE's size to charge ratio. Advantages to AF4 include larger collection volumes for further analysis, the ability to handle larger biomolecules, the adaptibility to run buffers at high salt concentrations, and a gentle separation mechanism. AF4 has been applied to a vast number of systems, including polymers, nanoparticles, proteins, viruses, and cells.[9-23]

Recently published work from our group revealed the feasibility of using AF4 to detect human immunoglobulin E (IgE) by using a ssDNA aptamer tag and separating the bound aptamer/protein complex from free aptamer.[24] In that work, different factors, including incubation and carrier buffer composition, focusing time, and focusing flow rate, were investigated on what affected the binding between aptamer and protein. It was found that one of the important binding factors was a carrier solution composition that allowed the ssDNA to fold into the appropriate secondary structure, in this particular case the presence of $MgCl_2$. Applying the optimized conditions to the AF4, an IgE LOD of 33 nM was achieved. The LOD was hindered by the use of only a single FITC label per protein molecule. In the current investigation, we were able to decrease our aptamer concentration by using an Alexa Fluor® 488 label. This reduced the necessary concentration of DNA to allow us to calculate K_d values. Upon applying the method to thrombin and its corresponding aptamer, we could not detect the aptamer or the complex. Not all ssDNA structures are suitable for AF4 analysis. Due to its highly flexible nature, potential for secondary structures, and a very large length to width ratio, DNA did not behave like globular proteins. In this study, we explored how ssDNA behaved in AF4, based on retention times and recovery, looking at length and potential secondary structure effects. With this understanding, we would be able to improve future experimental designs for use of aptamer affinity tags and potentially use AF4 to analyze folding of DNA and RNA.

2. Material and Methods

2.1 Chemicals

All chemicals used in this study were purchased from Fisher Scientific (Pittsburgh, PA, USA). Phosphate buffered saline (1xPBS) , used as both the carrier solution and the sample buffer, was prepared to final concentrations of 137 mM NaCl, 10 mM phosphate, 2.7 mM KCl, and 1.0 mM $MgCl_2$ and adjusted to a pH of 7.40 (± 0.03) with 6 N HCl. The buffer was filtered with a 0.2 um nitrocellulose filter (Whatman, Piscataway, NJ). All DNA sequences were purchased from IDT Technologies (Coralville, Iowa, USA) and underwent standard desalting (Table 4.01). Dilutions were prepared in 1xPBS to a final concentration of 1 μM for unlabeled ssDNA and 2 nM or 10 nM for the fluorescently labeled Weigand aptamer (WA) and Streptavidin aptamer (SA) sequences, respectively.

Human immunoglobulin E (IgE) was obtained from Abcam (Cambridge, Massachusetts, USA). Streptavidin was purchased from Sigma Aldrich (St. Louis, MO). Stock protein solutions (1.00 mg/mL) were stored in small aliquots at -20 °C and underwent only one freeze-thaw cycle to preserve protein quality. The protein stock was diluted tenfold and one hundred fold in 1×PBS for IgE and Streptavidin, respectively, stored at 4 °C, and used within 48 hrs.

Table 4.01. Table of ssDNA sequences and corresponding molecular weights.

Name	MW (kDa)	Sequence (5'-3')
A10	3.07	$[A]_{10}$
A20	6.20	$[A]_{20}$
A30	9.33	$[A]_{30}$
A40	12.47	$[A]_{40}$
A50	15.60	$[A]_{50}$
WA	11.29	5'-GGGGCACGTTTATCCGTCCCTCCTAGTGGCGTGCCCC-3'
cWA	8.99	5'-CACGCCACTAGGAGGGACGGATAAACGTG-3'
SA	18.31	5'-CTATACTCCACTTTGCTATTTCTCGGTTCCTTCACGCGCC GATCGCAGGCTGATGAATTG-3'
I9-102	20.62	5'-CAGCTGACGTACGTGCATGGCAAACACACTTCATCCGTA CCTTCTAGTGGGTGTGTAGCAAGCGCGC-3'
TA	5.66	5'-ATAGGTTGGTGTGGTTGG-3'

2.2 AF4 conditions

An AF2000 asymmetrical flow field flow fractionation system manufactured by Postnova Analytics (Salt Lake City, UT, USA) was used in this study. The separation channel had a depth of 350 μm, and the injection loop volume was 20 μL. A regenerated cellulose membrane with a molecular weight cutoff (MWCO) of 5 or 10 kDa was used where stated. All separations were done with an input (tip) flow of 3.30 mL/min and a cross flow of 3 mL/min, for a detector output flow rate of 0.30 mL/min. During the focusing step, the input flow was 0.2 mL/min and the crossflow was 3.00 mL/min with a focus time of 6 min. A SPD-20A Prominence UV/Vis detector at 280 nm was used to monitor the eluent for unlabeled DNA, and a 474 scanning fluorescence detector with an excitation wavelength of 495 nm and an emission wavelength of 525 nm (Milford, MA, USA) was used to monitor the fluorescently labeled DNA.

2.3 Affinity Measurements

The aptamers were held constant at final concentration of 2 nM or 10 nM for IgE and Streptavidin, respectively, with increasing protein concentration. The IgE aptamer was denatured in a boiling water bath for 2 minutes, cooled in an ice bath for 5 minutes, and then an increasing amount of protein was added (V_{final} 30 μL) and allowed to incubate at room temperature for 30 minutes. The entire sample was then injected into the sample loop to ensure consistent and complete loading of the 20 μL loop. The Streptavidin aptamer and protein were mixed without denaturing and immediately

injected into the AF4 system. The following equation was used to calculate the K_d of the aptamer for the protein (Equation 4.01).

$$\frac{I_o}{I} = 1 + \frac{[P]_o}{K_d} \qquad \text{Equation 4.01}$$

Where I_o is the peak area (or height) of the free aptamer in the absence of protein, I is the peak area (or height) of the free aptamer in the presence of protein, and $[P]_o$ is the concentration of the protein. The equation assumed that protein was in excess, the limiting component was the aptamer peak, and only one aptamer binds per protein. Peak area was used for IgE calculations while height was used in the streptavidin case due to poor resolution between the free DNA and aptamer/protein complex. In the affinity measurements, the DNA was the limiting factor and the protein was in excess, meaning that most of the protein remained unbound.

2.4 DNA Folding and Modeling

All sequences were modeled using Mfold [25] to obtain projected secondary structure with the exception of the thrombin aptamer (TA) as it had a G-quadruplex structure not determined by Mfold (Figure 4.01). Molecular modeling was performed using the AM1 force field using SPARTAN v. 6.0 to obtain three dimensional structures.[26] Sequences were modeled in Spartan and measured as both the unfolded linear form and with the Mfold predicted intramolecular bonding. Theoretical lengths were calculated between the two furthest atoms on the molecule using Spartan.

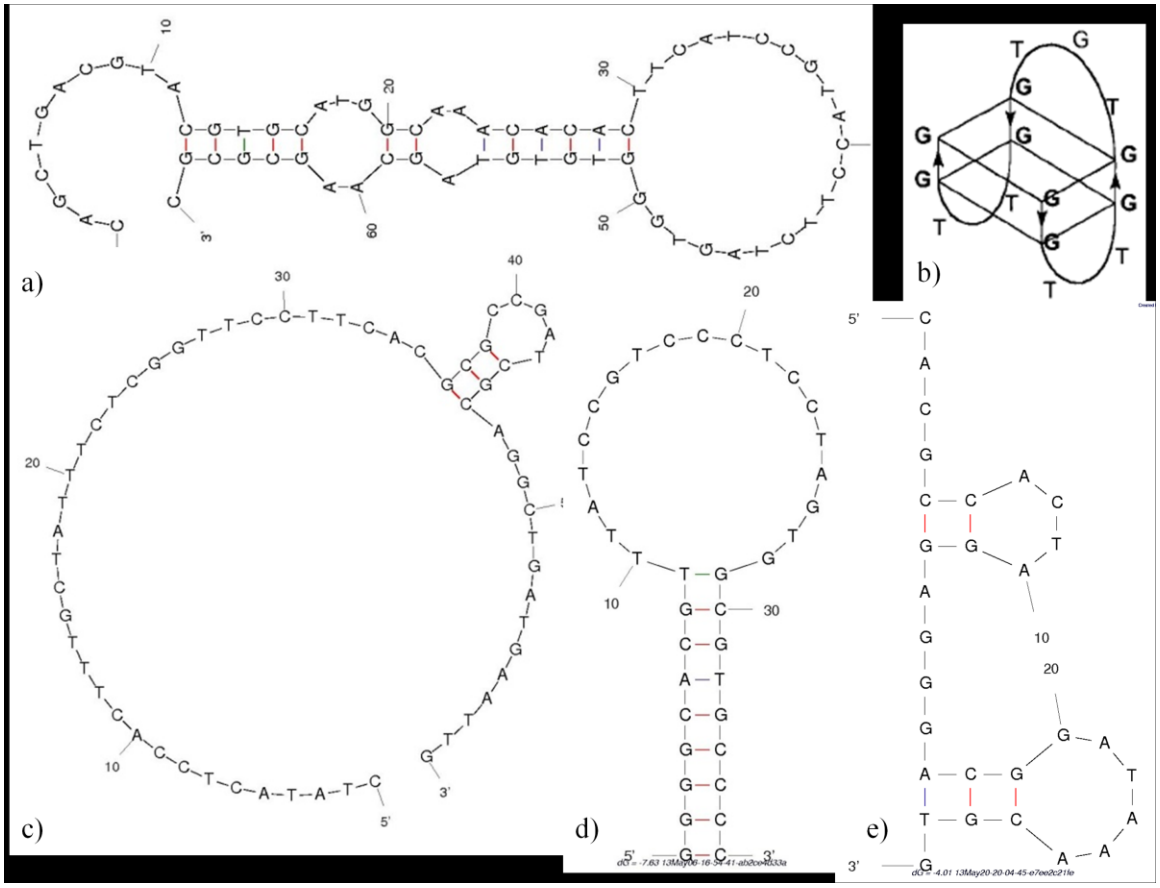

Figure 4.01. Structures of a) I9-102, b) thrombin aptamer (TA), c) streptavidin aptamer (SA), d) Weigand aptamer (WA), and e) complementary WA (cWA).

2.5 Recovery and Folding Equilibrium Calculations

To determine the recovery of different ssDNA sequences, the sample was injected into the system with a tip flow of 0.30 $mL \cdot min^{-1}$ and no cross-flow (NCF). The sample did not undergo focusing. The area for this NCF was assumed to be 100% recovery of the DNA. The percent recovery was calculated by dividing the area of the peak run under standard conditions (A) by the NCF area (A_{NCF}) (Equation 4.02).

$$\%\, Recovery = \frac{A}{A_{NCF}}\, x\, 100\% \qquad \text{(Equation 4.02)}$$

The percentage of the time the ssDNA spent folded in the AF4 system was determined by using the following equation where T_L and T_F were the theoretical times the ssDNA would spend in the system linear and folded, respectively, and T_R was the experimentally determined retention time of the denatured ssDNA (Equation 4.03).

$$\%\, Time\ Folded = \frac{T_L - T_R}{T_L - T_F}\, x\, 100\% \qquad \text{(Equation 4.03)}$$

3. Results and Discussion

3.1 Affinity Measurements

The IgE aptamer used for affinity measurements was discovered by Weigand (D17.2) and was referred to as the Weigand aptamer (WA). The decrease of the free DNA peak was plotted against the concentration of IgE and the K_d was calculated from the inverse of the slope of the linear fit (Figure 4.02a). The WA K_d was calculated to be 16.6 nM in the AF4 which is very near to the literature value of 10 nM. This shows that the AF4 is capable of accurately obtaining affinity measurements, indicating that the

separation mechanism is quite gentle on the complexes. The K_d value was also measured for the Streptavidin aptamer (SA) and calculated to be 400 nM (Figure 4.02b). This is higher than the literature value of 56 nM. The SA K_d deviation from literature was attributed to the poor resolution obtained between the aptamer and protein/aptamer complex. Since the peaks were poorly resolved, the K_d was calculated from the height instead of the area reduction of the free DNA peak. The molecular weight (MW) of the SA was 18.3 kDa. Streptavidin has a MW of 60 kDa. If the SA were a globular shape, the MWs of the aptamer and protein should be resolvable. However, ssDNA has a very high length to width ratio. Therefore, the retention time parameter versus MW cannot be directly compared between proteins and ssDNA.

3.2 Linear ssDNA

Varying lengths of ssDNA were analyzed on the AF4. In order to reduce sample complexity, the sequences were entirely made of adenosine triphosphate removing any intramolecular interaction possibilities. The retention times were plotted against the MW and had a linear relationship (Figure 4.03a). In addition, recovery was calculated for both a 5 and 10 kDa MWCO membranes (Figure 4.03b). Longer tubing was needed to maintain the appropriate backpressure for the channel with the 5 kDa MWCO membrane which resulted in an increase of the path length to the detector, elongating retention times. The percent recovery of the ssDNA was found to increase with increasing length. Expectedly, the 10 kDa MWCO membrane recovery achieved 100% recovery at the 12.47 kDa (40 nt) ssDNA. The 5 kDa MWCO membrane did not obtain 100% recovery

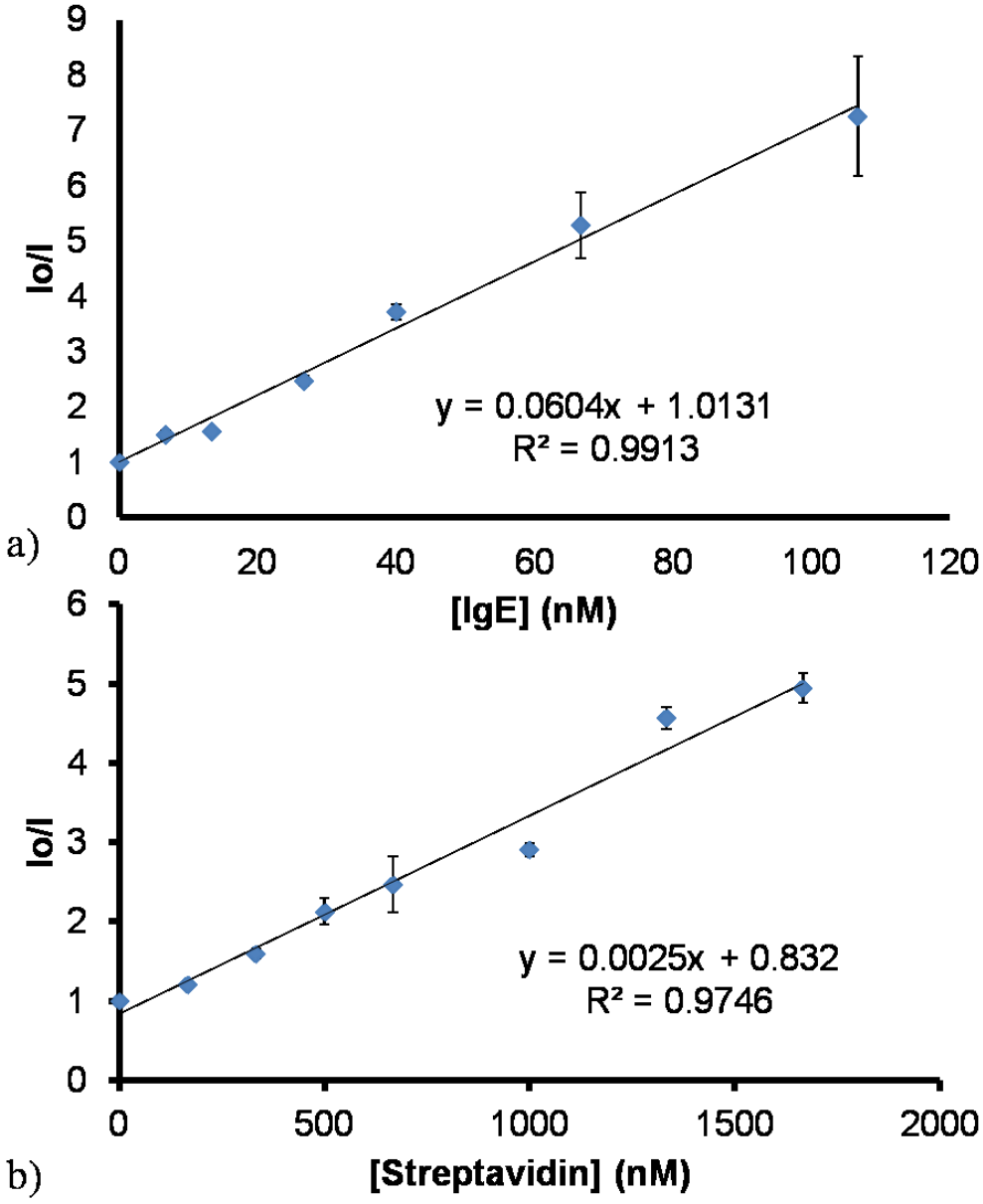

Figure 4.02. Affinity curves for a) IgE and b) Streptavidin.

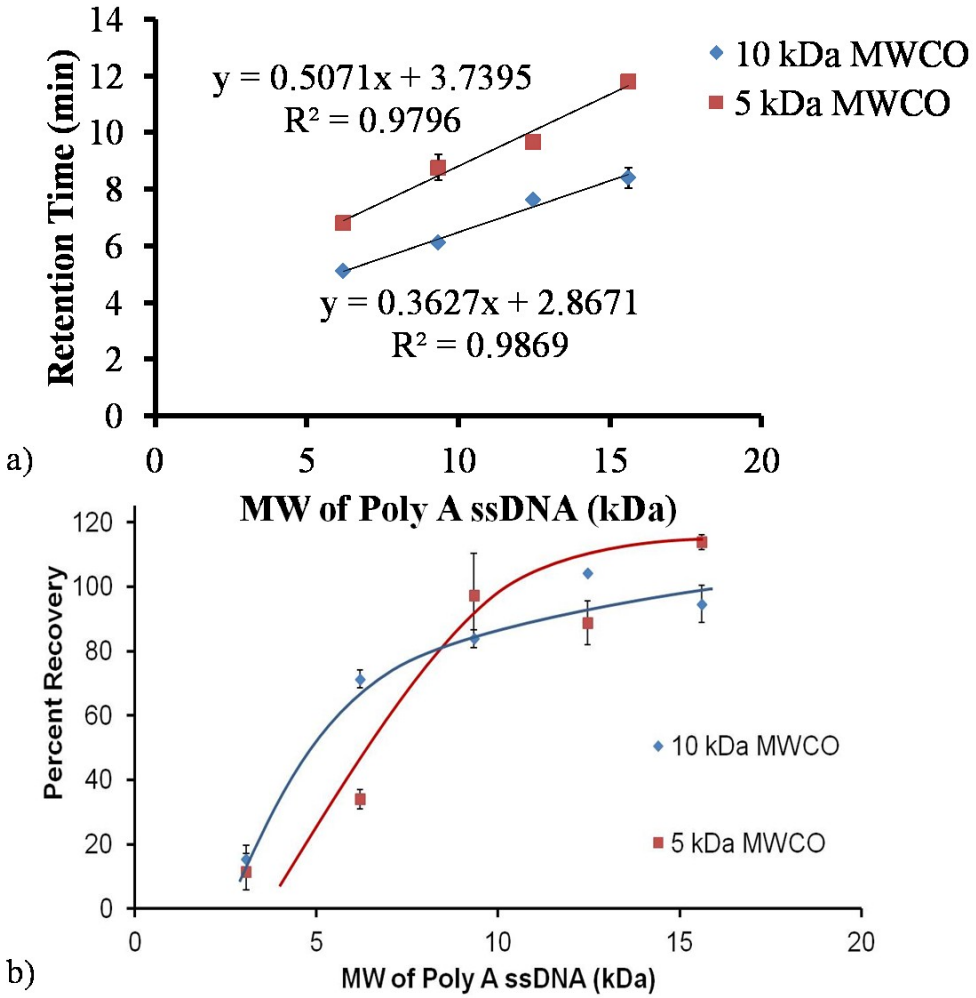

Figure 4.03. a) Retention times and b) percent recoveries for the poly A ssDNA with both the 5 kDa and 10 kDa MWCO membranes.

until the 9.33 kDa (30 nt) ssDNA. The 6.20 kDa (20 nt) ssDNA only had a 34% recovery. This difference seen between the 5 and 10 kDa membranes could be explain based on pore density. In work done by Ramamurthy et. al, they used solute transport to determine pore size and density of different sulfonated MWCO membranes.[27] They discovered that while the 11 kDa MWCO membrane had a pore size of 2.19 nm compared to the 3.5 kDa membrane's 0.7 nm diameter, the pore density increased from 447 to 1291 pores·μm^{-2}, respectively. From this, it could be assumed that the 5 kDa has higher pore density than the 10 kDa, resulting in a greater loss of the ssDNA despite a larger MW than the cut off. MWCO sizes are measured based on the retention of globular proteins while ssDNA high length to width ratio may not translate to the accurate MWCO measurements. The results suggest careful analysis of recovery when choosing to use ssDNA for affinity tags.

3.3 Secondary Structure: Intramolecular Effect

Most aptamers will have intramolecular interactions which cause secondary structure formation. Therefore, the aptamer will not spend the entire time in the channel in the linear form. Instead, it should form an equilibrium between the folded and linear forms. To investigate the behavior of more complex DNA, several aptamers were chosen from literature which form a variety of shapes including stem loops, bulges, and a g-quadruplex (Figure 4.01). Retention times and percent recoveries were compared for each aptamer with and without denaturing, and with both the 5 and 10 kDa MWCO membranes.

The recoveries of the aptamers followed the same trend as the poly A sequences (Figure 4.04a). The major difference seen was the thrombin aptamer (TA) with a MW of 5.66 kDa and had a recovery of 48.4 and 12.8% for the 10 and 5 kDa MWCO, respectively. When compared with the A20 linear ssDNA with a MW of 6.20 kDa, the large drop in recoveries , 71.35 to 48.32 percent for the 10 kDa membrane and 34.02 to 12.68 percent for the 5 kDa membrane, cannot fully be explained by the small decrease of 0.54 kDa in molecular weight between A20 and TA. Therefore, secondary structure may play a role. TA forms a G-quadruplex (Figure 4.01) which tightly folds the sequence and makes it appear smaller in the system, allowing it to more readily pass through the pores of the membranes.

Retention times were consistent for all aptamers, with no significant change despite denaturing (Figure 4.04b). The denaturing method was a simple boiling water bath which would increase the temperature and break the hydrogen bonds that form the intramolecular bonding. Once injected into the AF4 system, the sample was cooled from the solution exchange that occurs during the focusing step. This suggests that the folded state of the aptamer is rapidly changing. As the aptamer folds onto itself, the overall diameter of the molecule becomes smaller which would cause an earlier elution time when compared with the linear form. The aptamers were modeled using Spartan, in both the linear and their Mfold-projected folded forms. Spartan was used in order to project the tertiary structure of the aptamers in their minimized energy form. It is important to note that Spartan calculations are done with gas phase modeling, not in an aqueous environment where solution effects might play a role. In this work, we only use Spartan

as a basic measurement tool to compare the behavior of the folded DNA to the linear poly A sequences. The distance across the longest length of the molecule were measured on Spartan and converted to a theoretical retention time using the polyadensosine distances and retention times (Table 4.02 and Figure 4.05). In every case, the experimentally measured retention times of the aptamers were later than the predicted folded and earlier than the linear forms. This suggests that the aptamers spends part of the time both in the linear and folded forms and elute based on the percentage of time the aptamer spends in the folded state. Using the theoretical retention times for linear and folded forms and the experimentally measured retention time, the percentage time the aptamers were folded was calculated. It was found that the longest aptamers, SA and I9-102, spent the least amount of time folded, with less than 25% time folded. SA and I9-102 also relied on more internal binding to form secondary structure, while the other three sequences formed secondary structure with the end bases and had percentage time spent folded greater than 50 %. The end bases are more flexible than internal bases and should have a higher chance of meeting the correct complementary sequences to bind.

3.4 Secondary Structure: Intermolecular Effect

In two of the sequences tested, WA and cWA, a second peak was seen at later retention times (Figure 4.06a and b). Since intramolecular interactions cause the molecule to fold and correspond to earlier retention times, it was determined that the second peaks were most likely intermolecular effects. The binding together of two or more molecules

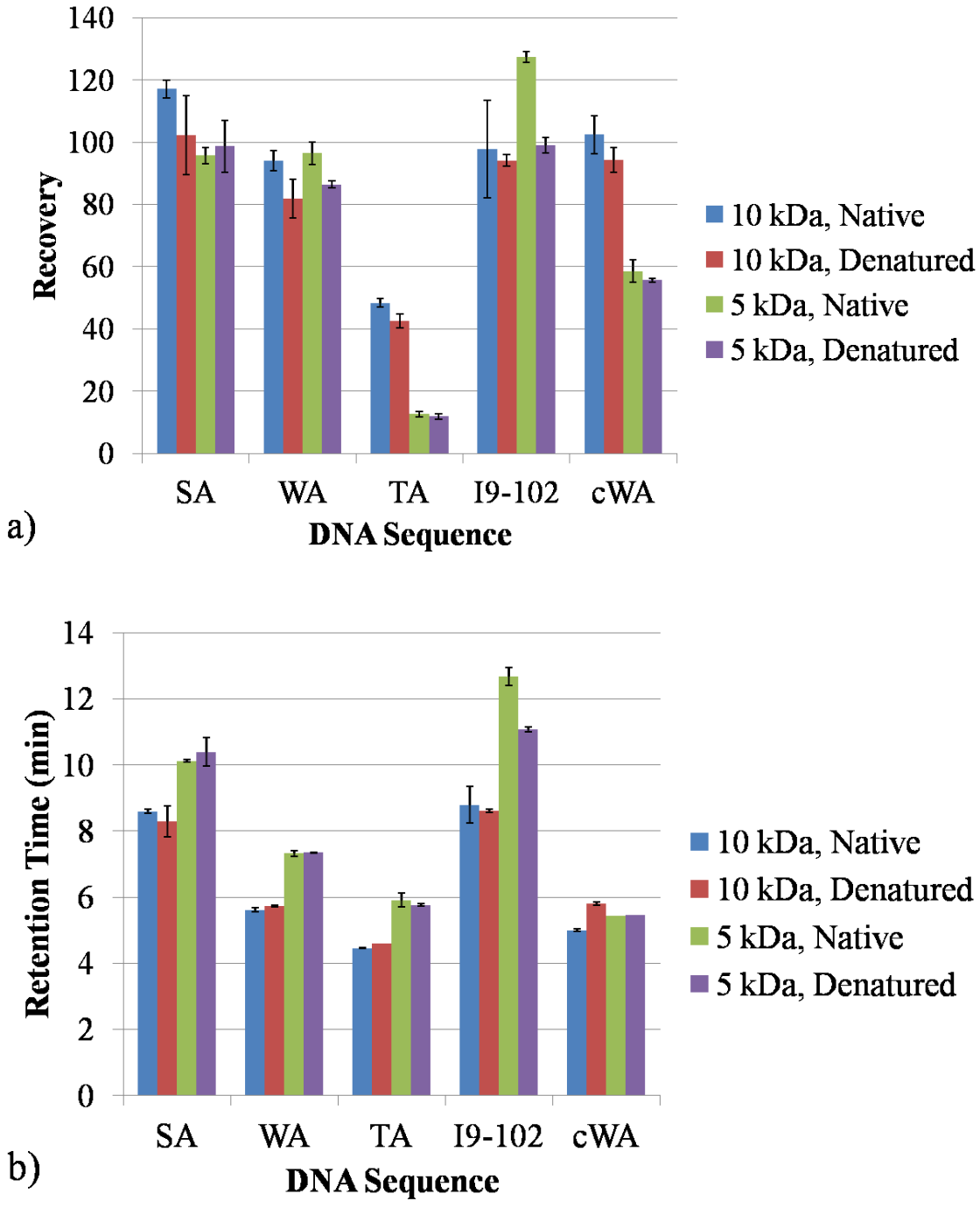

Figure 4.04 a) Percent recoveries and b) retention times of the aptamers comparing native with denaturing on both the 5 kDa and 10 kDa MWCO membranes.

would cause an increase in size, resulting in a later elution times. The difference seen between native and denatured samples for intermolecular is due to the slow re-annealing time. The DNA was injected immediately after denaturing. This was further supported by the lack of the peaks after the samples were denatured. To determine how the ssDNA was binding intermolecularly, the structure was examined. The WA and cWA are both stem loop structures that intramolecularly self-binds at the ends. These ends may also bind intermolecularly with each other. If the aptamers were binding intermolecularly, they would behave more like the poly A sequences as the secondary structure would be disrupted for the formation of linear DNA. To determine the feasibility, the average retention times for the second peak of the WA and cWA were converted to a theoretical MW based on the poly A calibration curve. The projected MWs for the WA and cWA intermolecular peaks were 33.44 and 15.12 kDa, respectively. In the case of the WA, a trimer formation of the WA would create a molecule with a MW of 33.86 kDa which is in very good agreement with the theoretical MW calculated based on the retention time of the secondary peak (Figure 4.06c). For the cWA sequence, the calculate MW of the second peak was 15.12 kDa. This MW is smaller than a dimer of the cWA (17.97 kDa). For the WA, the formation of the trimer would completely disrupt secondary structure, creating a completely linear molecule. However, the formation of a dimer of cWA would still allow part of the secondary structure to remain (Figure 4.06d). The presence of the secondary structure would cause the earlier formation as mentioned earlier.

Table 4.02. Table containing Spartan length measurements in linear and folded aptamer states, the experimental retention times of the aptamers and the calculated retention times (min) for linear and folded based on Spartan measurements. All information was used to calculate the percentage time folded for each aptamer.

Sequence	Linear (Å)	Folded (Å)	T_R	T_L	T_F	% Time Folded
WA	226	98.6	5.61	7.06	4.94	68.5
cWA	164	74.1	5.00	6.03	4.54	68.8
SA	352	181	8.60	9.15	6.31	19.3
I9-102	390	134	8.79	9.79	5.53	23.3
TA	94.3	48.4	4.47	4.87	4.11	54.4

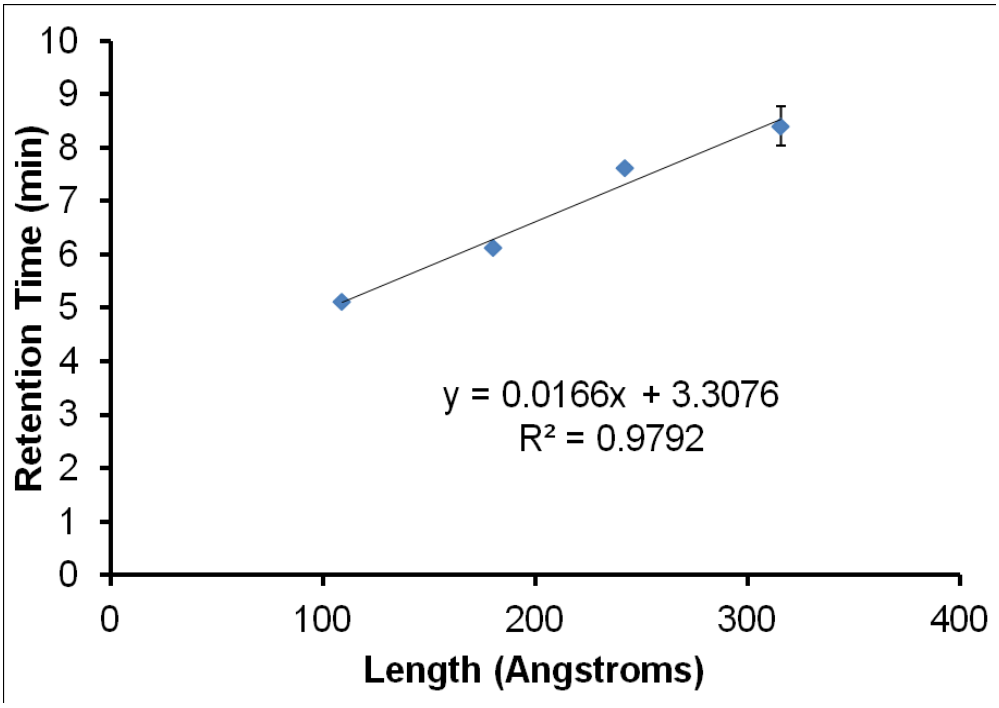

Figure 4.05. Calibration curve comparing length in Angstroms of the linear poly A ssDNA to retention time in the AF4.

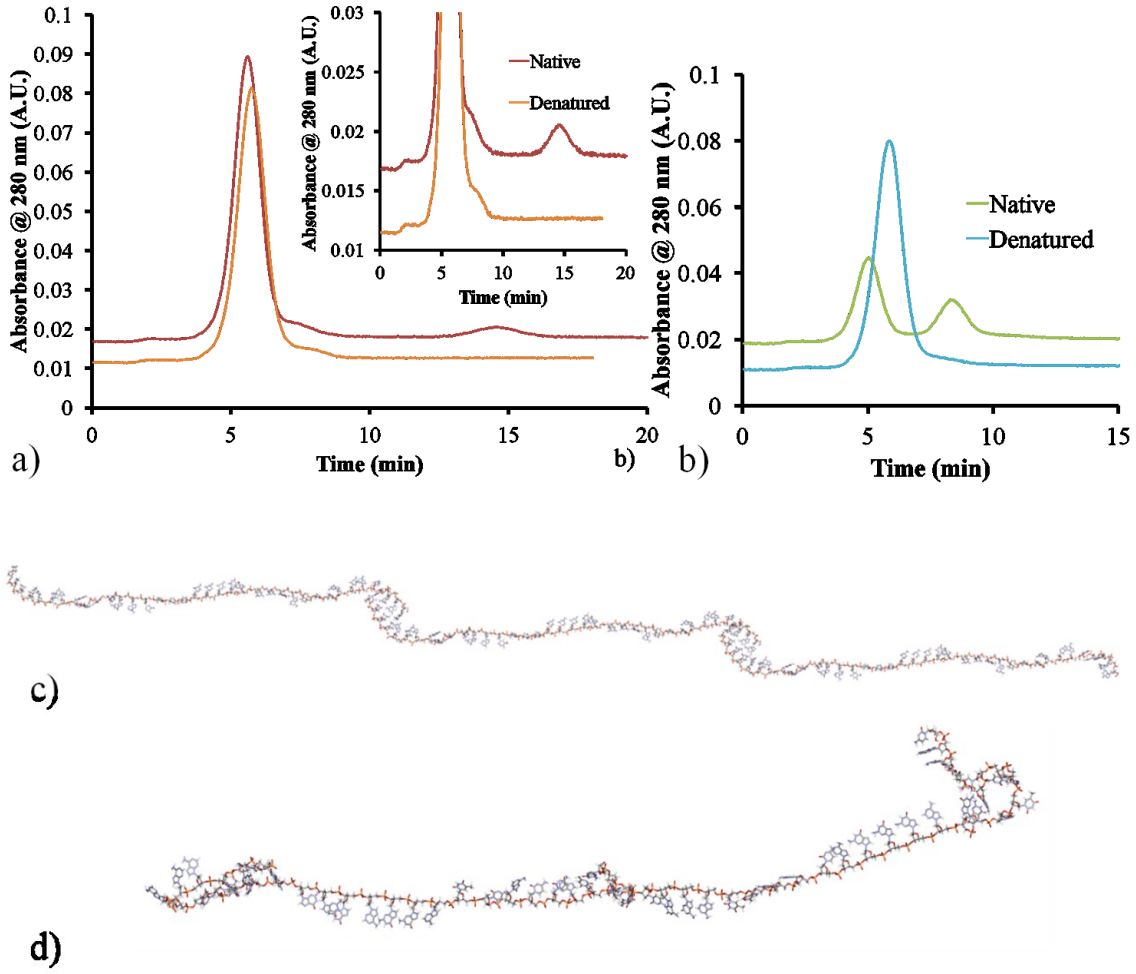

Figure 4.06 Elution profiles for the a)WA b) cWA showing a second peak in the native, non-denatured form. Spartan representations of the intermolecular interaction caused by the c) WA trimer and d) cWA dimer.

4. Conclusions

In this study, it was shown that accurate affinity calculations can be made on the AF4 with proper separation between the free aptamer and aptamer/protein peaks. Additionally, the behavior of short sequences of ssDNA was investigated and it was found that sequences below 10 kDa have limited recovery despite the use of lower MWCO membranes. When considering the use of aptamers as affinity tags in the AF4, the MW of the aptamer should be considered. Finally, the secondary structure of the aptamers can play a role in the retention time and, ultimately, how resolvable they are from their target proteins. Therefore, this method would not be suitable for smaller proteins. Based on the later retention times of the ssDNA with proteins of comparable MW, protein targets ($\geq$ 60 kDa) and larger biomolecules such as viruses and cells would be the most appropriate targets in AF4.

Acknowledgments

Michael C. Young prepared many of the Spartan figures used for calculations.

References

1. Li, N.; Zeng, S.; He, L.; Zhong, W., Probing Nanoparticle-Protein Interaction by Capillary Electrophoresis. *Anal. Chem. (Washington, DC, U. S.)* 82, (17), 7460-7466.

2. Ren, L.; Kim, H. K.; Zhong, W., Capillary Electrophoresis-Assisted Identification of Peroxyl Radical Generated by Single-Walled Carbon Nanotubes in a Cell-Free System. *Anal. Chem. (Washington, DC, U. S.)* **2009,** 81, (13), 5510-5516.

3. Mendonsa, S. D.; Bowser, M. T., In Vitro Evolution of Functional DNA Using Capillary Electrophoresis. *Journal of the American Chemical Society* **2003,** 126, (1), 20-21.

4. Mendonsa, S. D.; Bowser, M. T., In Vitro Selection of High-Affinity DNA Ligands for Human IgE Using Capillary Electrophoresis. *Analytical Chemistry* **2004,** 76, (18), 5387-5392.

5. Dvorak, M.; Svobodova, J.; Benes, M.; Gas, B., Applicability and limitations of affinity capillary electrophoresis and vacancy affinity capillary electrophoresis methods for determination of complexation constants. *Electrophoresis* 34, (5), 761-767.

6. Lu, C.; Li, H.; Wang, H.; Liu, Z., Probing the Interactions between Boronic Acids and cis-Diol-Containing Biomolecules by Affinity Capillary Electrophoresis. *Anal. Chem. (Washington, DC, U. S.)* 85, (4), 2361-2369.

7. Jia, Z.; Choi, D. S.; Chokshi, H., Determination of drug-polymer binding constants by affinity capillary electrophoresis for aryl propionic acid derivatives and related compounds. *J. Pharm. Sci.* 102, (3), 960-966.

8. El-Hady, D. A.; Albishri, H. M., Hyphenated affinity capillary electrophoresis with a high-sensitivity cell for the simultaneous binding study of retinol and retinoic acid in nanomolars with serum albumins. *J. Chromatogr. B: Anal. Technol. Biomed. Life Sci.* 911, 180-185.

9. Rebolj, K.; Pahovnik, D.; Zagar, E., Characterization of a Protein Conjugate Using an Asymmetrical-Flow Field-Flow Fractionation and a Size-Exclusion Chromatography with Multi-Detection System. *Anal. Chem. (Washington, DC, U. S.)* 84, (17), 7374-7383.

10. Guan, X.; Cueto, R.; Russo, P.; Qi, Y.; Wu, Q., Asymmetric Flow Field-Flow Fractionation with Multiangle Light Scattering Detection for Characterization of Cellulose Nanocrystals. *Biomacromolecules* 13, (9), 2671-2679.

11. Juna, S.; Huber, A., Determination of molar mass distribution of tapioca starch using asymmetrical flow field flow fractionation. *Starch/Staerke* 64, (2), 87-96.

12. Melucci, M.; Zambianchi, M.; Barbarella, G.; Manet, I.; Montalti, M.; Bonacchi, S.; Rampazzo, E.; Rambaldi, D. C.; Zattoni, A.; Reschiglian, P., Facile tuning from blue to white

emission in silica nanoparticles doped with oligothiophene fluorophores. *J. Mater. Chem.* 20, (44), 9903-9909.

13. Ma, P.-l.; Buschmann, M.; Winnik, F. M., Analysis of DNA/chitosan nanoparticles by field flow fractionation. *Polym. Prepr. (Am. Chem. Soc., Div. Polym. Chem.)* 51, (2), 172-173.

14. Zattoni, A.; Rambaldi, D. C.; Reschiglian, P.; Melucci, M.; Krol, S.; Garcia, A. M. C.; Sanz-Medel, A.; Roessner, D.; Johann, C., Asymmetrical flow field-flow fractionation with multi-angle light scattering detection for the analysis of structured nanoparticles. *J. Chromatogr., A* **2009,** 1216, (52), 9106-9112.

15. Hawe, A.; Romeijn, S.; Filipe, V.; Jiskoot, W., Asymmetrical flow field-flow fractionation method for the analysis of submicron protein aggregates. *J. Pharm. Sci.* 101, (11), 4129-4139.

16. Freitag, A. J.; Wittmann, K.; Immohr, L. I.; Winter, G.; Myschik, J., Asymmetrical flow field-flow fractionation: a preparative tool to obtain endotoxin-free protein species. *G.I.T. Lab. J., Eur.* 15, (11-12), 17-18.

17. Huerzeler, C.; Klein, T. In *Asymmetric FFF in biotechnology*, CRC Press: pp 136-138.

18. Schultes, S.; Mathis, K.; Zillies, J.; Zwiorek, K.; Coester, C.; Winter, G., Analysis of polymers and protein nanoparticles using Asymmetrical Flow Field-Flow Fractionation (AF4). *LC-GC Eur.* **2009,** 22, (8), 390-392, 394, 396, 398-400, 402-403.

19. Pease, L. F., III; Lipin, D. I.; Tsai, D.-H.; Zachariah, M. R.; Lua, L. H. L.; Tarlov, M. J.; Middelberg, A. P. J., Quantitative characterization of virus-like particles by asymmetrical flow field flow fractionation, electrospray differential mobility analysis, and transmission electron microscopy. *Biotechnol. Bioeng.* **2009,** 102, (3), 845-855.

20. Chuan, Y. P.; Fan, Y. Y.; Lua, L.; Middelberg, A. P. J., Quantitative analysis of virus-like particle size and distribution by field-flow fractionation. *Biotechnol. Bioeng.* **2008,** 99, (6), 1425-1433.

21. Citkowicz, A.; Petry, H.; Harkins, R. N.; Ast, O.; Cashion, L.; Goldmann, C.; Bringmann, P.; Plummer, K.; Larsen, B. R., Characterization of virus-like particle assembly for DNA delivery using asymmetrical flow field-flow fractionation and light scattering. *Analytical Biochemistry* **2008,** 376, (2), 163-172.

22. Lee, H.; Williams, S. K. R.; Wahl, K. L.; Valentine, N. B., Analysis of whole bacterial cells by flow field-flow fractionation and matrix-assisted laser desorption/ionization time-of-flight mass spectrometry. *Anal. Chem.* **2003,** 75, (11), 2746-2752.

23. Reschiglian, P.; Zattoni, A.; Roda, B.; Casolari, S.; Moon, M. H.; Lee, J.; Jung, J.; Rodmalm, K.; Cenacchi, G., Bacteria sorting by field-flow fractionation. Application to whole-cell Escherichia coli vaccine strains. *Anal. Chem.* **2002,** 74, (19), 4895-4904.

24. Schachermeyer, S.; Ashby, J.; Zhong, W., Aptamerâ€“protein binding detected by asymmetric flow field flow fractionation. *Journal of Chromatography A*, (0).

25. Zuker, M., Mfold web server for nucleic acid folding and hybridization prediction. *Nucleic Acids Res.* **2003,** 31, 3406-3415.

26. Dewar, M. J. S.; Zoebisch, E. G.; Healy, E. F.; Stewart, J. J. P., Development and use of quantum mechanical molecular models. 76. AM1: a new general purpose quantum mechanical molecular model. *Journal of the American Chemical Society* **1985,** 107, (13), 3902-3909.

27. Singh, S.; Khulbe, K. C.; Matsuura, T.; Ramamurthy, P., Membrane characterization by solute transport and atomic force microscopy. *Journal of Membrane Science* **1998,** 142, (1), 111-127.

Chapter Five

Conclusions and Future Outlook

The scope of this dissertation explored the feasability of applying F4 and AF4 for bioanalysis. In chapter two, the carrier solution composition effect on the recovery of protein and nanoparticles was studied on F4. It was found that higher salt concentrations, those greater than 50 mM, increased the recovery of proteins, while it decreased the recovery of unmodified nanoparticles (NPs). Overall, salt was found to reduce the surface zeta potential of the NPs reducing the electrostatic repulsion between the NPs and membrane, thereby increasing adsorption. This effect was not as prominent for particles with smaller diameters as they did not come close enough to the membrane for electrostatic repulsion to be necessary. Additionally, carboxylated NPs (COOH-NPs) were stabilized by their highly negatively charged surfaces. Ultimately, for future applications AF4 is suitable for biomolecules and may be used with nanoparticles if special attention is given towards the carrier solution's effect on the surface charge of the particles.

Future Outlook: AF-SELEX

In this dissertation, it was shown that the binding between ssDNA and proteins is maintained for specific binding situations while minimizing non-specific binding. These ssDNA, or aptamers, are short single stranded DNA or RNA that form bind to targets with high specificity and affinity. First discovered in the early 1990s, aptamers were

found to have dissociation constants (K_d) in the nanomolar to sub-nanomolar range for proteins and in the micromolar range for small molecules.[1] With similar K_d values as antibodies, but more rugged structure that can withstand harsher environments and labeling, aptamers are attractive alternatives to the antibodies in biosensing. Since their discovery, aptamers have used in a large range of applications such as detection, affinity purification, and even as drugs.[2-10]

Initial aptamer selections were done with RNA.[11] The process to select aptamers starts with a ssDNA library. The library contains the known primer regions and in the center contains an unknown random region. The number of possible sequences is dependent on the number of random nucleotides (N) in the unknown region 4^N. This process is called systematic evolution of ligands by exponential enrichment (SELEX). In SELEX, the target is first incubated in the library. The bound ssDNA is separated from the unbound, amplified via polymerase chain reaction (PCR), and the resulting amplified DNA is then incubated with the target again (Figure 5.01). Every selection round will increase the number of binding DNA, which creates a more competitive environment as the DNA with lower K_ds will out-compete the other sequences. Finally, the end pool should contain only high binding aptamers. The ssDNA is then cloned and sequenced.

Traditionally, the separation process of the bound from unbound DNA is done using a nitrocellulose filter.[11] The mixture of protein and DNA is passed through a nitrocellulose filter. The protein and bound aptamers are retained while the unbound sequences pass through the filter. To increase the binding affinity of the sequences, a slightly denaturing solution such as a low concentration of urea may be used to wash the

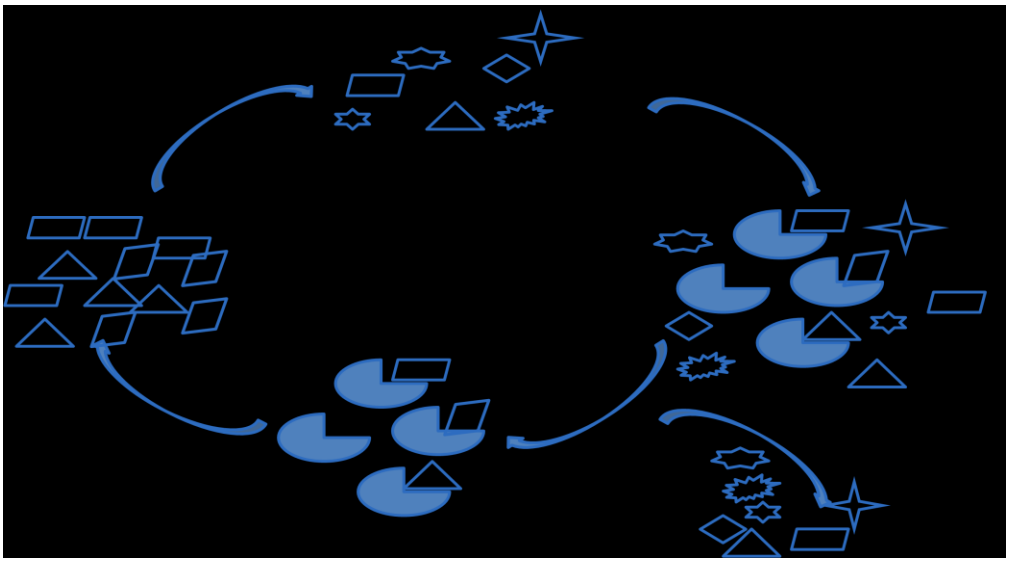

Figure 5.01. Schematic of SELEX process.

protein to remove weakly bound sequences. The protein is then washed with a strongly denaturing solution to release the aptamers. This number of selection cycles until sufficiently binding aptamers are found can exceed 25 cycles.

The large number of required rounds can be attributed to poor separation efficiency of the unbound DNA from the bound DNA. In 2003, Bowser et al used capillary electrophoresis (CE) to separate bound DNA from unbound, called CE-SELEX.[12] The increased separation efficiency resulted in an aptamer pool with nanomolar K_d values in only four selection rounds. CE is also suitable for finding aptamers for small molecules which could not be done in the traditional membrane separation. However, there are still a few limitations with CE-SELEX. There must be separation between the analyte and DNA, with the method working best for slightly positive targets since DNA is highly negatively charged. Since CE injections are on the nanoliter scale, collection and PCR amplification of such low copy number DNA can be particularly difficult. Also, the buffer conditions used to incubate the target and DNA pool need to contain sufficiently low ionic strength which can result in aptamers that bind in non-biologically relevant conditions.

In chapter 3, it was shown that the buffer conditions are very important for the formation of the aptamer's secondary structure. Therefore, the end binding environment should be considered when selecting for aptamers. AF4 has the salty buffer adaptability that CE lacks. Therefore, AF4 could potentially be used as a separation method for SELEX (AF4-SELEX). Some AF4-SELEX limitations do exist. Since AF4 has a lower MWCO based on the membrane pore size, AF4-SELEX would not be suitable for small

molecule targets. There must be a size separation in order to collect the bound complex. For a ssDNA pool consisting of aptamers with approximate molecular weights of 40 kDa, in order to obtain separation from the protein/aptamer complex, the protein should be at least 100 kDa in size. Therefore, AF4-SELEX would be better suited to larger targets such as large proteins, viruses, and cells.

The first step for developing AF4-SELEX is to select aptamers against a protein. The standard protein for SELEX method development is IgE. Once the method is proven successful on IgE, AF4-SELEX will be applied to viruses. Viruses are typically on the order of 50 nm or larger in diameter making them an excellent target for selection. The final AF4-SELEX project would deal with finding aptamers that inhibit viruses from binding to cells. Here, the idea stems from incubating cells with viruses and the ssDNA pool, and then collecting those viruses that do not bind to the cells. This would prevent viruses from amplifying in the host. These types of aptamers would make excellent anti-viral drug candidates.

Future Outlook: Biosensing

In another potential use for AF4, with the application of aptamers, protein detection in complex media could be achieved. One of the biggest challenges for sensitive detection is the background signal. As the aptamer does not significantly alter the molecular weight of the protein, the AF4 could first be used to do the protein separation to minimize the background. Even in complex solutions, where the protein

could not be distinguished using standard UV detection, the aptamer would bind specifically to the target allowing quantitation with a fluorescence detector. Once the feasibility of protein detection in complex sample is shown, multiplex detection would be the next step on AF4. By utilizing different aptamers to target each of the proteins, the AF4 would separate the proteins based on size, and the fluorescence detection would be detected. This method would work best for proteins that had significant enough size difference to be fully resolvable.

In complex samples, multiple target proteins could co-elute. In order to detect co-eluting proteins, fluorophores with different emissions could be used. However, there would still be a limited number of fluorophores that may be used simultaneously without spectral interference. Another aptamer labeling option would be the use of small metal NPs. The metal NPs could then be detected by ICP-MS. This would add to the number of possible labels used increasing the multiplex potential. Ultimately, the AF4 will have an interesting future in the application of bioanalysis.

References

1. Wiegand, T. W.; Williams, P. B.; Dreskin, S. C.; Jouvin, M. H.; Kinet, J. P.; Tasset, D., High-affinity oligonucleotide ligands to human IgE inhibit binding to Fc epsilon receptor I. *J Immunol* **1996,** 157, (1), 221-230.

2. Yoshida, W.; Yamamoto, H.; Ikebukuro, K., An Optical Biosensing System Based on Interference-Enhanced Reflection with Aptameric Enzyme Subunits of Thrombin. *Anal. Lett.*, Ahead of Print.

3. Li, L.; Ge, P.; Selvin, P. R.; Lu, Y., Direct Detection of Adenosine in Undiluted Serum Using a Luminescent Aptamer Sensor Attached to a Terbium Complex. *Anal. Chem. (Washington, DC, U. S.)*, Ahead of Print.

4. Wu, Y.; Liu, L.; Zhan, S.; Wang, F.; Zhou, P., Ultrasensitive aptamer biosensor for arsenic(III) detection in aqueous solution based on surfactant-induced aggregation of gold nanoparticles. *Analyst (Cambridge, U. K.)* 137, (18), 4171-4178.

5. Lee, C.-Y.; Wu, K.-Y.; Su, H.-L.; Hung, H.-Y.; Hsieh, Y.-Z., Sensitive label-free electrochemical analysis of human IgE using an aptasensor with cDNA amplification. *Biosens. Bioelectron.*, Ahead of Print.

6. Zhou, D., Quantum dot-nucleic acid/aptamer bioconjugate-based fluorimetric biosensors. *Biochem. Soc. Trans.* 40, (4), 635-639.

7. Carrasquilla, C.; Lau, P. S.; Li, Y.; Brennan, J. D., Stabilizing Structure-Switching Signaling RNA Aptamers by Entrapment in Sol-Gel Derived Materials for Solid-Phase Assays. *J. Am. Chem. Soc.* 134, (26), 10998-11005.

8. Cui, Z.; Zhang, Z.; Ren, Q.; Wei, H.; Zhang, X. In *Quantum dot-aptamer nanoprobe to label influenza virus for single virus imaging*, American Chemical Society: pp HEALTH-521.

9. Zelada-Guillen, G. A.; Riu, J.; Duzgun, A.; Rius, F. X., Immediate Detection of Living Bacteria at Ultralow Concentrations Using a Carbon Nanotube Based Potentiometric Aptasensor. *Angew. Chem., Int. Ed.* **2009,** 48, (40), 7334-7337, S7334/1-S7334/5.

10. James, W., Aptamers in the virologists' toolkit. *J Gen Virol* **2007,** 88, (2), 351-364.

11. Tuerk, C.; Gold, L., Systematic evolution of ligands by exponential enrichment: RNA ligands to bacteriophage T4 DNA polymerase. *Science* **1990,** 249, (4968), 505-510.

12. Mendonsa, S. D.; Bowser, M. T., In Vitro Evolution of Functional DNA Using Capillary Electrophoresis. *Journal of the American Chemical Society* **2003,** 126, (1), 20-21.